NAVAL
POSTGRADUATE
SCHOOL

MONTEREY, CALIFORNIA

THESIS

EVALUATION OF EM PROPAGATION MODELS USING DATA FROM WALLOPS ISLAND EXPERIMENT (2000)

by

Andrew J. Moys

September 2003

Thesis Advisor:	Kenneth L. Davidson
Second Reader:	Wendell A. Nuss

THIS PAGE INTENTIONALLY LEFT BLANK

REPORT DOCUMENTATION PAGE			Form Approved OMB No. 0704-0188
Public reporting burden for this collection of information is estimated to average 1 hour per response, including the time for reviewing instruction, searching existing data sources, gathering and maintaining the data needed, and completing and reviewing the collection of information. Send comments regarding this burden estimate or any other aspect of this collection of information, including suggestions for reducing this burden, to Washington headquarters Services, Directorate for Information Operations and Reports, 1215 Jefferson Davis Highway, Suite 1204, Arlington, VA 22202-4302, and to the Office of Management and Budget, Paperwork Reduction Project (0704-0188) Washington DC 20503.			
1. AGENCY USE ONLY *(Leave blank)*	**2. REPORT DATE** September 2003	**3. REPORT TYPE AND DATES COVERED** Master's Thesis	
4. TITLE AND SUBTITLE: Evaluation of EM Propagation Models Using Data from Wallops Island Experiment (2000)			**5. FUNDING NUMBERS**
6. AUTHOR(S) Andrew J Moys			
7. PERFORMING ORGANIZATION NAME(S) AND ADDRESS(ES) Naval Postgraduate School Monterey, CA 93943-5000			**8. PERFORMING ORGANIZATION REPORT NUMBER**
9. SPONSORING /MONITORING AGENCY NAME(S) AND ADDRESS(ES) N/A			**10. SPONSORING/MONITORING AGENCY REPORT NUMBER**
11. SUPPLEMENTARY NOTES The views expressed in this thesis are those of the author and do not reflect the official policy or position of the Department of Defense or the U.S. Government.			
12a. DISTRIBUTION / AVAILABILITY STATEMENT Approved for public release; distribution is unlimited.			**12b. DISTRIBUTION CODE**

13. ABSTRACT ***(maximum 200 words)***

The Royal Navy and the United States Navy emphasise utilising the environment to achieve a tactical edge. Such approaches are outlined in Sea Power 21. This thesis recognises accurate characterisation of the physical battlespace as vital to concepts of both self-defence (Sea Shield) and strike (Sea Strike). Electromagnetic (EM) propagation is presented as a vital factor in the performance of a wide variety of ship, land, and airborne sensors and weapon systems. Atmospheric influences on EM propagation are related to gradients of temperature and humidity within the atmosphere. It is emphasised that modern maritime warfare is increasingly concentrated in the coastal theatre, an area in which atmospheric variability is often at maxima in both the vertical and horizontal. This thesis examines, using currently available technology and operational methods, how well the physical EM battlespace is described. Propagation models from the UK and US are used to evaluate the propagation environment within the coastal zone, using measured data, collected from the East Coast of the USA, at Wallops Island during 2000, as a comparison. The main findings relate to the large potential errors, due the inability to measure and characterise the variability of the coastal environment under simulated, operational scenarios.

14. SUBJECT TERMS EEMS, AREPS, RF Propagation, Refractivity, Coastal Variability, Wallops Island, Surface Ducting and Evaporative Ducting Effects, Operational Simulation			**15. NUMBER OF PAGES** 162
			16. PRICE CODE
17. SECURITY CLASSIFICATION OF REPORT Unclassified	**18. SECURITY CLASSIFICATION OF THIS PAGE** Unclassified	**19. SECURITY CLASSIFICATION OF ABSTRACT** Unclassified	**20. LIMITATION OF ABSTRACT** UL

NSN 7540-01-280-5500 Standard Form 298 (Rev. 2-89)
Prescribed by ANSI Std. 239-18

THIS PAGE INTENTIONALLY LEFT BLANK

Approved for public release: distribution is unlimited

EVALUATION OF EM PROPAGATION MODELS USING DATA FROM WALLOPS ISLAND EXPERIMENT (2000)

Andrew J. Moys
Lieutenant Commander, Royal Navy
B.Sc., Queen Mary College, University of London, 1987

Submitted in partial fulfillment of the
requirements for the degree of

MASTER OF SCIENCE IN METEOROLOGY

from the

NAVAL POSTGRADUATE SCHOOL
September 2003

Author: Andrew J. Moys

Approved by: Kenneth L. Davidson
Thesis Advisor

Wendell A. Nuss
Second Reader

Carlyle H. Wash
Chairman, Department of Meteorology

THIS PAGE INTENTIONALLY LEFT BLANK

ABSTRACT

The Royal Navy and the United States Navy emphasise utilising the environment to achieve a tactical edge. Such approaches are outlined in Sea Power 21. This thesis recognizes accurate characterisation of the physical battlespace as vital to concepts of both self-defence (Sea Shield) and strike (Sea Strike). Electromagnetic (EM) propagation is presented as a vital factor in the performance of a wide variety of ship, land, and airborne sensors and weapon systems. Atmospheric influences on EM propagation are related to gradients of temperature and humidity within the atmosphere. It is emphasised that modern maritime warfare is increasingly concentrated in the coastal theatre, an area in which atmospheric variability is often at maxima in both the vertical and horizontal. This thesis examines, using currently available technology and operational methods, how well the physical EM battlespace is described. Propagation models from the UK and US are used to evaluate the propagation environment within the coastal zone, using measured data, collected from the East Coast of the USA, at Wallops Island during 2000, as a comparison. The main findings relate to the large potential errors, due the inability to measure and characterise the variability of the coastal environment under simulated, operational scenarios.

THIS PAGE INTENTIONALLY LEFT BLANK

TABLE OF CONTENTS

THIS PAGE INTENTIONALLY LEFT BLANK

LIST OF FIGURES

THIS PAGE INTENTIONALLY LEFT BLANK

LIST OF TABLES

THIS PAGE INTENTIONALLY LEFT BLANK

ACKNOWLEDGMENTS

I would like to offer my thanks and appreciation to all those persons who extended their time and professional expertise as I produced this thesis. Heartfelt thanks goes to Professors Davidson and Nuss, Paul Frederickson, Tamar Neta, Bob Creasey, Wendy Townshend (MWC, UK), Janet Stapleton (NSWC-DD) and all the staff at NPS.

NPS faculty, staff and equipment participation in Wallops'2000 was sponsored by the Office of Naval Research (Code 322MM) through Naval Surface Warfare Command, Dahlgren Division (NSWC-DD). The participation of NPS staff in the production of the analyses and evaluations, was sponsored by the US Navy's Space and Naval Warfare Command (SPAWAR, PMW-150).

I would also like to thank the Directorate of Naval Surveying, Oceanography and Meteorology for funding my attendance at NPS and the Maritime Warfare Centre for allowing me to use EEMS for this study.

Finally to my parents and dog, Baggins, back in UK, and also to Tracey Delk and Henry Howell for enduring throughout.

THIS PAGE INTENTIONALLY LEFT BLANK

I. INTRODUCTION

A. NAVAL STRATEGY

The Royal Navy's, The Fundamentals of British Maritime Doctrine (Directorate of Naval Staff Duties, 1995) emphasises, that it is the "duty of Command to take account and advantage of the environment", and that "expertise in environmental prediction must be available to a commander if he is to exploit the maritime environment fully and minimize its adverse effects".

Surface based and airborne search radars and most command and control communications and missile guidance systems all function within that part of the radio frequency spectrum liable to propagation anomalies, as a result of meteorological influences. Complementary electronic warfare, whether it is in a jamming role (electronic countermeasures) or in an intercept capacity (electronic support measures), must be conducted in these same frequency bands, and can be greatly increased in their effectiveness by a thorough knowledge of the propagation characteristics present.

The meteorological factors that favour unusual radio and radar performance are well established, although this is not to say that all the answers are known. Additionally lack of high vertical resolution measurements in the surface layer and the paucity of upper air meteorological data generally over the sea has posed, and continues to pose, difficulties when attempting to identify and forecast such conditions. At the same time, increased sophistication of the offensive and defensive assets available in fighting the war at sea, has made knowledge of how the environment may be affecting the propagation assume even greater importance. Within the framework of the 4-D Cube (a four-dimensional, common picture compilation of the battlespace environment) such information is vital to the warfighter in obtaining a clear, concise and accurate evaluation of both weapons systems performance and the threat assessment.

Both the United States Navy (USN) and the Royal Navy (RN) have placed great emphasis on the use of the environment for operations and strategic planning. The US Navy's Naval Transformation Roadmap, Sea Power 21 (2003), under the category of Sea Strike and Sea Shield, and The Navy Strategic Planning Guidance With Long Range

Planning Objectives (Chief of Naval Operations, 2000) emphasize the need to build an information and knowledge superior force to counter the ever-increasing diversity and complexity of threats likely to be faced in the future. Potential adversaries are expected to continue to acquire increasingly sophisticated and effective weapons, sensors and platforms over the coming few decades. The performance of these systems against defensive resources will become ever more dependent upon the atmospheric and oceanic conditions than ever before.

At the time of writing, a number of sophisticated models are available to describe the effects of the atmosphere on radio and radar propagation. These models utilise actual meteorological measurements, or input data from environmental models, such as the UK Met Office's Meso-scale Model or the US Navy's COAMPS model.

This thesis examines the current level of predictability, using a comparison of realistic operational methods and data collected during Microwave Propagation Measurement Experiment (MPME) at Wallops Island during April and May 2000. This dataset is unique in many ways, not least due to the fact that actual propagation conditions and meteorological data were measured, during a number of different synoptic meteorological conditions.

1. Defending Against the Threat

Potential adversaries are expected to pursue area denial strategies for the next 15 to 20 years. Unlike those of the previous generation, these challenges are expected to be land-based and in the littoral environment, rather than in open ocean.

The level of sophistication and performance of future weapons is expected to increase substantially, with the survivability of both weapon and platform increasing through the use of advanced countermeasure designs and multi-spectral signature control as demonstrated by the RN's Type 23 Frigate and future Type 45 Frigate. Increasingly, these weapons systems will be supported by more sophisticated sensors, many of these will be particularly sensitive to the variability of the Marine Atmospheric Boundary Layer (MABL). The concept of Sea Shield currently identifies the threats as follows:

a. Anti-Ship Cruise Missiles (ASCM)/Unmanned Aerial Vehicles (UAV)

One of the most significant systems to consider both currently and in the future is also one whose performance is significantly affected by the atmosphere. It is the Anti-Ship Cruise Missile (ASCM). Such systems have been proven effective in the Falklands Conflict during which, HMS Sheffield and the Atlantic Conveyer were sunk by the Aerospatiale Excocet system. In the ensuing years both air defence and missile design has improved significantly. The current design trends of the ASCM include:

- Significant increases in the terminal velocity from predominantly sub-sonic speeds to supersonic speeds in the next decade, and hypersonic speeds by 2020.
- Reduction in Radar and IR signatures
- Ever increasingly complex terminal manouevers.
- Reductions in flight profile altitudes.

All of the above features are designed to make the detection and targeting on incoming missiles more difficult. Future ship designs will require more advanced sensors to detect increasingly stealthy missiles, improved stealth characteristics to complicate enemy target acquisition, effective soft and hard-kill capabilities, and the ability to sustain damage, whilst maintaining the ability to function and fight. Increasingly such weapons are likely to be launched by UAVs, which by nature of their small radar cross-section are difficult to detect.

b. Surface to Air Missiles

Advances in the design and effectiveness of basic missile design, propulsion systems, guidance systems and warheads will all increase the capability of air defence systems, both ashore and afloat. The countermeasures to both manned and unmanned aircraft will improve rendering missile attack more difficult. Stealth measures will also continue to evolve, but above all the use of Electronic Warfare support will remain critical.

c. Surface Vessels

Current build specifications for naval surface vessels, include measures for the reduction in radar cross-sections and multi-spectral low observability (IR, visual, magnetic and acoustic). Fire control systems now encompass the entire spectrum of electromagnetic/electro-optical (EM/EO) emissions including radar, EO, IR and laser for anti-air warfare (AAW), anti-surface warfare (ASUW) and undersea warfare (ASW). Increasingly the threat from smaller vessels, such as speed-boats or skiffs/Dows armed with portable missile systems, or insertion teams, armed with surface-contact munitions is being considered. Such vessels have a very small radar cross-section (RCS) and are thus naturally difficult to detect.

d. The Sub-Surface Threat

The 1980's and early 1990's saw submarine technology advance to a state where the tactical advantage of ship-borne sonars and towed arrays was severely eroded and the detection of submarines by passive acoustic methods alone very difficult. A number of other methods including detection of periscopes and masts through EM/EO sensors has become of greater significance. Indeed, in littoral and coastal shelf regions, the practice of radar flooding is a major tactic in the detection and deterrent of submarines.

B. METOC OPERATIONAL/MISSION SUPPORT

Many of the capabilities outlined in Sea Power 21 require mission support implicitly or explicitly from environmental products provided by the Meteorological and Oceanographic (METOC) Branch. Much of the data will be input in to Tactical Decision Aids (TDAs), which require high quality data to be input from in-situ observations or from environmental models such as the Coupled Ocean Atmosphere Meso-scale Prediction System (COAMPS) run by the Fleet Numerical Meteorological and Oceanographic Center (FNMOC) at Monterey, CA. Environmental products are used for a whole host of naval purposes including the support of flying missions, naval gunfire support, ship safety and routing, EM/EO propagation conditions for the detection of and

vulnerability to various missile systems and aircraft, snort masts, periscopes, surface vessels of varying sizes (including rigid inflatable boats) and swimmers.

EM/EO propagation is extremely sensitive to environmental variability and the most critical to weapons systems deployment. Accurate assessment of the environment's effect on weapon system performance is dependant upon both, the ability of propagation models to describe radio paths and interference patterns, and of production of four-dimensional representations at high resolutions of the atmosphere. Recent research and initiatives into the relative importance of various atmospheric parameters include:

- The SMOOS (R) continuous shipboard measuring system;
- The Aegis Class specific Shipboard Weapons System Performance System (SEAWASP);
- Rocketsondes;
- The Tactical Dropsonde (T-Drop).

Each of the above suffers limitations to their operational use: the SMOOS(R) shipboard measuring system requires a bulk parameterization, which may be unreliable under stable atmospheric conditions; standard RAWINDSONDES provide accurate in-situ soundings, but lack resolution near surface, are relatively expensive, require stores of ancillary equipment such as helium and trained METOC personnel to operate the system; rocketsondes and T-drops are also relatively expensive, but tactically more flexible and require less ancillary equipment and manpower.

Many of the currently operating systems were developed independently of each other and consequently suffer problems in the sphere of inter-operability. Thus the systems are rarely tested against each other or evaluated as a complete product. This lack of quantification leads to vital information often being discarded, by both operators and the Command, in favour of using the same result that worked the last time around.

The thesis has been formatted to give detailed background radar and meteorological/tactical effects information from Chapters III until VI, model descriptions and experimental set-up can be found in Chapters VII and VIII, synoptic descriptions in Chapter IX, analysis of results in Chapters X and XI and summary/conclusions in Chapter XII.

THIS PAGE INTENTIONALLY LEFT BLANK

II. BACKGROUND

A. PURPOSE

A purpose of this thesis is to examine the meteorological influences that produce variations in propagation, in particular evaporative, surface based and low-level elevated ducts. The effects of the features will be examined principally by using a propagation tactical decision aid (TDA) from the United Kingdom, called the Electromagnetic Effects Modelling System (EEMS), and the results compared to measured propagation taken at WALLOPS 2000. The standard US TDA Atmospheric Refractive Effects Prediction System (AREPS) will also be used for comparison purposes. The AREPS TDA is used by the Royal Navy (RN) and United States Navy (USN) as well as by other NATO navies.

Any attempt to measure, and indeed, model the atmosphere and it's effects will be limited by errors in data collection and subsequent analysis. One of the main features of any such exercise is to limit and minimize the errors to a satisfactory level. Broadly speaking, the total error associated with the process of predicting EM propagation for ship-borne sensors is the sum of:

- Instrument and measurement error;
- Errors associated with applying relatively coarse operational data to existing theory of the MABL;
- Temporal and spatial environmental variation;
- Propagation model errors and initialization problems (target, transmitter and receiver characteristics).

The thesis will examine the role of these errors and make conclusions regarding their impact on operations and tactics.

B. WALLOPS 2000 EXPERIMENT

During April and May of 2000, a number of radio frequency (RF) field tests were conducted by the US Navy's Surface Warfare Center, Dahlgren Division (NSWC-DD), Dahlgren, VA, at the US Navy's Surface Combat Systems Center (SCSC), Wallops Island, Virginia. The tests supported the Office of Naval Research (ONR 351) funded

"Interactive Adaptation of Fire Control Sensors to the Environment" task by collecting pertinent propagation and METOC data in environments designed to simulate those encountered by a warship. In fact the experiments are all conducted within the littoral environment and were subject to both synoptic and meso-scale meteorological influences. Such an environment is typical of those in which littoral combat might take place, and thus some significant tactical advice can be gleaned from the results. Experiment objectives and designs are detailed in the Site Test Plan and Procedures for the Microwave Propagation Measurement Experiment at the SCSC Wallops Island Test Facility (NSWC 2000).

The principal objective of the experiments was to develop methods by which ships could remotely sense low altitude propagation and clutter using ship-borne fire control sensors and locally derived meteorological observations. This operationally obtained data would be used to improve sensor and combat system performance through a semi-automatic adaptation to existing conditions.

Two main elements of this objective, which apply to this thesis, were to:

- Evaluate the degree to which meteorological data and meso-scale model data can be used to accurately predict the true propagation conditions;
- Validate various propagation models and meteorological data collection techniques.

A number of groups were involved in both the planning and execution of the experiment:

- Naval Surface Warfare Center, Dahlgren Division, Dahlgren, VA (NSWC-DD)
- Johns Hopkins University, Applied Physics Laboratory, Laurel, MD (JHU/APL)
- Naval Postgraduate School, Department of Meteorology, Monterey, CA (NPS/MR)
- Space and Naval Warfare Command (SPAWAR) Systems Center, San Diego, CA (SSC)

1. Basic Test Scenario

The basic field-test scenario consisted of a transmitter on the project vessel, *R/V Sealion,* and receivers located ashore. The shore-based receivers were used to directly collect propagation data over the sea as the vessel moved along a pre-determined path. Meteorological data were collected from a number of platforms at various positions along the path as below:

- Onboard the *R/V Sealion* (operated by NSCWC-DD) as it traversed the pre-determined propagation path.
- Onboard a leased a helicopter (instrumented by JHU/APL) along the same path as the *R/V Sealion* using a vertical saw-tooth pattern flight profile.
- Onboard the R/V Chessie (operated by JHU/APL), which employed both SEAWASP instrumentation and a towed instrumented catamaran.
- From shore based tower, using NASA equipment.
- From several buoys, including the Naval Postgraduate School Flux Buoy (this is the main source of meteorological data used by the author due to its high quality, consistency and continuity of data).

The collection of radar and meteorological data commenced on 03 April 2000 and ceased on 12 May 2000. On the days when radar data was collected, there were generally several collection periods or runs. At the beginning of a run, the *R/V Sealion* commenced data collection immediately offshore near the receiver station. The vessel then followed a predetermined path for each collection run, along one of three radials, 135 degrees, 150 degrees and 165 degrees (all radials are measured from true north). The radials were selected daily to minimize wave impact on the collection vessel and it's crew. Typical collection runs extended approximately 20nm down-path, although in some cases this was extended to 35nm. This thesis uses data collected from runs, undertaken on four separate days.

THIS PAGE INTENTIONALLY LEFT BLANK

III. RELEVANT BASIC CONCEPTS OF RADAR SYSTEMS

A. BASIC PRINCIPLES

1. Electromagnetic Waves

Radio waves are waves of electromagnetic energy. An electromagnetic (EM) wave consists of an electric and magnetic field, which are mutually perpendicular to each other (Figure 1.). The fields oscillate sinusoidally, and are in phase with each other i.e. the maximum value of the sinusoids on the electric and magnetic components occurs at the same time. The direction of propagation of the wave is perpendicular (transverse) to the directions of oscillation of the electric and magnetic fields, and EM waves are therefore known as transverse.

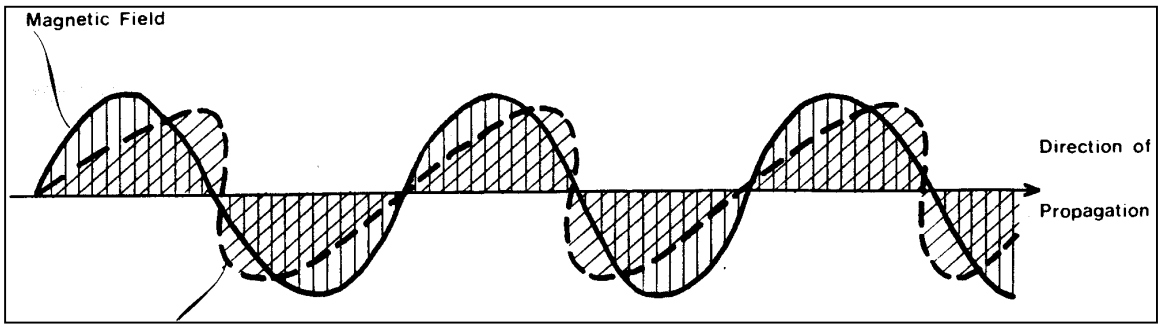

Figure 1. An electromagnetic wave – horizontal polarisation.

When the planes containing the electric and magnetic fields are fixed in space, the wave is said to be plane polarised. With radio waves, the plane containing the electric field is conventionally referred to as the plane of polarisation. An aerial with horizontal dipole elements will produce an electric field in the horizontal (as in the case of Figure 1.) and the radiated wave is said to have horizontal polarisation. Almost all radar systems are horizontally polarised. Some communications systems employ vertical polarisation. Circular (or more generally, elliptical) polarisation occurs when the plane of polarisation rotates in space about the axis of propagation at the frequency of the EM wave. Circular polarisation of the signal is sometimes used by radar systems to reduce the level of clutter produced by precipitation.

2. Types of Transmission

Radar systems employ two types of energy transmission: Pulse and Continuous wave (CW). Pulsed radar transmits radio frequency energy in a series of pulses, separated by non-transmission intervals, also known as rest time. Target echoes are processed during these rest times. CW radar sends out a continuous signal with a separate receiver capturing the returns. CW radar processes moving target information by analyzing the Doppler shift of the return echoes. Pulse radar is used primarily for detection and track, whereas CW radars are typically used for fire-control purposes. In the Wallops Island experimental procedure, CW provided the best means to map the propagation path. Since ducting conditions are wavelength (frequency) dependant, not pulse or shape-dependant, the CW results can be extrapolated to pulse systems.

3. Frequency and Wavelength

Radio waves occupy the lower part of the electromagnetic spectrum, extending from 300 GHz to below 3kHz, corresponding to wavelengths from 0.1cm to 100km respectively. In view of this wide range of frequencies (8 decades), it is not surprising that radio waves exhibit different properties in the way they propagate in, and interact with, the atmosphere and Earth's surface. Different technologies are also required for their generation and detection. It is convenient to subdivide the radio spectrum into frequency bands, each covering a decade in frequency; within each band, the radio waves exhibit broadly similar characteristics. Figure 2 illustrates the standard radio wave band nomenclature. In most instances it is most common to reference radio waves in terms of frequency.

An alternative, finer subdivision of the electromagnetic spectrum is commonly used for radar systems. Each band has a single, NATO agreed, letter designator, as give in Table 1.

Commercial radar and communications systems generally use different waveband designators (Table 2). These designators were at one time also used within the RN.

This study concentrates of two frequencies, 3.7 GHz, and 9.1 GHz, which equate to F and I band in the NATO nomenclature or S and X in the civilian. S (E/F) band radar

is predominately used for air search, whereas X (I/J) band is used for surface search, fire control and navigation/air traffic control purposes. I band radar is also used by the RN in their Airborne Early Warning (AEW) Sea King AEW 7 aircraft.

Waveband	Frequency Range
A	0 –250 MHz
B	250-500
C	500-1000
D	1-2 GHz
E	2-3
F	3-4
G	4-6
H	6-8
I	8-10
J	10-20
K	20-40
L	40-60
M	60-100

Table 1 Military radar frequency band designators

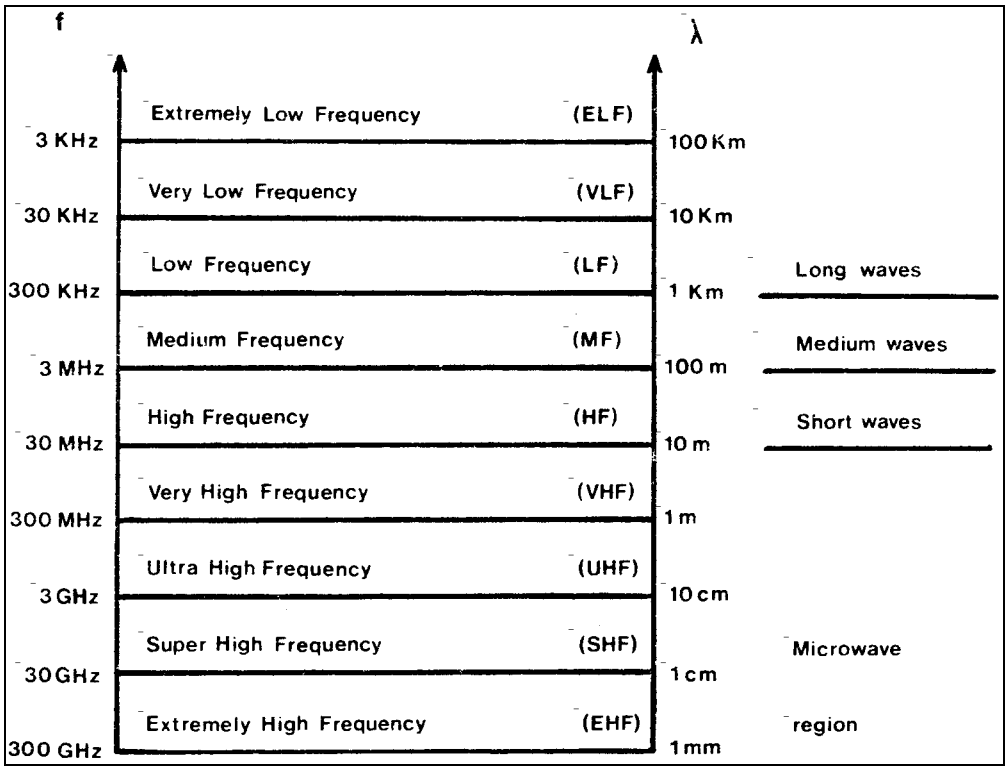

Figure 2. Radio wave band nomenclature.

Waveband	Frequency Range
L	1-2 GHz
S	2-4
C	4-8
X	8-12
Ku	12-18
K	18-27
Ka	27-40

Table 2 Civil radar and communications frequency band designators

B. RADAR PERFORMANCE FACTORS

A number of different factors may affect the performance of a radar system. The main ones are carrier frequency (f), pulse shape, pulse width and pulse repetition frequency, the power relation (peak to average power), beamwidth, and scan rate. The values of each of these for any given system will depend upon the use, accuracy, range, practical size limitations and generation of and receipt of the signal.

1. Signal-to-Noise Ratio

Radar antennae transmit powerful pulses of EM energy, but only a small fraction of this will be incident on a distant target. The return energy from this target will then be reflected over a wide angle and thus, only a very small percentage of the transmitted energy will return to the radar antennae.

The absolute lower limit of the sensitivity of a radar receiver is determined by a phenomenon called noise. Noise consists of any unwanted voltage inputs to the receiver that may ultimately obscure a weak return signal. Noise may be generated by a number of sources, ranging from atmospheric disturbances to deliberate attempts made by and opposing force to saturate or jam the return echo. These effects are generally transitory in nature, and system performance is actually determined by the self-noise generated within the radar circuitry itself.

The threshold level of a system, the level, which must be exceeded for a signal to be registered, can be manually or automatically set within the radar. Noise signals vary markedly in practice and a typical pattern is shown in Fig. 3. If a threshold level is set too high to allow noise signals to register, the sensitivity of the radar will be considerably reduced. If the threshold is set too low, then many false indications will register, and in this case the noise signals will complicate the picture to the detriment of detecting the actual target of interest. In this case, late or missed detections are likely as both operator and processor will be overwhelmed with many false targets, and the elimination of these. This effect, or property, of the radar will be very difficult to determine when propagation becomes enhanced. In such a case, a compromise has to be made by adjusting the radar system, either manually or automatically, according to the specific conditions encountered. The threshold level can then set the false-alarm rate of the radar.

2. Receiver Sensitivity

The sensitivity of a radar system is a dominant term of the radar range equation. Equation 1 describes the relationship between the receiver sensitivity and the smallest discernable signal (S_{min}):

$$sensitivity(dbm) = 10\log_{10}\left[\frac{S_{\min}}{1milliwatt}\right] \qquad \text{Eqn. III-1}$$

3. Pulse Width

The width of the pulse will determine the range resolution of the radar, the maximum and minimum detection ranges. Pulse width will determine the length of the propagating pulse within the medium. The range resolution is found using the radar range formula:

$$range = \frac{ct}{2} \qquad \text{Eqn III-2}$$

In this equation (c) is the speed of light, and (t) is the pulse width. In Fig 4, two targets are less than the range resolution apart. The leading edge of the pulse will be striking the farthest target, whilst the trailing edge of the pulse is approaching the closest target. As the two pulses return to the radar, the leading edge of pulse B is hidden in pulse A and thus only one target would be detected.

The foregoing discussion suggests that narrow pulse is desirable, but is not always the case. For detection to occur, a target must return an echo that is strong enough to be indicated on the scope or plan position indicator (PPI). The energy in the returned echo may be increased by increasing the peak-transmitted power or by increasing the pulse width. Increasing the pulse width is the more practical of the two options, as increasing peak power will increase the weight, cost and energy requirements of the radar.

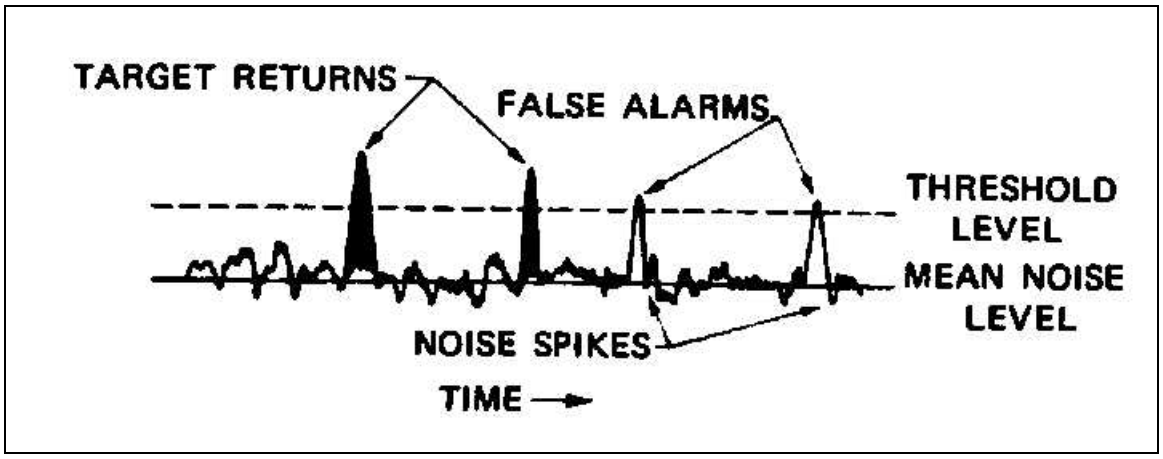

Figure 3. Schematic representation of received radar signals with noise (from Frieden, 1985).

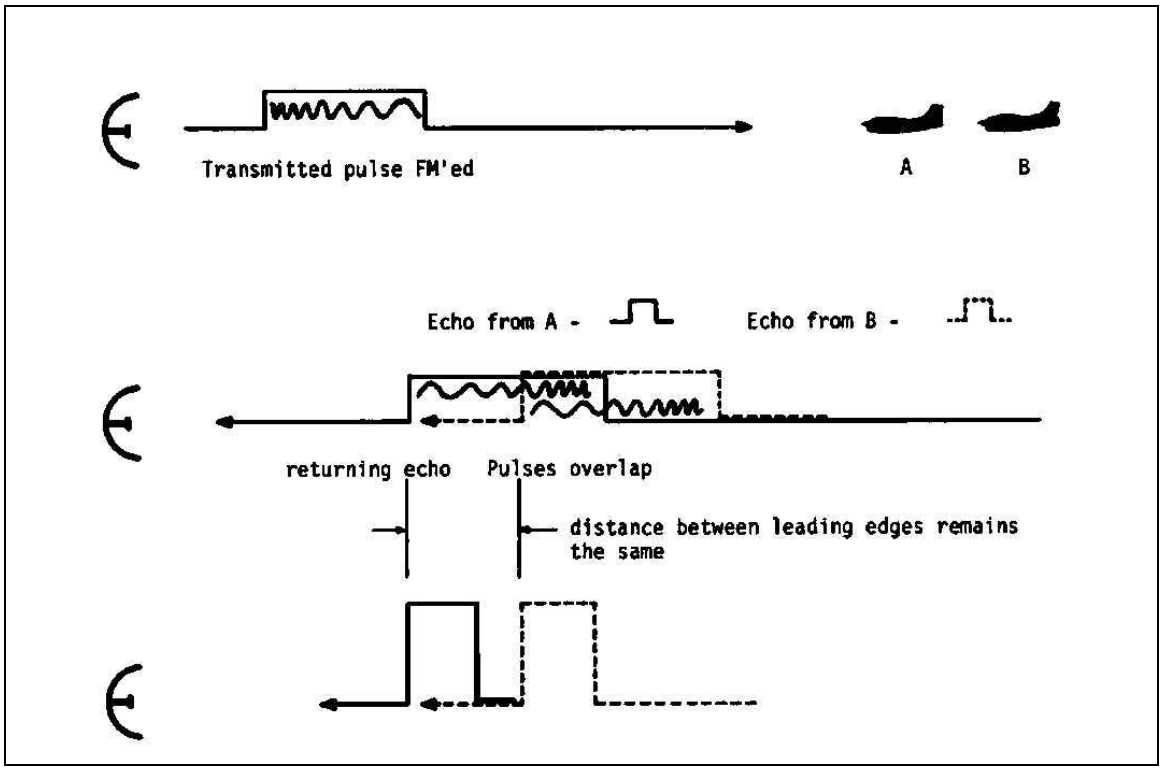

Figure 4. Effects of pulse width on target resolution (from Frieden, 1985).

4. Carrier Frequency

The selection of an appropriate carrier frequency is dependant upon several factors, including the directivity and resolution desired, and the existing design limitations on electronic equipment.

For quasi-optical antenna systems, the higher the frequency, the shorter the wavelength and therefore the smaller the antenna required. Conversely, for an antenna of fixed dimensions, using higher frequencies will increase the directivity. Higher frequencies will also provide increased target resolution and enable the detection of smaller sized targets because of the shorter wavelength.

The disadvantages of high frequencies include greater propagation loss and inherent difficulties of generating and amplifying the RF energy. The greater resolution provided by the higher frequency also creates greater sea-clutter and backscatter. The operator is then presented with a major difficulty since the higher frequency radar will better couple with lower duct heights, whilst simultaneously aggravating the clutter and false alarm problem.

5. Antenna Gain

The gain of a radar system is a very important property. It is a measure of the ability of an antenna to concentrate energy in a particular direction. Two different but related definitions of antenna gain are the *directive gain*, (or *directivity*), and the *power gain* (simply *gain*).

a. Directive Gain

The directive gain of a transmitting antenna (G_D) is the ratio of the maximum radiation intensity versus average radiation intensity, where the radiation intensity is the power unit solid angle radiated in the direction (θ,φ) and is denoted $P(\theta,\varphi)$.

The directive gain and the beam-width are closely related. If θ_B and φ_B are the azimuth and elevation angle half-power beam-widths, then Eqn III-3 gives the relationship:

$$G_D = \frac{4\pi}{\theta_B \times \varphi_B} \qquad \text{Eqn. III-3}$$

b. Power Gain

The definition of directive gain is based primarily on the shape of the pattern of radiative transmission. The power gain (G) includes the effects of antenna losses and any other loss that lowers the antenna efficiency. The power gain is defined by the ratio of the maximum radiation intensity from an antenna of interest versus the radiation intensity from an omni-directional source with same power input.

6. Antenna Aperture

A secondary effect of antenna design is its effectiveness as a collector of energy. The amount of power available to the receiver is a function of the energy density of the returning echo and the effective area of the antenna. The antenna effective area or aperture (A_e) is related to the carrier frequency of the radar, the construction of the antenna, and the antenna physical size. The difference between the physical area of the antenna and A_e is a measure of its efficiency as given in Eqn III-4:

$$A_e = \rho_a A \qquad \text{Eqn. III-4}$$

The power gain and antenna aperture are related by Eqn III-5:

$$G = \frac{4\pi A_e}{\lambda^2} \qquad \text{Eqn III-5}$$

C. THE SIMPLIFIED RADAR RANGE EQUATION

Several of the aforementioned factors affecting radar performance are combined to develop the basic radar range equation.

If the peak power output of a radar transmitter (P_t) radiates uniformly in all directions, the power density (power per unit area) at any distance (R) from the radar can be determined by dividing the transmitted power by the surface area of an imaginary sphere of radius R as shown in Eqn III-6.

$$PD_{omni} = \frac{P_t}{4\pi R^2} \qquad \text{Eqn III-6}$$

Similarly, the power density of a directional antenna is related to P_t by the power gain as shown in Eqn III-7.

$$PD_{directional} = \frac{P_t G}{4\pi R^2} \qquad \text{Eqn III-7}$$

The above relationship defines the power that reaches a target at distance R from the radar. The power reflected by the target is a function of the radar cross section of the target (σ) as shown by Eqn III-8.

$$P_{target} = \frac{P_t G \sigma}{4\pi R^2} \qquad \text{Eqn III-8}$$

The power returning to the radar is again a function of the surface area of a sphere of radius R shown in Eqn III-9.

$$P_{echo} = \frac{P_t G \sigma}{\left(4\pi R^2\right)^2} \qquad \text{Eqn III-9}$$

Finally, only the antenna captures only a portion of the returned echo power. Given the effective area of the antenna (A_e), then the echo power, (P_r), received at the radar is given by Eqn. (III-10):

$$P_r = \frac{P_t G A_e \sigma}{\left(4\pi R^2\right)^2} \qquad \text{Eqn III-10}$$

If the smallest magnitude of echo power that the receiver resolves from the input noise (S_{min}) is equated to P_r, then the maximum range of the RADAR is found by solving Eqn III-11 and Eqn III-12.

$$S_{\min} = \frac{P_t G A_e \sigma}{\left(4\pi R^2\right)^2} \qquad \text{Eqn III-11}$$

$$R_{\max} = \left[\frac{G \sigma A_e P_t}{\left(4\pi R^2\right)^2 S_{\min}}\right] \qquad \text{Eqn III-12}$$

IV. METEOROLOGY OF RADIOWAVE PROPAGATION

A. INTRODUCTION

In this chapter the meteorological and ocean surface factors that are known to affect radio wave propagation will be considered. Conditions that lead to a phenomenon referred to as ducting are of primary interest, as these have the greatest effect on the coverage of radar and communications systems. The initial discussion will be based on the meteorological mechanisms that lead to ducting (and super-refraction), rather than on the type of duct formed (surface duct, elevated, or elevated layer surface duct). It is important to note, however, that is the duct type (classified on the basis of refractive index profile), rather than the originating meteorological mechanism that is important in terms of operational effects (these effects will be dealt with in Chapter V).

1. Refractivity

Refraction modifies the direction of propagation of a wave-front. A ray describes the wave-front propagation direction and is normal to the wave-front. Refraction is described by the index of refraction, (n), and defined by the ratio of wave speed in free space (c) to wave speed in the medium (v), Eqn. (IV-1). EM rays bend toward regions of slower wave propagation speeds or higher n. Gradients in the index of refraction across the propagation path cause refraction, or ray curvature, effects. For most conditions, the responsible gradient of the index of refraction affecting operations is that occurring in the vertical (dn/dz), where z is height.

Since the normal value of n for the atmosphere is close to unity, a more convenient and useful index-of-refraction is used, refractivity N. Eqn. (IV-2) is the relationship between the index-of-refraction (n) and the refractivity (N). For microwave frequencies and below, Eqn. (IV-3) (Bean and Dutton, 1968) relates N to the routinely measured atmospheric variables of absolute temperature (T), partial pressure of water vapor (e) and total atmospheric pressure (P) where T is in degrees Kelvin, and P and e are in millibars (mb).

$$n = \frac{c}{v} \qquad \text{Eqn IV-1}$$

$$N = (n-1)\times 10^6 \qquad \text{Eqn IV-2}$$

$$N = 77.6\frac{P}{T} - 5.6\frac{e}{T} + 3.73\times 10^5 \frac{e}{T^2} \qquad \text{Eqn IV-3}$$

Most applications of EM refractivity consider propagation between two points on earth where the earth's curvature is important. A useful parameter is modified refractivity (M) which is the refractivity corrected for the gradient that would cause the ray to propagate parallel to the earth's surface. This refractivity gradient is approximately –0.1568m^{-1}. Eqn. IV-4 is the expression for M where (r_e) is the earth's radius (6.378×10^6m) and (z) is the height above the surface in meters.

$$M = N + \frac{z}{r_e \times 10^{-6}} = N + 0.1568z \qquad \text{Eqn IV-4}$$

In a standard atmosphere (Bean and Dutton, 1968), the refractivity decreases with height. In most situations, the behavior of the M profile is more complicated. The vertical gradients of N or M (dN/dz or dM/dz) define the four general refractive categories shown in Fig 3. Radar propagation is determined by the vertical gradient of M (dM/dz) rather than by its absolute value. When $dM/dz=0$, the EM ray curvature is equal to the earth's surface; when $dM/dz>0$, EM rays curve away from the earth's surface; when $dM/dz<0$, EM rays curve downward toward the earth's surface. If a negative dM/dz layer extends to the surface, then EM rays are trapped between the surface and the top of the layer, a phenomenon known as a surface duct, which significantly affects surface-based transmitters. The propagation conditions illustrated in Figure 5, describe the general effect of dM/dz.

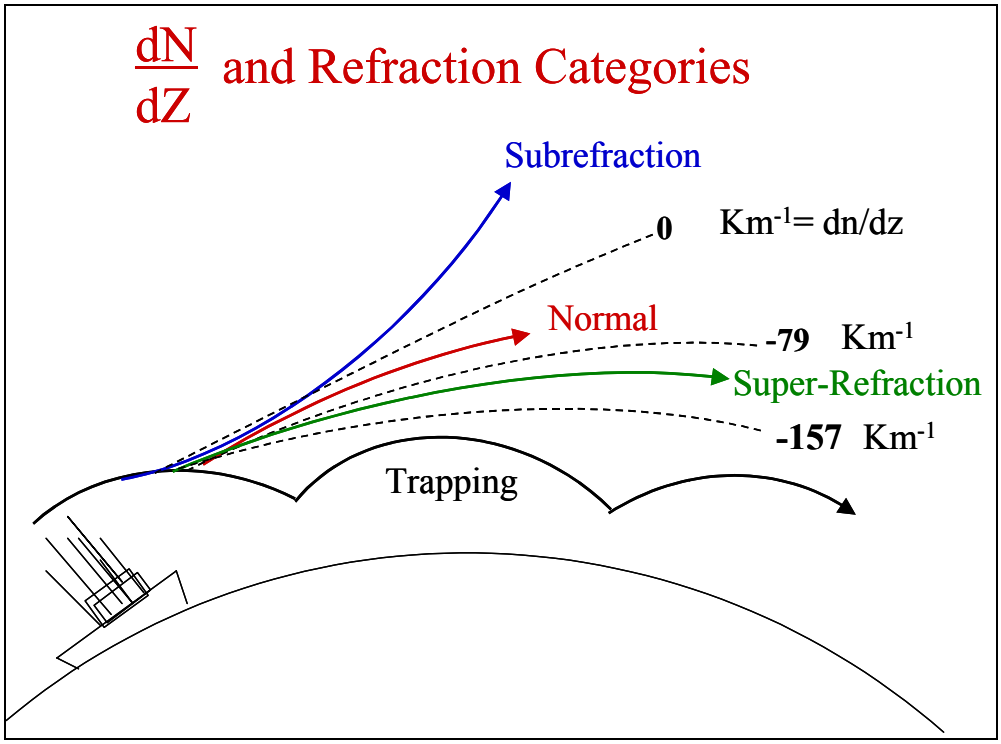

Figure 5. Refraction Categories

Standard refraction is related to a well-mixed atmosphere in which the pressure, temperature and water vapour content of the air decrease steadily with height. The rate of decrease of pressure with height varies little with height, so that variations in the refractive index profile, compared with that under standard refraction, must result from a temperature and/or a humidity structure that differs from that in a simple well-mixed atmosphere. In general it can be stated that:

- On any particular occasion both the temperature lapse and the hydrolapse (a rapid change in moisture content with height) must be taken into account; however,
- The hydrolapse generally plays a more important role than the temperature lapse.

2. Ducting and Super-Refraction

Ducting and super-refraction require a decrease in refractivity with height at a rate greater than in the standard atmosphere, from Eqn IV-4, this will be satisfied by either (or both):

- A lapse rate of temperature *less* than standard, or an *increase* in temperature with height.
- A hydrolapse *greater* than standard.

In practical terms:

- A steep hydrolapse (i.e. a sharp drying out with height) favours super-refraction or a duct: a weak hydrolapse normally leads to standard refraction at best.
- A temperature inversion (i.e. an increase of temperature with height) favours super-refraction or a duct; a temperature inversion without a strong hydrolapse seldom results in duct, except at low temperatures.
- A combination of *both* a steep hydrolapse *and* a temperature inversion provides the ideal conditions for duct formation.
- A strong lapse rate of temperature (such as occurs adjacent to the surface under convective conditions) opposes super-refraction or duct formation, but if the hydrolapse is intense, the effect of the hydrolapse can override the temperature lapse and a duct can form.

3. Sub-Refraction

Sub-refraction requires an increase in refractivity with height (or at least a decrease at a rate less than in the standard atmosphere). This is satisfied by, either (or both):

- A lapse rate of temperature *greater* than standard.
- A hydrolapse *less* than standard, or an *increase* in moisture content with height.

In practical terms:

- An inversion of hydrolapse (i.e. an increase of moisture content with height), even if accompanied by a temperature inversion, will invariably lead to sub-refraction.

4. Formation of Ducting Conditions

As described in the previous section, IV A 2, ducting is associated with dry air overlying relatively moist air and is enhanced by the overlying air being warmer. The evaporation duct is the most widespread and persistent form of duct that is encountered in the maritime environment. It is caused by the extremely large hydrolapse that normally exists in the first few metres above the sea surface. This influence by water vapour gradients is generally strong enough to form a duct almost irrespective of the temperature lapse rate.

Differential advection and subsidence are two meteorological mechanisms that can lead to super-refraction and the formation of ducts. *Both* lead to a large hydrolapse *and* a temperature inversion that are normally required for a duct to exist. In coastal regions, the relative role of these two factors will play an important role in the type of duct formed, if any.

Although humidity decreases over a wet surface, advection and subsidence are the main features and mechanisms leading to ducting in the open-ocean, there are other causes of ducting that may be encountered. These tend to be more localized or of more limited duration. Nonetheless these factors can be important in certain instances, especially in the littoral zone. They are the sea breeze (a special case of advection), frontal and land effects.

Apart from refraction there are other influences on radio wave propagation of which are important to be aware of but will not be addressed in field test results in this thesis. In particular, the effects of rain and atmospheric gases become important at the higher microwave and millimetre wave frequencies, and can result in a reduction of communication or detection range. Radar backscatter from rain also gives rise to clutter.

During the Wallops Island 2000 precipitation effects can be largely discounted as can the effects of absorption by atmospheric gases, all the other mechanisms described, however, play a measurable and major role in the refractivity at one time or another during the field test. Each of these features and/or mechanisms will be addressed separately in the following sections.

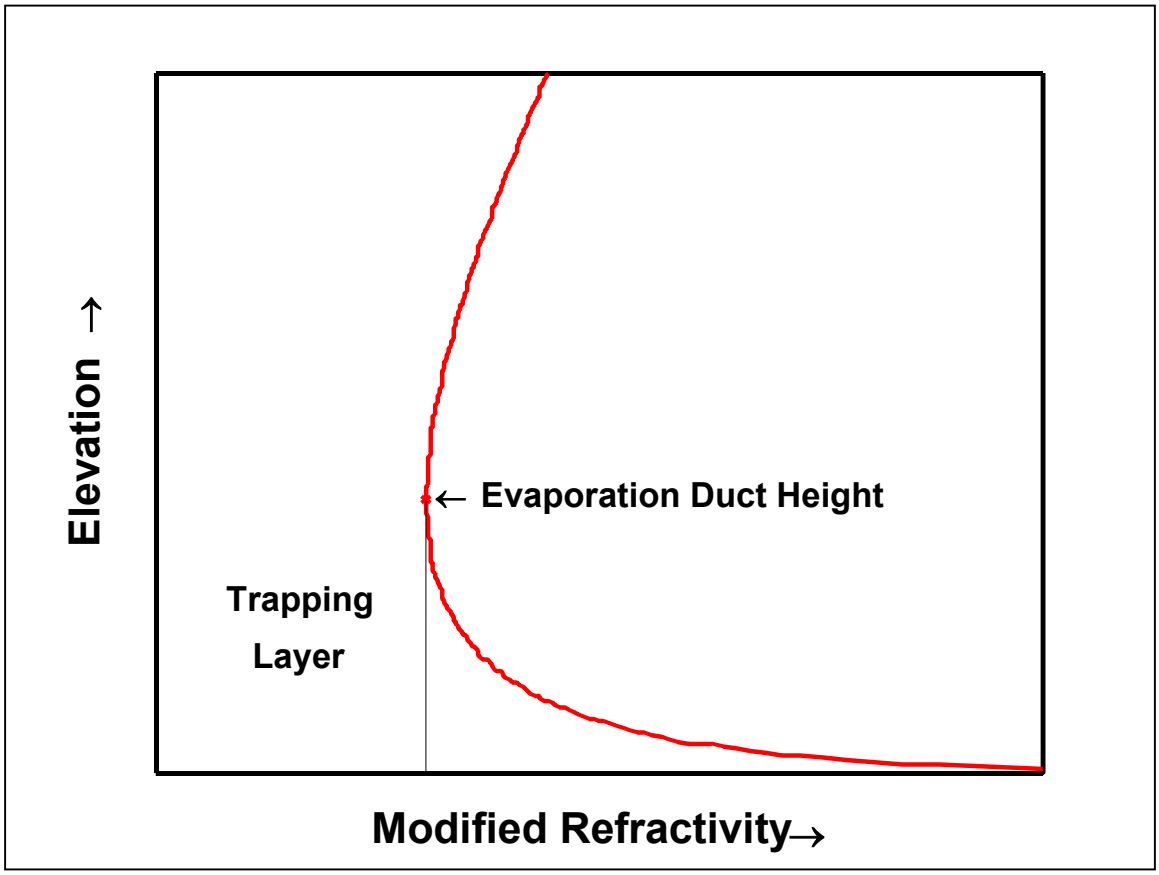

Figure 6. Schematic plot of a typical vertical modified refractivity profile with corresponding evaporation duct height and trapping layer (from Frederickson *et al* 2000b)

B. THE EVAPORATION DUCT

A trapping layer requires the air temperature to increase with height and/or humidity to decrease with height. Above the ocean, these conditions exist almost permanently producing the evaporation duct.

An *M* profile leading to a typical evaporation duct situation is illustrated in Figure 6. The top of the trapping layer, where d*M*/d*z*=0, is referred to as the 'evaporation duct height'. Since d*M*/d*z*<0 below this level, it is the 1st level level of the minimum value of *M above the surface*. Further, it is not a distinct level since dM/dz ~ 0. The evaporation duct approximates a wave-guide refracting (upper) and reflecting (lower) boundaries.

Such a wave-guide will cause EM waves to propagate over the ocean surface for much greater distances than expected, over the geographic horizon. For this reason it is obvious that information on the presence and properties of the evaporation duct is critical to properly assess EM propagation conditions near the ocean surface.

The evaporation duct is the most common cause of anomalous propagation on ship-based radar and communication systems in the open ocean situation away from the influence of the coast. Even in coastal situations it is often the dominant mechanism, except when localized coastal advection, or sea-breeze effects, become important. Because of this, much effort has gone into understanding the evaporation duct. There are well established boundary layer models based on the similarity theory of turbulence: these enable the evaporation duct height to be estimated from a bulk measurement of sea temperature, and the dry and wet bulb air temperatures and wind velocity measured several feet above the surface. A detailed analysis of these models is undertaken in Chapter VI, but the basic premise is that the level of turbulence is principally a function of two parameters:

- The wind speed.
- The temperature difference between the sea and the overlying air.

The most common situation is an unstable boundary layer. In broad terms, this occurs when the temperature of the sea is higher than that of the air. The temperature lapse is usually much in excess of that in a standard atmosphere, which on its own would produce sub-refraction, but the effect is outweighed by the strong hydrolapse. When the air temperature is higher than that of the sea, the boundary layer is stable, and this can give rise to large duct widths (30m or more).

C. SURFACE-BASED DUCT

Whereas the evaporative duct is formed by the strong, negative humidity gradient immediately above the ocean surface, the surface-based duct tends to be the result of synoptic weather conditions favorable for the creation of larger than normal gradients some distance above the surface, i.e. elevated trapping layer. The feature associated with the surface based duct is referred to as the temperature inversion. The direct causes of duct or temperature inversion formation or temperature inversion, strong temperature and

humidity gradients, are the result of: a) subsidence or differential advection and b) boundary-layer mixing. Figure 7, illustrates profiles of M versus height, for evaporation, surface based and elevated ducts.

1. Marine Layer Temperature Inversions

A marine layer capped by an inversion is a common feature of the atmospheric marine boundary layer. The increase in the temperature with height due to subsidence aloft with mixing immediately above the surface can be large enough that the temperature actually increases with height, creating an inversion. Temperature decreases from –0.6^{o}C to near 1^{o}C per 100 meters with in the standard atmosphere (with no inversion). The inversion region is hydrostatically stable because of the temperature increase so mixing or overturning of the air column does not occur. Because of the subsidence of dry air above and well-mixed marine (moist) layer below, the temperature inversion coincides with a region of rapid decrease in humidity. Therefore, inversion formation over the sea is conductive to duct formation because of its associated positive temperature gradient and large negative humidity gradient.

2. Subsidence or Differential Advection

Downward vertical motion, called subsidence, acts to produce the positive temperature gradients and more negative humidity gradients and thus promotes duct formation (see Figure 8). Downward moving air, as often found in and near surface high-pressure regions and immediately behind cold fronts, conserves its moisture content during descent, but warms due to adiabatic (compression) heating. The resulting air has a higher temperature, and thus by definition, lower relative humidity following descent. This downward vertical velocity achieves it's maximum at some distance above the surface, since the vertical velocity of the air parcel must be zero at the surface. (The parcel cannot penetrate the ground.). Both the increase in temperature and decrease in relative humidity enhance duct formation by decreasing dM/dz. The same end result of dry warm air over relatively cool moist air can be achieved with upper level horizontal advection as would occur in synoptic scale circulations or in local land-sea circulations where the flow aloft is from land to sea. This is referred as differential advection.

3. Boundary-Layer Mixing

Turbulence generated at the earth's surface creates a 'boundary-layer' capped by a region of enhanced temperature and humidity gradients at its top (see Figure 7). The region of strong gradients separates the underlying well-mixed layer from the overlying non-turbulent regions. This often creates the strong gradients associated with a trapping layer near the top of the boundary layer. The top of the trapping layer is also the top of a duct or wave-guide. The responsible turbulence is created by the surface in two ways:

(1) Thermally generated turbulence: Heating of the earth's surface heats the air immediately at in contact with the surface. This creates hot buoyant parcels of air that rise and mix the air above, thereby creating turbulence.

(2) Wind generated (or mechanical) turbulence: The requirement that the wind velocity must be zero at the surface creates a gradient in wind speed close to the surface, thereby creating turbulence.

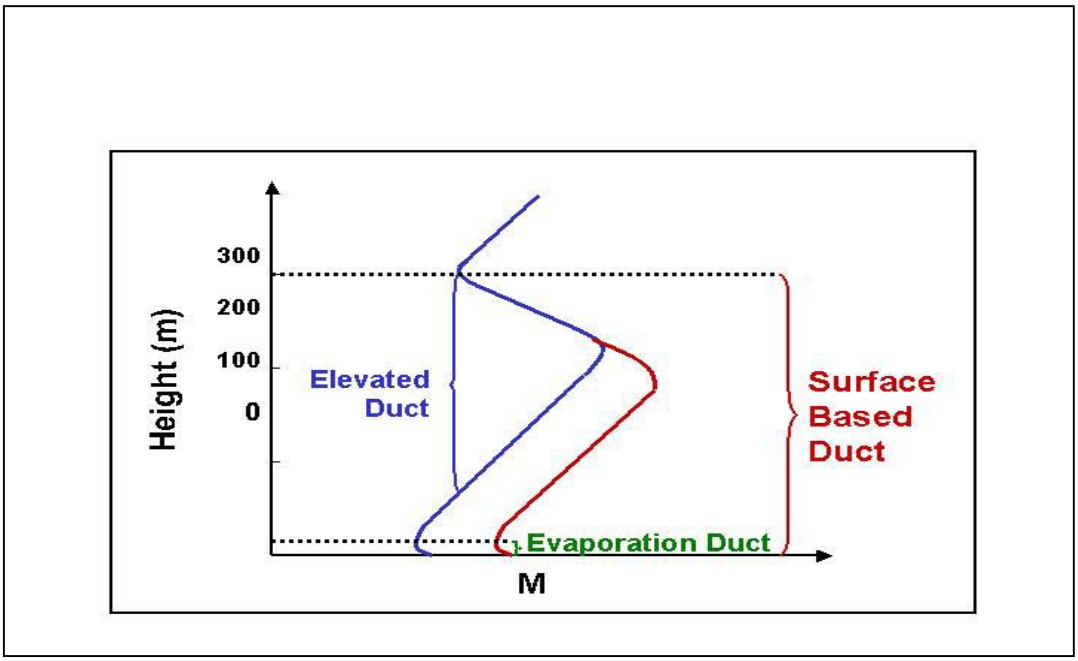

Figure 7. Graph of M versus height, demonstrating example profiles for evaporation, surface based and elevated ducts.

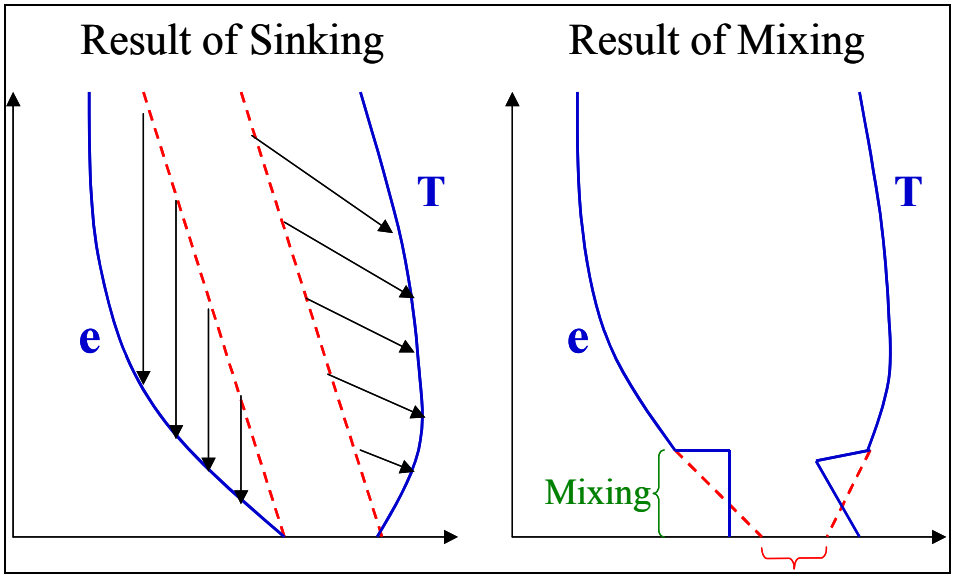

Figure 8. Types of inversions: (a) subsidence reaching the surface, (b) subsidence above a mixed layer.

V. OPERATIONAL ASPECTS OF NON-STANDARD PROPAGATION

A. INTRODUCTION

The operational (tactical) effects of non-standard propagation depend upon several factors. The presence of ducting or other refractive conditions is clearly of primary importance. However, operational assessment must also take into account the capabilities of the radar, communications, or electromagnetic spectrum surveillance system. Because operational application is an objective of this thesis, this chapter describes in general terms the operational effects of each type of duct.

An accurate tactical assessment ideally requires the use of a propagation assessment tool (such as EEMS or AREPS), particularly if the meteorological environment is complex.

For simplicity, the discussion will highlight the important features of individual ducts. It is important to bear in mind that multiple ducts will often occur simultaneously:

- In stable conditions, or near the coast, a surface based duct due to subsidence or advection is likely to occur in conjunction with the evaporation duct. Since this is likely to be stronger, and will certainly be deeper, than the evaporation duct it will dominate, and thus tactical advice must be based on the surface duct conditions.
- Surface and elevated ducts may occur simultaneously. In this case the tactical advice will depend on whether a surface or airborne platform is under consideration.

The occurrence of significant multiple ducts, makes the use of an accurate propagation assessment tool vital for tactically significant forecasts.

B. SYSTEM CONSIDERATIONS

The tactical importance of ducting cannot be assessed without considering the configuration and capabilities of the system under evaluation.

1. Transmitter/Target Height

The most obvious factor is the height of the transmitter relative to the duct. To obtain full reception/detection capability of a duct, the transmitter and receiver/target should be situated within the duct. Thus the evaporation duct has most influence on surface-to-surface paths whilst an airborne (AEW) system will obtain greatest detection ranges in an elevated duct; however, surface ducts can adversely affect AEW systems due to the occurrence of radar holes.

2. Frequency

The depth of a duct, (i.e. evaporative or surface-based duct), determines the range of frequencies that are trapped by the duct. This frequency dependence is a critical factor in evaluating the ducting condition. Eqn (V-1) is an approximation for the minimum trapped frequency (f_{min}) by a duct of depth (d):

$$f_{\min} = \left(\frac{3.6 \times 10^{11} Hz}{meters^{-3/2}} \right) d^{-3/2} \qquad \text{Eqn V-1}$$

Waveband	Frequency	Wavelength	Minimum Duct Width (m)
VHF	200 MHz	1.5m	140
	300 MHz	1m	110
UHF	400 MHz	70cm	85
	1.5 GHz	20cm	37
	3 GHz	10cm	23
SHF	4 GHz	7cm	18
	10 GHz	3cm	10

Table 3 Guideline minimum surface duct width for trapping.

Duct versus trapped frequency relationships, shown in Table 3, indicate that the typical evaporative duct of 10-20m depth will not appreciably affect the 2-4Ghz (E/F band) search frequencies used by most three dimensional air-search radars. Long- range two-dimensional radars that operate at frequencies below 1Ghz (C band) will not experience ducting effects until the duct depth exceeds 40 meters. Only the highest frequency radars (I/J band), which are associated with surface-search, fire-control radars and missile-seeker illumination, truly benefit from the typical 10-15m evaporative ducts found in most coastal and open ocean regions.

Note also:

- That the trapping efficiency of a duct of a given width increases as the strength of the duct increase i.e. with increasing M-deficit in the ducting layer.
- That the corollary to stronger trapping within a stronger duct is that there will be a reduction in the amount of energy that is propagated outside it. When pronounced, this can lead to a radio or radar hole immediately above the duct.

3. Reciprocity "Failure"

Although the principle of reciprocity always holds (i.e. the path loss between points A and B is the same as that between points B and A), system considerations may result in an apparent "failure" of reciprocity in the presence of ducting. Consider a case of an AEW helicopter using a narrow beamwidth radar against a surface vessel. If the surface vessel is using an electronic support measures (ESM) receiver with a relatively wide beam width aerial, the detection probabilities of the helicopter and the ship could be affected very differently by the presence of ducting (a narrower beam will couple more energy into the duct than the wider beam). Thus, it is not safe to assume that because an adversary can detect your ship, then your systems will be able to detect him, even if this is the case under standard atmospheric conditions.

C. ASPECTS OF EVAPORATION DUCTS

The average evaporation duct is so shallow as to lie well below the level at which most communication and radar aerials are situated in ships. Nevertheless, coupling of energy into the duct does take place. The effect on system performance depends on frequency, but with EM systems operating above 3 GHz (wavelength less than 10cm), surface detection ranges and detection ranges versus very low flying aircraft and missiles can be increased significantly beyond that under standard refraction.

For a given height of evaporation duct, range enhancement will not only depend on the height of the aerial with respect to the duct, but will also increase with increasing frequency of the transmission, and for a given frequency it will increase with increasing thickness of the duct. At the same time, the distance at which transmissions can be intercepted will generally be increased.

Transmissions, within the UHF wave-band frequency, are rarely affected by the nature of the evaporation duct. However, if the duct is well developed some extension in surface coverage is possible, but only with transmissions greater than 1 GHz .

Navigational radar is not particularly sensitive to the evaporation duct because of the relatively low powers and fairly high system detection thresholds involved.

For a submarine at periscope depth, the aerials will normally be located within the evaporation duct. This will increase the effectiveness of the duct in extending the horizontal coverage of centimetric transmissions. Except in fog or drizzle (normally indicative of sub-refraction) or in heavy precipitation (resulting in pronounced signal attenuation), submarine surface search ranges will therefore be greatly increased compared with those resulting from simple radio sight considerations, and depending upon the height of the evaporation duct, complete trapping could occur. Although this would suggest increased ESM intercept range against the submarine, it need not be necessarily so. If the top of the duct is below the height of the ESM receiver, the signal received could be extremely weak; if the transmission is confined to a single sweep, it might even be missed. This is an example of “reciprocity failure” whereby a submarine may be able to detect a surface vessel while an ESM receiver on board the vessel may me unable to detect the submarine’s emissions.

D. ASPECTS OF SURFACE BASED DUCT

Because trapping of energy in a duct is strongest for a transmitter in the duct, a surface duct is of greatest significance for surface-based systems. The main effect for surface-to-surface paths is range enhancement, which can be very significant. Surface-to-air paths will suffer from radar holes. The effect on airborne systems will depend on the heights of the transmitter and target relative to the duct.

Surface ducts have broadly similar propagation characteristics whether they are caused by surface-based layers (advection, including sea breeze fronts), or by elevated layers (subsidence inversions). The principle differences between surface ducts caused by surface layers and by elevated layers are:

- For an elevated layer to produce a surface duct, it must be much stronger than is required of a surface advection layer (weaker elevated layers will give rise to elevated ducts or super-refracting layers). Because the layer height (and therefore the duct width) will generally be much larger than that of surface layers, trapping of EM waves will be stronger. Indeed, elevated layer, surface ducts will often trap all frequencies with which we are concerned, operationally.
- Elevated layer, surface ducts will be accompanied by "skip-distance effects". For surface-to-surface transmissions this can lead to a "blind zone" between the normal radio horizon and the range at which ducted signals return to the surface. This blind zone does not occur for surface layer, surface ducts.

1. Surface-Based Systems

a. Range Enhancement

Surface ducts have the potential to produce greatly extended communication and detection ranges when both transmitter and receiver/target are within the duct. Even the shallower surface ducts are likely to extend to a height above most ship's aerials and will lead to complete trapping of all SHF (centrimetric) transmissions, particularly at the higher frequencies. The enhancement will increase with increasing frequency of transmission. Multiple-time-around radar echoes are likely if the duct extends far enough.

Range enhancement for a surface-based radar will not necessarily increase with increasing duct width:

- Higher layers (particularly elevated layers) are generally weaker, giving rise to weaker trapping.
- Energy leaving a transmitter at a given elevation angle will arrive at a higher layer with a greater angle of incidence (due to the Earth's curvature), and is therefore less likely to be trapped.

Both of these effects will reduce the amount of energy that can be propagated forwards in the duct. Clearly, ranges achieved will be highly dependent on the power of transmission.

In the case of advection and sea-breeze ducts:

- Range enhancement will be most pronounced in directions parallel to the coast.
- The likelihood of diurnal variation in duct activity (maximum intensity during the afternoon and evening) should be borne in mind.
- In lower latitudes, with strong sea breeze effects, the resulting ducts may be several hundred feet deep, resulting in complete trapping of surface based SHF and UHF transmissions, possibly even affecting the VHF waveband.

b. ESM/ECM

ESM intercept ranges on surface-to-surface paths will be greatly extended, as will the range at which electronic countermeasures (ECM) can be effective. Trapping of UHF transmissions is possible, particularly on the higher part of the frequency range, and for lower aerial heights.

c. UHF Communications

Effective UHF communications between a ship and another ship or low flying aircraft is normally dictated by standard radio horizon considerations. In the presence of strong ducts, UHF communications ranges can be greatly extended when compared to normal conditions. This can allow a wider dispersal of a force or a helicopter to maintain radio contact at extended ranges when flying at low levels. One disadvantage of this effect is the increased level of interference.

d. EMCON Policy

The presence of a surface duct is a vital consideration in deciding emission control (EMCON) policy. Although surface ranges would be greatly extended so would intercept distance(s) by any adversary. The following should be noted:

- Even low power sources such as flight deck communications have been intercepted at quite extreme ranges under conditions of severe ducting.
- In deciding whether to break or maintain radio silence, it should be remembered that, in general, if a target can be detected, it will also probably be capable of detecting own ship emissions. It may be, therefore, that a passive policy is the one to be preferred.
- If an active transmission policy is elected, then RADAR transmissions should be confined to the lower frequency A and B band systems. These will be less prone to trapping than the higher frequencies.

Much will depend on whether a significant surface duct is present. Unfortunately positive identification of the deeper surface ducts and their dimensions, requires refractivity data. If this necessitates launching a radiosonde, this will in itself breaking radio silence.

e. RADAR Holes

Whenever range enhancement occurs in one direction, there must be an associated reduction in range capability in another direction, since the total power radiated by the radar or communication system is constant. In the case of a surface duct, this often manifests itself as a radar or radio hole in the region above the duct. Normally some energy will leak through the upper surface so that the region will not be completely "blind". However when the duct is strong, and the sea surface is relatively smooth, leakage from the duct may be minimal and radio/radar coverage will be very weak. It can be seen that the close an attacking aircraft flies to the top of the duct (but making sure not to be in it), the closer it can approach a force or unit with a much reduced chance of radar detection.

2. Airborne Systems

For AEW helicopters operating within the duct, detection ranges against surface targets and airborne targets within the duct will be greatly extended, but at the expense of targets above, where a reduction in detection ranges will occur.

For AEW helicopters operating above the duct, some extension in surface detection capability is still possible due to coupling of energy into the duct, although it will be, by no means as dramatic as that when operating in the duct. Range enhancement under these conditions will depend upon aircraft altitude. The amount of energy trapped will generally decrease with increasing altitude above the duct. This may mean that a target's transmissions will not be interceptible by airborne ESM when operating at altitudes above the duct. The roughness of the sea surface and its effect on the scattering of EM energy can influence this situation.

E. ASPECTS OF SKIP DISTANCE EFFECTS

A complicating factor that can arise with surface-to-surface transmissions within a duct produced by an elevated layer is that the surface coverage is not always continuous. Depending on the height of the layer, waves traversing the layer may not reach the Earth's surface within the maximum range of waves propagating directly along the surface. This will lead to a blind zone between the direct and indirect waves. Blind zones will not be apparent unless targets are known to be both within and beyond them at the same time, with only the more distant targets being detected. Figure 9 shows the skip distance effect.

By analogy with the corresponding ionospheric effect in the reception of medium and short radio waves, the distance between the transmitter and the nearest point at which an indirect wave reaches the surface may be described as the skip distance of the transmission. As a rule of thumb, the skip distance will approximate to one fiftieth of the height (in feet) in nautical miles (e.g. a 1500ft layer will give a skip distance of 30nm).

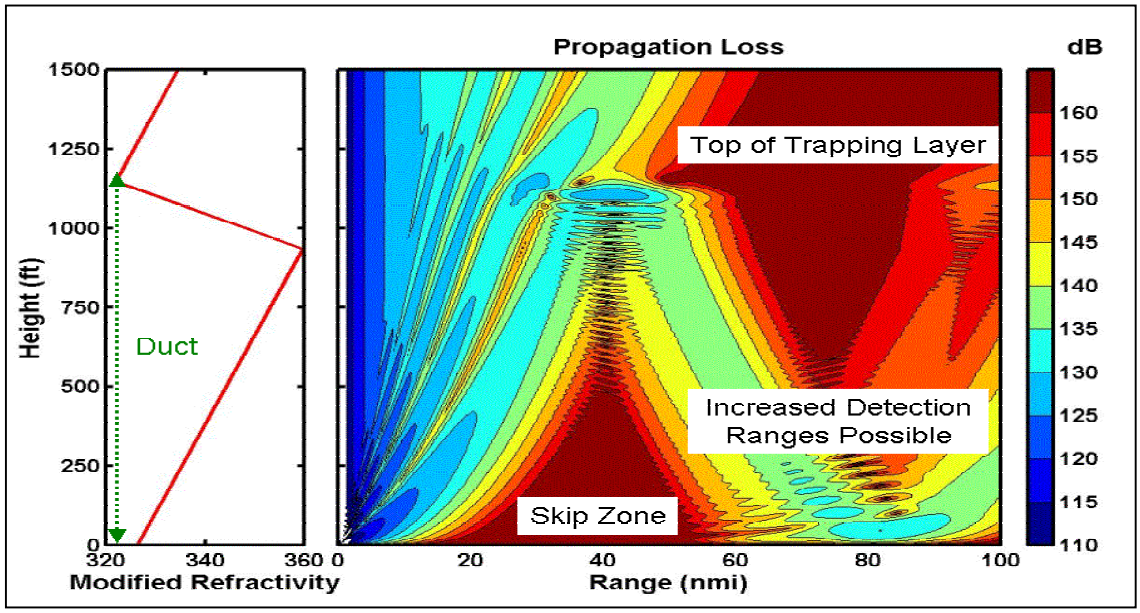

Figure 9. Skip distance effects.

Beyond the range at which the indirect wave first reaches the surface, enhanced detection capability will occur, but it will not be uniform with range. If the strength of a radar return falls below the system threshold for detection, further blind zones can occur. This can happen with surface ducts caused by surface as well as elevated layers. A predicted coverage feature is that the presence of an evaporation duct with the surface based duct will remove the 1st skip zone.

F. ASPECTS OF FADING

A characteristic feature of signal strength measurements under ducting conditions is that *while the signal maintains a high average level, it is often subject to frequent and sometimes quite intense “fading”. A radar echo from a target at long distance might therefore appear only intermittently. Fading results from:

- Destructive interference between signals arriving at the detector via two or more paths, known as multipath propagation.
- Spatial irregularities and temporal variation in the height and intensity of the ducting layer.

Multipath fading is caused by phase variations between the multiple paths that a signal takes through the atmosphere between a transmitter and receiver during ducting

conditions. The interference between these signals results in fading of the combined signal in an unpredictable fashion. One of the paths may involve a ground reflection in a similar manner to the mechanism that gives rise to the interference lobes seen in a coverage diagram. Phase variations in the atmosphere will cause the positions of the lobes to vary and can give rise to fading. Severe multipath fading is common on overland paths subject to ducting caused by nocturnal radiation inversions. The effect is particularly strong during the formation and break-up of the ducting layers.

In the case of elevated layers, a particular fading mechanism is associated with the temperature inversion which normally accompanies them: the inversion is a region of sharp density changes and as such, over a given area or distance, will be prone to vertical oscillations as a result of gravity waves. These waves can encompass a wide variety of wavelengths and will be superimposed on the inversion layer, which in itself, may be sloping. The effect of the wave motion is to compress and alternately stretch the depth of the refractive layer so inducing variations in the refractive index gradient through the layer. At any given point, therefore, the refractive layer will vary both in height and strength with time. Gravity waves may be generated by vertical wind shear or by turbulent processes from beneath. In this latter respect, it is likely that the wave motion will be more marked over land and downwind from land-masses, than over the open ocean. This last observation can have significant implications for the METOC forecasting for the littoral environment.

G. ASPECTS OF SEA CLUTTER

The term sea clutter is used to describe the radar return received from the sea surface. The strength of the return depends both on the roughness of the sea and the overlying wave guide, Pappert, et al (1992). With wind speed less than 5kts, sea return is minimal; it increases rapidly with wind speed between 5kts and 20kts and more slowly thereafter. The clutter pattern is stronger and covers a larger area in an upwind direction than either downwind or crosswind. The effects of sea clutter increase with increasing frequency of the transmission because of both the scattering effects of the sea and the wave-guide versus frequency trapped relationship.

Sea clutter adversely affects system performance: if the sea clutter return is stronger than a target at the same range, then it will be difficult or impossible to detect the target. Many radar systems employ a Moving Target Indicator (MTI) to enhance the radar's ability to detect a fast-moving target against a slower-moving clutter background. MTI is normally sufficient to overcome the sea-clutter problem when no strong ducting is present. However in the presence of a surface duct or of a strong evaporation duct, the sea clutter return can be greatly enhanced and impair the ability of the MTI to be able detect the moving target. In addition, enhanced propagation conditions can significantly extend the ranges affected by sea clutter.

Evaporation and surface based ducts generally result in the continuous enhancement of sea-clutter returns at all ranges. The strength of the sea return received by a radar system will depend on the height of the duct. In general, for a given wind speed, sea clutter becomes stronger and extends over greater distances as the height of the duct increases.

In the case of elevated layer surface ducts, due to the skip effect, wave paths traversing the elevated layer can lead to high sea returns being received from distances significantly beyond the limit of the clutter accompanying the ground waves. There are usually several discrete range interval of high sea clutter return because of the multi-hop nature of the propagation in this type of duct. These discrete intervals are normally independent of azimuth angle resulting in the appearance of a series of concentric arcs or rings (referred to as sea clutter rings) appearing outside the more conventional continuous pattern surrounding the radar when viewed on a PPI (plan position indicator) display. The clutter rings can result in the masking of air target at particular ranges. Figures 10 and 11 demonstrate clutter from evaporation and surface-based ducting respectively.

Airborne radars above the duct will also experience enhanced and extended sea clutter for a given wind speed under surface ducting conditions. In this case, clutter appears beyond the central sea return, although clutter rings as such are not observed. Their performance can be severely impaired, particularly for surface-search applications.

In coastal operations, land clutter may also be significantly enhanced and this can cause target masking and general confusion to the radar operator.

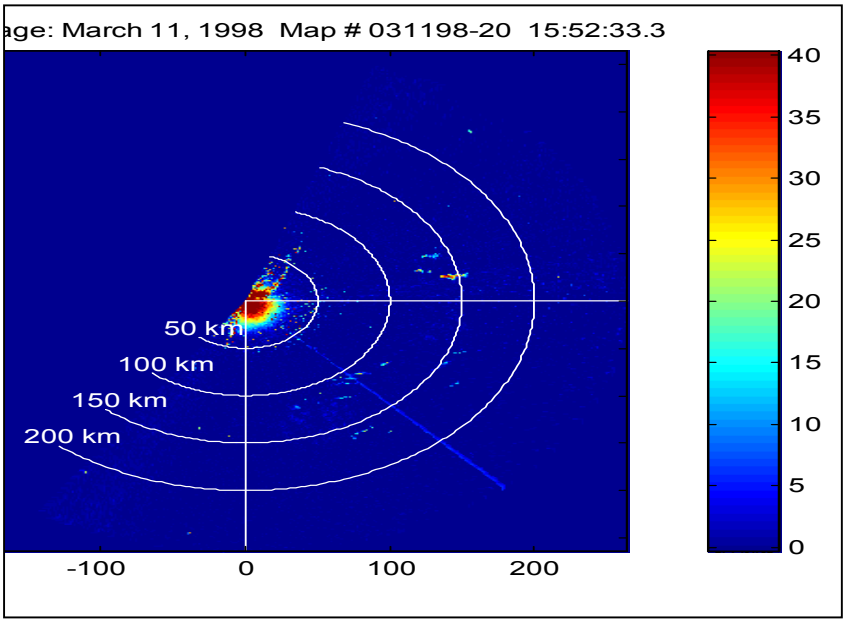

Figure 10. Clutter from evaporation ducting.

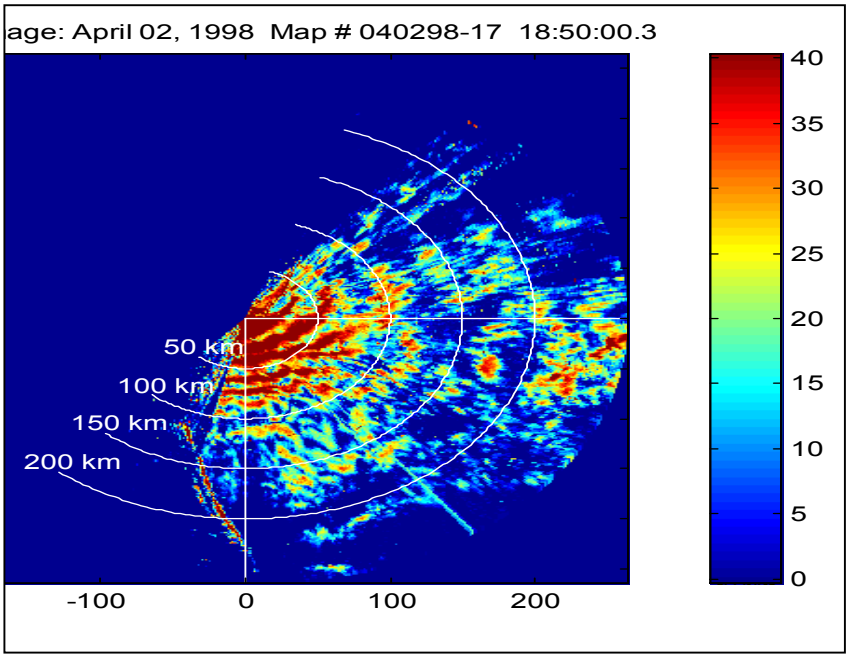

Figure 11. Clutter from surface-based duct.

VI. PROPAGATION MODELS

A. INTRODUCTION

In principle, the propagation prediction for any EM wave problem is provided by a solution of Maxwell's equations. Such a predictive model will be deterministic in its results (if the propagation medium is characterised exactly, the solution would also be an exact description of the propagation conditions for the given path at the given time. However, in practice it is much more complex than this scenario. Approximations and simplifications are required and no practical solution of Maxwell's equation (i.e. one that is analytically solvable or is numerically tractable) will be applicable to all propagation environments or problems. Different propagation environments and mechanisms will require different approximations and assumptions, and this has led to the development of various methodologies for solving EM wave problems. Several models and computer programs/packages have evolved to deal with different application areas. Two such packages are EEMS and AREPS, which are used to analyse the Wallops Island dataset.

Deterministic models are particularly relevant when a prediction/forecast of a specific system is required at a specific location and time (e.g. determining the optimum altitude for an airborne raid to fly, in order to evade detection by an enemy radar). It must be emphasised, however, that the accuracy of a prediction its critically dependant on the quality and quantity of real-time environmental data available. The lack of such high quality data is often likely to be more of a constraint on the final prediction, than the accuracy of the propagation model itself.

Because the propagation environment is never known exactly, a deterministic approach to the problem, may, in fact, be undesirable. Predictions are sometimes required, when no direct measurement of the environment is available. In such a case, a prediction may still be possible, but will be now, be based on climatological data, or on a measurement of a similar system within a similar environment. This empirical type of model will be sufficient for some applications, and due to its reduced complexity, be able to produce near-instantaneous predictions. Such models will be useful in long-term and system planning or for simulation purposes, where an average value is more applicable.

Tactical decision aids (TDAs), such as previously introduced EEMS or AREPS, require system information in addition to a propagation model and environmental data. Performance criteria for radar, communications and navigational systems is required as well as target, background and clutter characteristics will be necessary to estimate the detection capabilities of the system. The human is also an integral part of many detection systems, and as such, the performance of the operator should be taken into account and modelled.

B. ENVIRONMENTAL DATA

Measurement and assimilating information about the propagation environment is an integral part of any TDA. In some cases such data may be essentially static and obtained once (e.g. terrain data). However, the propagation medium itself will generally vary with time, and thus sensor must be deployed to obtain timely and representative measurements of the medium.

Direct sensing is currently the most widely available source of data in the troposphere, principally by means of radiosonde, rocketsondes or screen. Recent developments in remote sensing, however, show promise in obtaining refractive index information with greater spatial (horizontally) and temporal resolution than is possible by conventional methods (the vertical resolution is still not currently sufficient for operational purposes). Such remote sensors are less prone to detection than conventional methods and are thus ultimately the way forward.

Real-time deterministic prediction (now-casting) and forecasting models require regular updates of meteorological data (such a system is envisioned within the 4-D Cube framework). Forecasting of system performance will rely on accurate forecasts of the state of the propagation medium, and as such improvements will rely heavily on the development of numerical weather prediction models.

A description of the measurement and collection of environmental data will be conducted in Chapter VII and a review of atmospheric models made in Chapter XII.

C. BULK EVAPORATION DUCT MODELS

Direct measurement of the evaporation duct would require multi-level fixed sensors starting near the surface and extending to heights that cover the normal evaporation duct's vertical extent. Such an approach is, of course, unpractical, except under experimental conditions. The common evaporation duct height range is from 2 to 40 metres, above the highest level on most small combatants. Operational shipboard airflow measurements are the mean bulk measurements (wind speed, temperature, humidity and pressure) are taken onboard ships at some reference height (marine screen-level). Surface temperature can be and normally are obtained manually by METOC personnel or continuously by systems such as SMOOS(R)/SEAWASP, as used by the USN.

Bulk models for the surface-layer are what allow the use of mean single-height measurements in conjunction with value for the sea-surface temperature (SST) to estimate the temperature and humidity surface-layer profiles that are needed to calculate near-surface refractivity profiles. The refractivity profile is then interpreted for the presence and height of evaporation ducts. Empirically formulated models that relate the profiles to surface fluxes, so-called flux-profile models, are used to relate bulk measurement at a single level in the atmosphere and the surface. Monin-Obukhov Similarity (MOS) theory establishes the approach for the models. According to MOS theory, conditions are assumed to be horizontally homogeneous and stationary. The turbulent fluxes of momentum, sensible heat and latent heat are assumed to be constant with height in the surface layer. The surface layer is the lowest 10% of the turbulent atmospheric boundary layer, and generally extends upward to a height of roughly 10 to 200m.

As it turns out, propagation models applied in this thesis have different bulk-models imbedded in them. The EEMS TDA uses Battaglia's (1985) model for near neutral conditions.

In this model the duct height d (m) is given by:

$$d = 0.96(\mathrm{Ta} - \mathrm{Ts}) - 3.4(e\mathrm{a} - e\mathrm{s}) \qquad \text{Eqn VI-1}$$

where Ta (K) is the air temperature measured at 10m above mean sea level, Ts (K) is the SST, ea (mb) the water vapour pressure at 10m and es (mb) the water vapour pressure at sea level.

The AREPS TDA uses the Naval Postgraduate School (NPS) adapted LOB (Liu *et al.* 1979 and Fairall *et al.* 1996) bulk surface-layer scaling model (Frederickson *et al.* 2000a) within the MOS approach to determine the near-surface *M* profile and also the Paulus-Jenske model. The NPS model is also similar to a version described by Babin *et al.* (1997), which was formulated directly from the LOB. The NPS approach computes the modified refractivity (*M*) profiles and determines the evaporative duct height directly from this profile. Babin *et al.* (1997) used an iterative method to determine the evaporation duct height. The profile approach has the advantage that the *M* profiles themselves provide operational users with useful EM propagation information. The method also avoids the possibility that the iteration for duct height will not converge.

D. ELECTROMAGNETIC EFFECTS MODELLING SYSTEM (EEMS)

The EEMS TDA was originally developed as a technical demonstrator for a replacement for in-service radar propagation models such as IREPS (Integrated Refractive Effects Prediction System. It aims to provide greater accuracy in radar propagation modeling, combined with the improved execution times, which are required for operational use and the inclusion of operational parameters, such as target speed and radar antenna rotation rate. EEMS is able to compute and produce a number of different tactical decision aids. These cover airborne and surface-based probability of detection against a plethora of targets, both surface and above surface, ESM vulnerability, calculation of radar coverage against a threat to another unit (referred to as High Value Unit (HVU) protection mode. It contains interfaces to allow both Digital Terrain Elevation Data (DTED) and also data files from the Meteorological Office Meso-scale Model to be used as input and display accordingly.

EEMS Version 2 was developed for the Maritime Warfare Centre (MWC) under demand order agreement MWC/97/03, sub-task 030. Production and development of the EEMS TDA was sponsored and funded by CINCFLEET N3 Division (RN Headquarters - Operations).

The propagation model used within EEMS is TERPEM (TERrain Parabolic Equation Model). TERPEM is a propagation modeling tool for assessing the effects of atmospheric and terrain diffraction on radar and communications system in the frequency range 30 MHz to 100 GHz. Good agreement has been achieved between the output of TERPEM and that of AREPS (Thompson, 2002). The TERPEM code solves a parabolic form of the wave equation, which according to Dockery and Goldhirsh (1995) is the standard method for assessing the effects of meteorological environments on naval radar applications. Essentially the model solves a parabolic approximation to the wave equation through the use of split-step Fourier transforms. Although there are some useful simplifications made in TERPEM in order to improve run time where conditions are favourable (Levy, 1989, 1995; TERPEM user Guide, 1998), the basic approach within the ducting region follows that of Dockery (1998). TERPEM also allows for a rough sea by applying a correction factor derived from the model of Miller et al. (1984), with a root-mean-square (RMS) wave-height taken from the saturation curve spectrum of Phillips (1966).

This thesis uses output from the TERPEM model in three different formats:

- One-way-loss coverage diagrams.
- One-way-loss propagation factor diagrams, in which signal attenuation that would have occurred within free space has been factored out.
- One-way-loss curves at three different heights within the surface boundary region.

These output products will be compared with the direct propagation measurements from the Wallops Island MPME experiment and also output from the AREPS TDA.

EEMS/TERPEM can be used in either a range-independent or range-dependant mode (single vertical profile vs. multiple vertical profiles respectively). This thesis mainly concentrates on the range-independent mode in order to examine the data in the light of current operational practices and data availability. Some limited range-dependent runs will be made for comparison purposes, however.

E. ADVANCED REFRACTIVE EFFECTS PREDICTION SYSTEM (AREPS)

The second assessment tool used in this study was the Advanced Refractive Effects Prediction System (AREPS) developed by the Atmospheric Propagation Branch at the Space and Naval Warfare Systems Center (SSC), San Diego. AREPS computes and displays a number of tactical decision aids. These are for airborne and surface based radar probability of detection, electronic surveillance measure (ESM) vulnerability, UHF/VHF communications, simultaneous radar detection and ESM vulnerability, range-dependent ray-trace, and a surface search range table. All decision aids are displayed as a function of height, range and bearing. Detection probability, ESM vulnerability, communications and surface search range assessments are based on EM system parameters stored in a user changeable database. Paths containing land features depend on terrain either obtained from the National Imagery and Mapping Agency's (NIMA) Digital Terrain Elevation Data (DTED) or specified by the user.

Calculations performed in AREPS depend on atmospheric refractivity data derived from observations provided by radiosondes or other sensors. AREPS version 3.2 uses the Advanced Propagation Model (APM), to calculate range-dependent EM system propagation loss within a heterogeneous atmospheric medium over variable terrain, where the radio-frequency index of refraction is allowed to vary both vertically and horizontally while accounting for terrain effects along the path of propagation. The APM model is a combination of Fourier spectral and geometric solutions to the EM propagation equation for accuracy and speed in an operational environment.

VII. FIELD TEST PROPAGATION AND METEOROLOGICAL MEASUREMENT SYSTEMS

A. NSWC-DD MICROWAVE PROPAGATION MEASUREMENT SYSTEM II (MPMS II)

The Microwave Propagation Measurement System II (MPMS II) comprised of both transmitter and receiver subsystems. The transmitter subsystem was located aboard the *R/V Sealion*. It consisted of three co-located continuous wave (CW) transmitters each with its own vertically polarized log-periodic antenna mounted in the horizontal axis so that all antennas were at the same height. The transmitter assembly was mounted on a platform that traversed a 30 ft (9.1 m) tower, presenting a 3 to 33 ft (0.9–10.1 m) height above sea level. The receiver subsystem was located in a van that was positioned at the edge of the beach to the north side of building V-24 at the test facility. It included a 100 ft (30.5 m) tower with up to 4 receivers placed at heights typical of shipboard radar systems. The S-band receiver, typical of search radars, and a C-band (not examined in this thesis) receiver, typical of tracking radars, was placed 60 ft (18.3 m) above mean sea level. The X-band receiver, typical of fire-control systems and surface search radars, was placed 100 ft (30.5 m) above mean sea level. The receiver electronics were rack-mounted with control and display functions operating on a desktop computer system. MPMS II system parameters are summarised in Table 4.

Simultaneous Paths	40 (10 Transmitters, 4 Receivers)
Waveform	Continuous Wave
Transmitter Power	20dBm
Antenna	1-18 GHz Log-periodic (Vertically Polarized)
Antenna Gain	7.0 / 6.5 / 6.0 dB (3.7 / 5.1 / 9.3 Ghz)
Antenna Beam Width	60 deg minimum AZ and EL
Height Resolution	Transmitter 3-33 ft. Receiver fixed.
Receiver Bandwidth	N/A

Table 4 MPMS II System Parameters.

B. METEOROLOGICAL SENSORS ON *R/V SEALION*

The NSWCDD *R/V Sealion* is a 60 ft, ocean yacht equipped with the MPMS II transmitter sub-system and an additional independent meteorological measurement system.

The meteorological data collected included wind speed and direction, air temperature and relative humidity, pressure, solar radiation and water temperature. These measurements were made 8.5 m (27.9 ft) above the water line. Water temperature was obtained using a radiometer (8-14 μm) and a surface temperature probe (thermistor).

The basic task during the experiment was to transit outbound, away from the MPMS receiver tower on specified radials, to the distance of the radio horizon. Rocketsondes were launched at the start (3nm), midpoints (8 and 20nm) and end (30nm) of each radial run. Radials were selected to minimize sea-induced motion aboard the craft.

C. METEOROLOGICAL SENSORS ON *R/V CHESSIE*

The John-Hopkins University Applied Physics Laboratory (JHU/APL) project boat, *R/V Chessie*, is a 50 ft (15.2 m) sport-fisherman type boat used to collect various meteorological data to support computer modelling of the propagation environments.

The sensors aboard the *R/V Chessie* include the meteorological portion of the SEAWASP system, an instrumented towed sled, balloon dropsondes, and rocketsondes. These systems provided data from sea level to 3000 ft. Data from R/V *Chessie* is not used in this analysis

D. VERTICAL ASCENT MEASUREMENTS ON R/V'S *SEALION* AND *CHESSIE*

The rocketsonde system was developed with commercial off-the-shelf (COTS) hobby rocket components (Call, 1994). Figure 12 shows the component parts of the rocketsonde including the rocket body, nose cone, engine, and instrument package attached to a parachute. Figure 13 shows the rocketsonde assembly in the launcher and

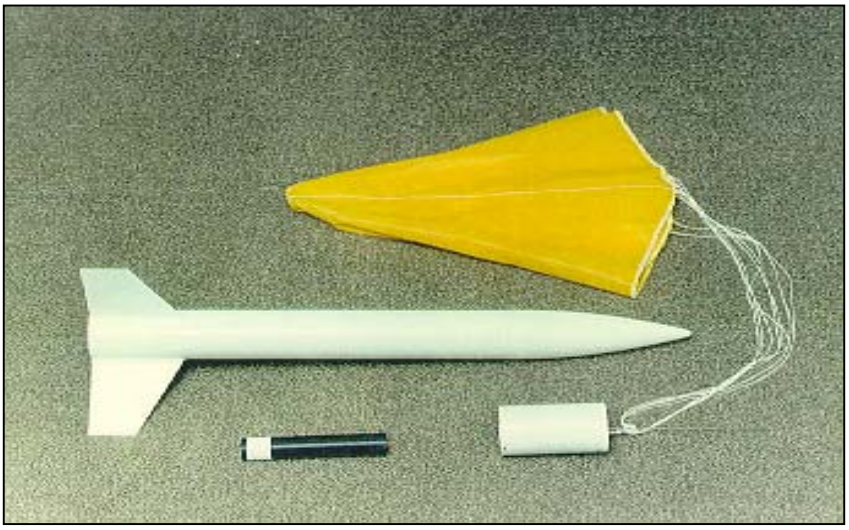

Figure 12. Rocketsonde components.

Figure 13. Rocketsonde assembly prepared for launching from USN ship.

the data acquisition computer system during a launch from a U.S. Navy aircraft carrier. The microprocessor controlled digital sensor package is carried aloft in a non-metallic rocket that is fabricated of paper and plastic. No special approval is required to launch rocketsondes as they are classified under the same rules as hobbyist model rockets. Table 5 lists dimensions, weight cost and other details for the rocketsonde. Similar information is provided on the RS-80 series radiosonde used onboard U.S. Navy ships at-sea with the MARWIN MW 12 Rawinsonde Set (MRS).

The accuracy, response time, and resolution of the both the rocketsonde and radiosonde pressure, temperature, and relative humidity sensors approach those of high quality laboratory instruments. The sensor responses are appropriate for the typical ascent/descent rates. The sensor types and specifications for both sonde systems are provided in Table 5. Both sonde systems transmit over a narrow 400-406 MHZ frequency band. The rocketsonde transmits every 1 to 2 seconds using an FM narrowband crystal-controlled transmitter. The slow parachute descent and high sampling rate of the sonde, provides a high spatial resolution profile of the atmosphere. The balloon launched radiosonde currently used onboard RN and USN ships ascends at approximately 4 m/s and provides the atmospheric parameters of temperature, pressure, and relative humidity roughly every 8 to 10 m. The rocketsonde on the other hand has a slower 2 m/s descent rate and provides data at intervals of 5 m or less. The higher vertical resolution will be demonstrated on the basis of refractivity gradient as well as refractivity profile comparisons for simultaneously launched sondes and RPO outputs (Baldauf, 1996).

Dimension/Weight/Cost	**Rocketsonde**	**Radiosonde (RS-80)**
Length	660 mm	147 mm
Diameter	63.5 mm	55x90 mm
Total Launch Weight	453 g	
Instrument Package Weight	113 g	Less than 200 g
Parachute Size	91.4 cm	
Rocket Propellant	Ammonium percholate-polyurethane	
Propellant Weight	56 g for 757-m altitude	
Total Cost Per Shot:	$ 200	$150 (includes sonde, balloon, helium)

Table 5 Rocketsonde and Radiosonde characteristics (from Baldauf, 1996)

SENSOR	ROCKETSONDE	RADIOSONDE (RS-80)
PRESSURE SENSOR		
Type:	Aneroid capacitance	Capacitive aneroid
Pressure Range:	1050 to 600hPa	1060 to 3 hPa
Accuracy:	1.0hPa	0.5 hPa
Resolution:	0.01hPa	0.1 hPa
Response/Lag Time:	<0.1 second	
TEMPERATURE SENSOR		
Type:	Bead thermistor	Capacitive bead
Temperature Range:	-55^{o} C to 50^{o} C	-90^{o} C to 60^{o} C
Accuracy:	0.3^{o} C	0.2^{o} C
Resolution:	0.01^{o} C	0.1^{o} C
Response/Lag time:	>1.0 seconds	< 2.5 seconds
HUMIDITY SENSOR		
Type:	Capacitance polymer	Thin film capacitor
Humidity Range:	0 to 100%	0 to 100%
Accuracy:	3% RH	2% RH
Resolution:	0.1% RH	1.0% RH
Response/Lag time:	<1.0 seconds	1.0 second

Table 6 Rocketsonde/Radiosonde (MRS) Sensor Performance Characteristics (from Baldauf, 1996)

E. NAVAL POSTGRADUATE SCHOOL FLUX BUOY

The Department of Meteorology, Naval Postgraduate School (NPS), was involved in WALLOPS 2000 experiments with the deployment of a 'flux' buoy on the NSWC-DD established propagation track. The buoy was deployed for the entire WALLOPS 2000 collection period and beyond, for a period extending from April through mid-June 2000. The continuous and high quality nature of the data collected allows direct comparisons throughout the period of the study. For this reason the flux buoy data is used for all surface and near surface measurements throughout this thesis.

The flux buoy (FB), shown in Figure 14, was a 2-meter diameter disk buoy instrumented with sensors to measure mean environmental parameters, atmospheric turbulence quantities and one- and two-dimensional wave spectra. The buoy was moored 7 nautical miles off shore near:

37° 45.8′ N, 75° 23.1′ W

The actual buoy location at a given time varied slightly from the above location depending upon the surface current, since the buoy is anchored with a 150-ft (45.7-meter) scope of chain. The mean water depth at the FB location was approximately 14-meters (46-ft).

The FB was deployed on 1 April 2000 and recovered on 10 June 2000. Mean meteorological and sea temperature data and wave spectra data were available for this entire period. During the initial deployment on 1 April 2000 a turbulence sensor, the sonic anemometer on the FB was damaged and was removed from the buoy. On 1 May 2000 a replacement sonic anemometer was mounted on the buoy at sea, allowing atmospheric turbulence data to be collected from 1 May until 8 June 2000, when the buoy was placed in 'hibernation' mode prior to recovery (Frederickson *et al.* 2000a).

The FB contained two separate data acquisition systems. One system obtained mean environmental data, and one obtained high frequency atmospheric turbulence and platform motion data. These two separate data acquisition systems are described in the next two subsections.

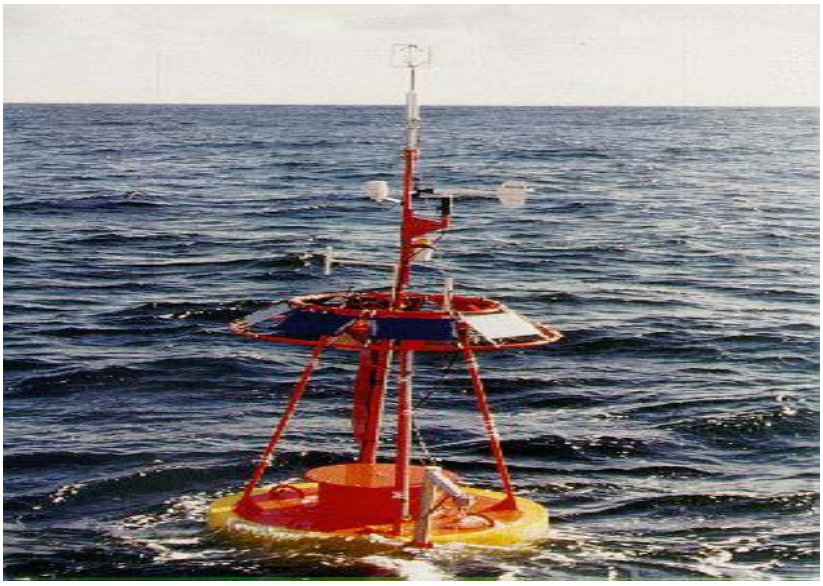

Figure 14. NPS Flux Buoy.

1. Mean Environmental Data System

The mean data acquisition system sampled environmental data from a suite of instruments at 1 Hz. These 1 Hz values were averaged into one-minute blocks that were then stored in the onboard computer. The wind direction and buoy heading were averaged to take into account changes across 360 – 0 degrees. The flux buoy mean sensors are described in Table 7.

Due to power constraints, the air temperature and relative humidity sensor (Rotronic MP101A) was mounted within a passively aspirated radiation shield, rather than a forced aspiration shield. For this reason the air temperature may have been slightly positively biased and the relative humidity may have been slightly negatively biased for low wind speeds during the day, and especially just after sunrise and just before sunset. Bulk surface layer parameters were computed from these mean data using the methods outlined sub-paragraph (3) below.

Measured Parameters	**Sensor Type**	**Manufacturer and Model**	**Height Above Surface**
Wind Speed/Direction	Propeller-vane anemometer	R. M. Young Wind Monitor Model 05106	3.90 meters
Air Temperature	Pt 100 RTD	Rotronic MP101A	3.94 meters
Relative Humidity	Rotronic Hygrometer	Rotronic MP101A	3.94 meters
Atmospheric Pressure	Barometer	A.I.R.	2.10 meters
Sea Surface Temperature	IR Temperature Transducer	Everest Model 4000	2.40 meters
Bulk Sea Temperature	Hull thermistor	NPS custom design	–1.17 meters
Buoy Heading	Compass	TCM-2	0.39 m

Table 7 Flux Buoy Mean Measurement Systems.

2. Turbulent Data System

The flux buoy turbulence data system measured atmospheric turbulence and buoy motion properties at a sampling rate of 5 Hz. These data were stored in the onboard computer in files containing a 77-minute time series record. The turbulence sensors are described in Table 8. These sensors had the capability to measure three-dimensional wind speed and sonic temperature and the buoy three-dimensional linear accelerations and angular rotations. Direct covariance momentum and sonic buoyancy fluxes and wave height spectra were derived from these high frequency measurements.

Measured Parameters	**Sensor Type**	**Manufacturer and Model**	**Height above Surface**
3-D Wind Speed & Sonic Temperature	3-D Ultrasonic anemometer	Gill Instruments Model 1210R3	5.23 meters
3-D Platform Motion	Accelerometers & Rate gyros	Crossbow DMU-VGX	0.39 meters
Buoy Heading	Magnetic compass	TCM-2	0.39 meters

Table 8 Flux Buoy Turbulent Measurement System.

3. Data Processing and Analysis Procedures

Mean or average atmospheric and sea surface descriptions were those used for comparisons in this study because the objective was to relate results to descriptions that would be available in an operational environment. In this regard, procedures for obtaining direct turbulence descriptions of the atmosphere surface layer will not be described although such descriptions were possible from the sonic anemometers. Similarly, detailed 2-dimensional surface wave descriptions were possible but will not be described.

The surface and near-surface measurements of wind speed, air temperature, float SST (found to be the most reliable), relative humidity (RH) and atmospheric pressure were inputted in to the respective TDAs to obtain bulk evaporation duct parameters. The calculated evaporation duct was then appended to the respective rocketsonde profile and the respective propagation model ran at varying combinations of frequency and height

parameters, according to the data in Table 4. Combinations of runs with rocketsonde and evaporation duct properties only were then run to simulate operational data limitations. The results of the various runs are analysed in Chapter XI.

THIS PAGE INTENTIONALLY LEFT BLANK

VIII. SENSOR PERFORMANCE AND DATA SELECTION

A. SENSOR PERFORMANCE

1. Mast-Mounted Systems

Positions of the NPS flux buoy, *R/V Chessie* and *R/V Sealion* during the various range tests on during April and May 2000 are shown in Fig 15. Continuously operating instrumentation on the three spatially separated platforms, along with regularly spaced rocketsonde launches, enabled examination of both the spatial and temporal changes in the boundary layer. This thesis uses data from *R/V Sealion* and the NPS flux buoy.

2. NPS Flux Buoy

The flux buoy provided the most complete and continuous data set of surface-layer and ocean surface properties for the entire experiment period. The fixed position of the buoy provided an excellent record of the temporal changes in the atmosphere over the recording period

Considerable differences in sea-surface temperature were found between the reports by the IR sensors, float thermistors and hull-mounted thermistors. Such differences in sea surface temperature results in greatly differing ASTD, which in turn, implies profoundly different duct heights when computed using the bulk parameterization methods. It is recognized that small changes in the ASTD result in dramatic changes in the computed duct height (Frederickson et al., 2000b). The most reliable and accurate measurement was found to be the float sensor on the NPS buoy and this data source was used throughout this study.

Inputs of wind speed, air temperature (at 3.94m), float SST, relative humidity (RH) and atmospheric pressure in to the TDAs are all taken from the NPS buoy.

3. Rocketsonde Profiles

The rocketsonde measurements were critical to this analysis on propagation data and influencing meteorological conditions because rocketsonde derived profiles provided information on the occurrence of a surface-based duct. Rocketsonde system reliability and performance throughout the WALLOPS 2000 experiments was mixed and varied. Of the 57 rocketsondes launched in total during the experiment; 18 failed to capture usable data. Of the 32 files identified as "good" quality, 7 were marked as "good with resolution." All of the rocketsonde launches yielding data from WALLOPS 2000 were examined for their suitability for this study. Reasons for disqualifying rocketsonde launches included: empty or incomplete sounding files; patently inadequate vertical resolution; obvious sensor failure; or failure to measure near the ocean surface. Four of the 32 "good" rocketsondes were used for this study, each representing four different complex meteorological situations on four separate days.

B. DATA SELECTION

The objective of this thesis is to describe the accuracy of EM propagation models in a realistic operational scenario, to discuss the advantages and disadvantages of current methodology used by naval operators and make tentative suggestions for future solutions.

For this reason the choice of which rocketsondes came down to those profiles in the position that a warship would most likely to be in an operational or exercise scenario.

During amphibious operations/supporting land based operations, naval warships can be anything from ½ nm to 70nm away from the coast. In recent conflicts, such as Iraqi Freedom, UK and US vessels were often approximately 30nm from the coast, or just beyond the horizon. Current standard naval practice is to stand off between 30-50nm when supporting operations ashore.

In view of this distance, only those launches taken at the end of the run were selected. Moreover to give the most complex and worst-case scenario, it was decided to use those launches taken closest to the time of daytime maximum heating (approximately 2-3 PM local time or 1800-1900Z). At this time the meso-scale meteorological influences are expected to be at their maximum effect. Thus the profile will be at its most

complex and challenging for the propagation models. In realistic terms, the time when a propagation forecast might be expected to be at it's most unreliable.

These two factors narrowed the selection down considerably. The final selection being made to examine any difference between stable and unstable cases, and those with no surface based ducting and those with.

The profiles chosen were:

- April 10th at 1820Z. A stable case without strong surface based ducting.
- April 29th at 1950Z. An unstable case with significant surface based ducting.
- May 1st at 1910. A stable case with weak surface based ducting.
- May 3rd at 1930Z. An unstable case with strong surface based ducting.

It was deemed that the differences in stable versus unstable cases was an important factor, as all the evaporation duct models are extremely sensitive to small changes in temperature and humidity fluctuations. The static stability above the surface boundary is also an important factor in determining the nature of propagation and this also influenced profile choice.

Once chosen, each of the profiles was input into the respective propagation models along with the data measurements from the NPS flux buoy. It was decided to use a single profile in the range-independent- mode as this procedure most closely resembles that currently used afloat by a METOC team.

This emphasis on considerations of selecting procedures for using data collected, addresses part of the question that this thesis attempts to answer, which is: "Using currently available software and realistic operational methods, how well are the propagation conditions modelled?"

As a METOC officer, this is perhaps the most important question that one should ask prior to giving tactical and defensive advice regarding the effect of the atmosphere on the ship's weapons and sensors.

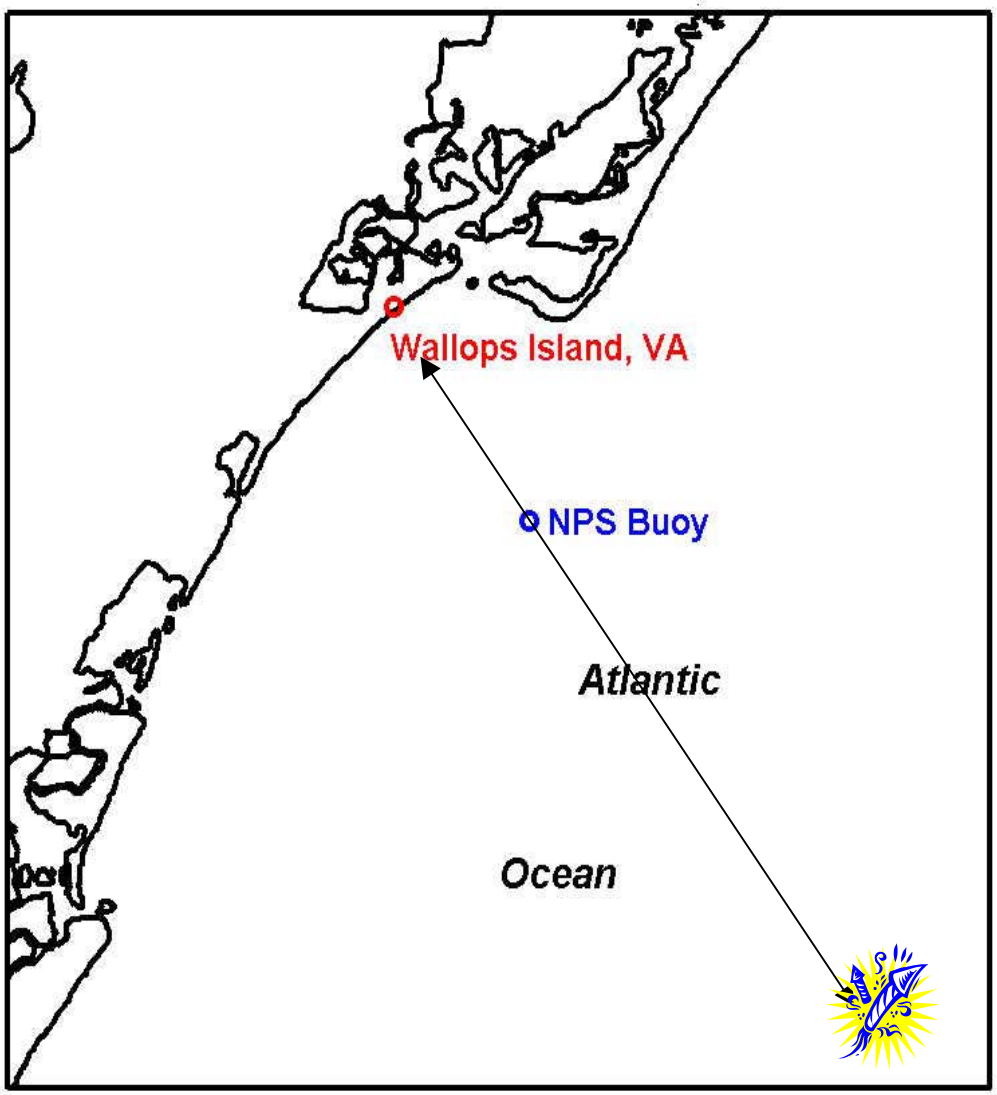

Figure 15. Map depicting positions of NPS flux buoy, the track run of R/V Sealion and the approximate launch position of the rocketsondes for 10th and 29th April, 1st, and 3rd May (actual distances along track were 33.5nm, 33.5nm, 35nm and 33.5nm respectively.

IX. SYNOPTIC SCALE METEOROLOGICAL DESCRIPTIONS

A. INTRODUCTION

This chapter is concerned with a description of the synoptic conditions pertaining to the times, centered on, rocketsonde launch obtained refractive profiles. Since these profiles determine the propagation conditions, it is important to relate significant features in them to the responsible synoptic scale phenomenon, if possible.

The objective of the description is to give an overview of the mechanisms responsible for the formation of the refractive conditions existing at the time of each launch.

A synoptic evolution for each day will be considered using:

- Synoptic charts at 4mb intervals with wind vectors appended for 1200Z each day covering 10 degrees latitude and longitude from Wallops Island
- Visible images from the GOES-E geostationary satellite at 1800Z each day.
- Meso-scale charts at 2mb intervals with wind speed at 6 hourly intervals, covering 5 degrees of latitude from Wallops Island.
- Skew-T diagrams for 1800Z each day, from surface to 400mb.
- Graphs of refractivity, both M and N, as output from EEMS.

Synoptic charts, skew-T diagrams and satellite imagery were obtained from the NOAA Air Resources Laboratory (ARL) website (2003). The charts are based on archive data from the NCEP Eta model. The horizontal resolution of the model was 40km, with 22 vertical levels and model output every 3 hours. Data from the ARL website is displayed at 80km resolution and at 6 hourly intervals.

B. SYNOPTIC EVOLUTION

1. 10 April 2000

Initially a 990mb low, centred just to the north of Newfoundland moves steadily northeast (Fig 16). The associated cold front, lies across Bay of Fundy and recurves southwest toward Cuba, then continues to move east (Fig 17). This leaves the area of interest (AOI) in a clear, moderate occasionally fresh, potentially unstable at low-levels (LL) WNW'ly airflow. The Bermuda High, 1031mb, extends a ridge northwest toward the AOI. As the day progresses (see Figs 18-21), pressure steadily rises over the AOI with a small ridge over the area by 1800Z. Winds are generally from the northwest at 10-15kts throughout the early part of the day but drop to 5-10kts by 1800Z.

The effects of this synoptic pattern (see Fig 22) would be to stabilize the vertical profile in the medium levels (6500-16,000ft) due to the increasing ridging, with a remnant layer of potential instability remaining at LL (below 6,550ft). By mid-afternoon the land temperature exceeds the SST, and thus immediately above the sea, a small layer of stability is expected due to offshore advection of warm air.

In terms of the refractivity (see Fig 23), the relatively warm, dry air flowing from overland will be expected to give a fairly strong evaporation duct, which in this case has a height of 37ft. Whilst the air is potentially unstable at LL, it is also dry aloft, and it would thus be expected to produce a super-refractive layer, of moderate extent, above the duct with no further ducting at LL, due to the potential instability. A series of super-refractive layers/elevated ducts would be expected above 850mb (5000ft) due to the subsidence associated with the ridging of high pressure.

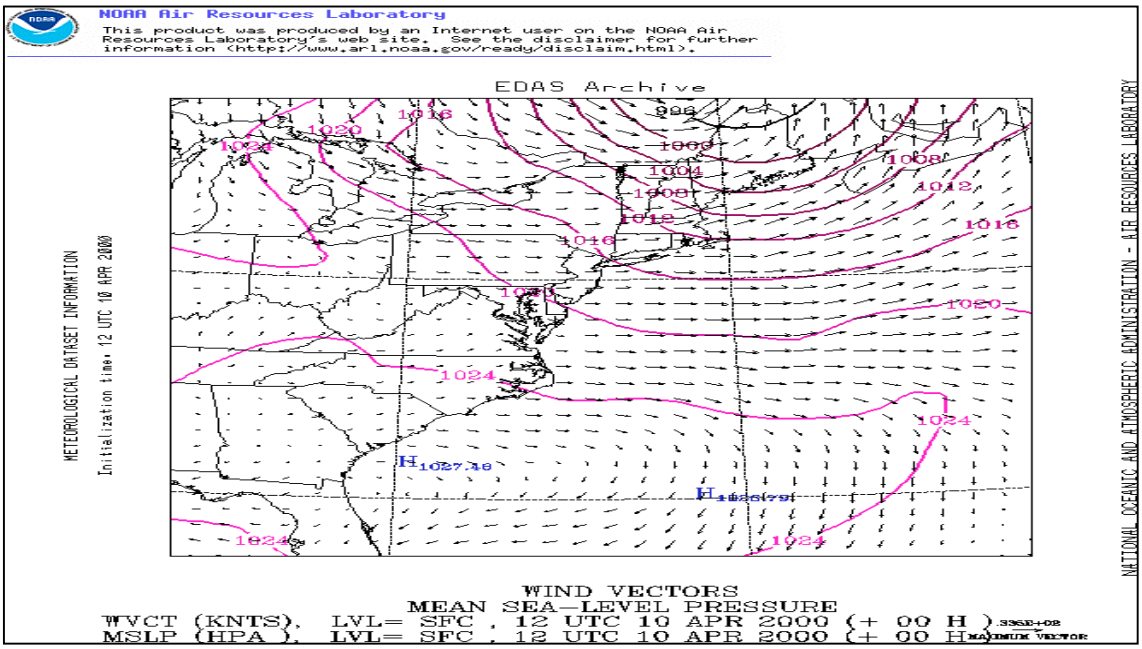

Figure 16. 10 Apr 1200Z. Synoptic chart at 4mb spacing.

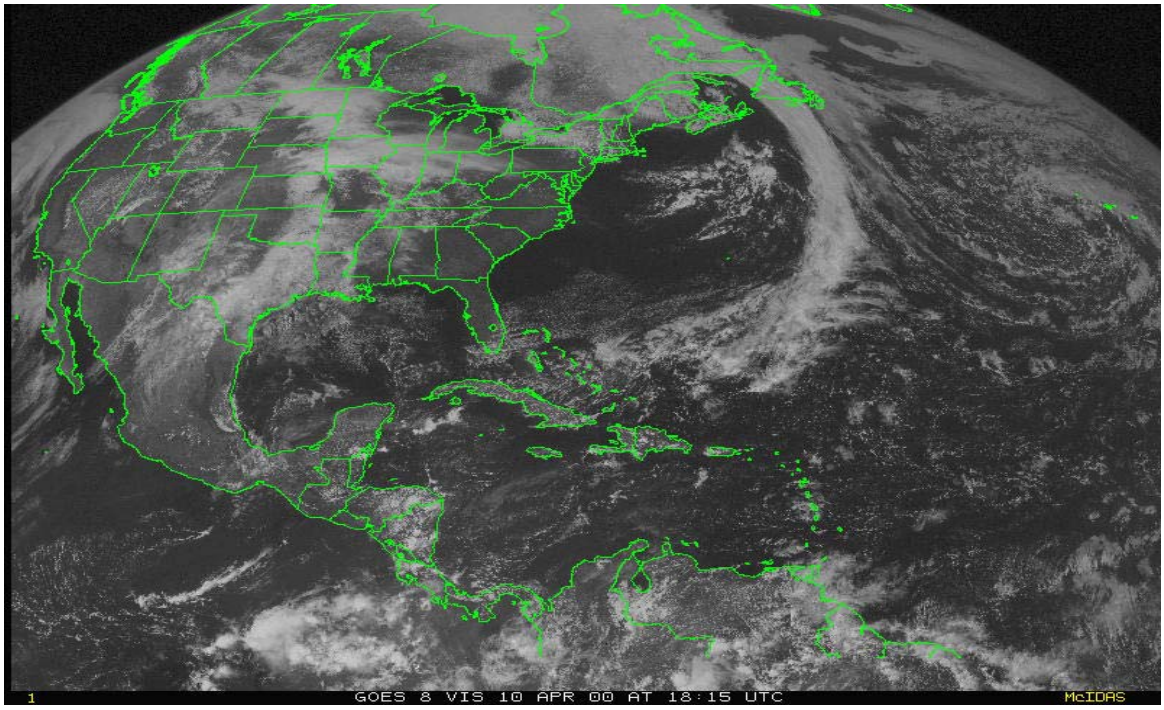

Figure 17. 10 Apr 1815Z. GOES-E visible satellite imagery.

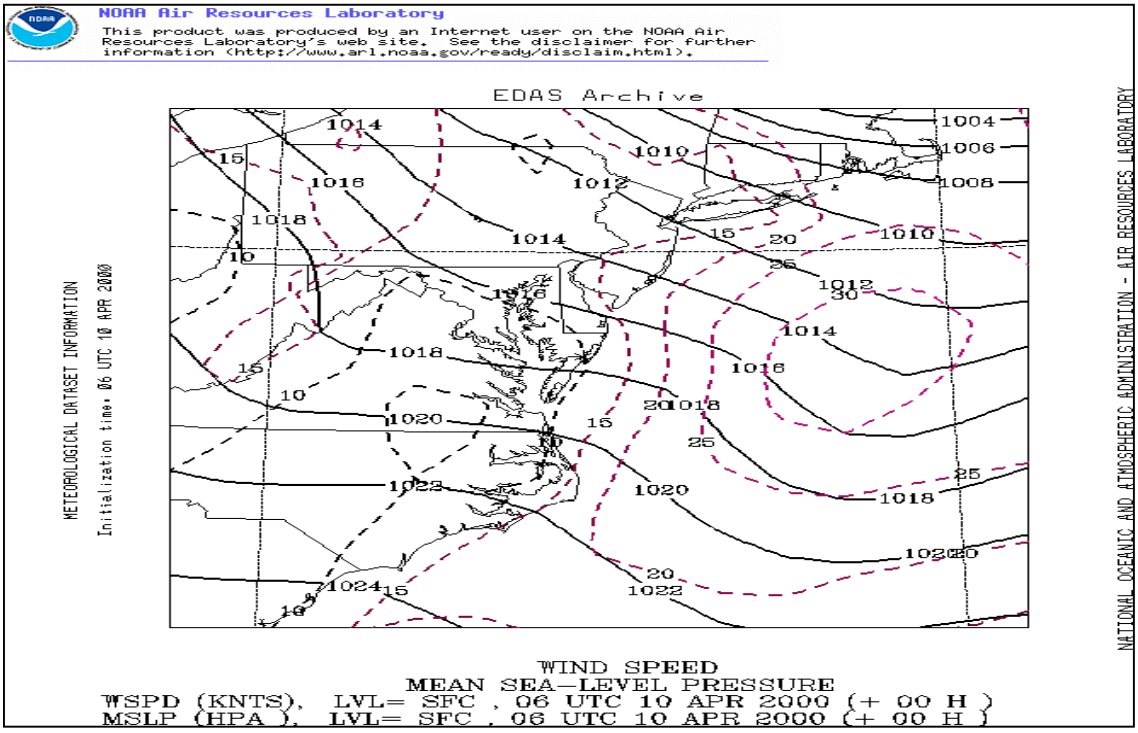

Figure 18. 10 Apr 0600Z. Synoptic chart at 2mb with wind speed.

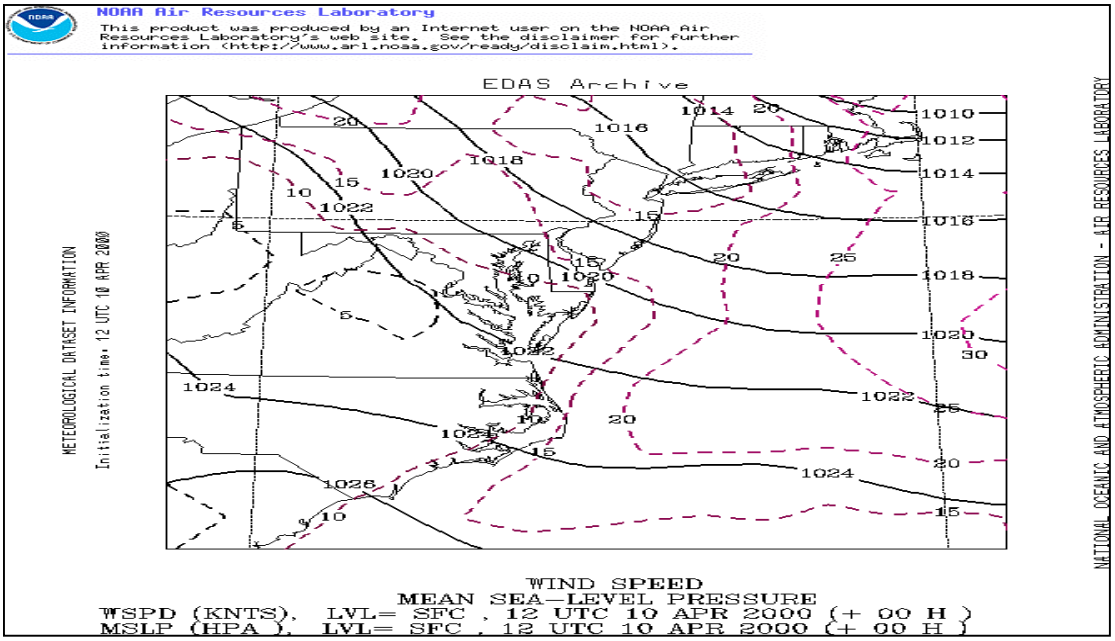

Figure 19. 10 Apr 1200Z. Synoptic chart at 2mb with wind speed.

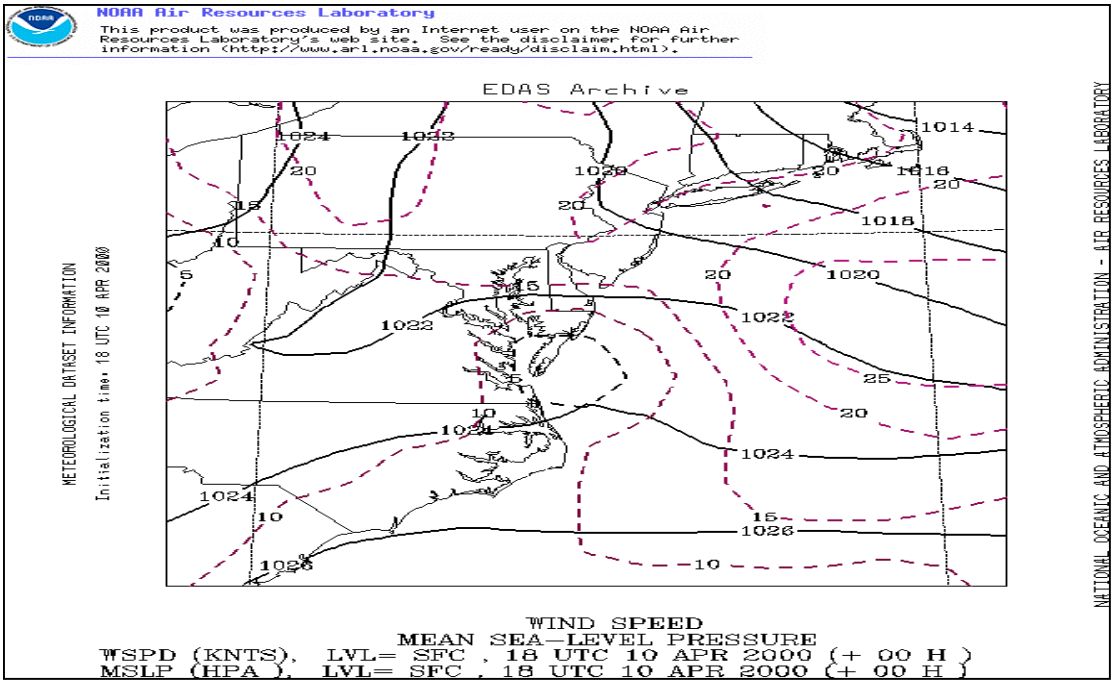

Figure 20. 10 Apr 1800Z. Synoptic chart at 2mb with wind speed.

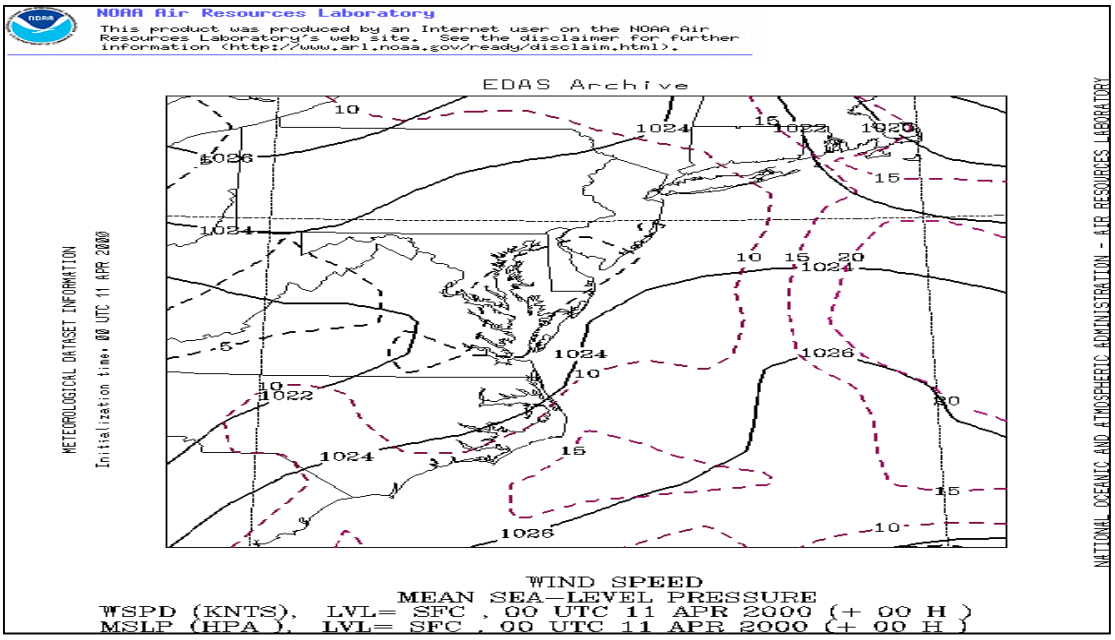

Figure 21. 11 Apr 0000Z. Synoptic chart at 2mb with wind speed.

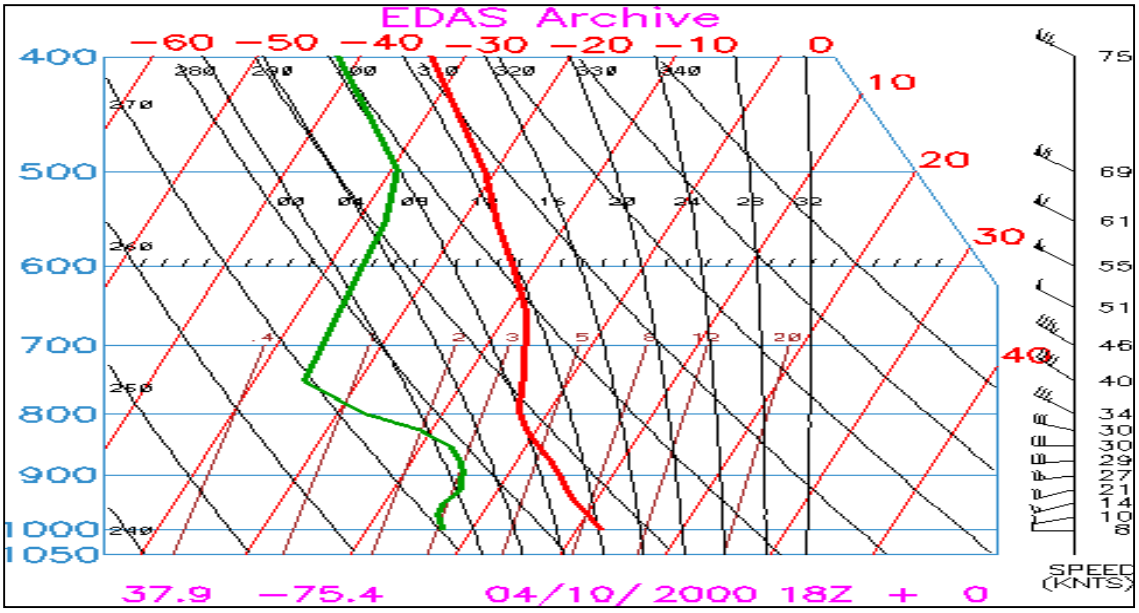

Figure 22. 10 Apr 1800Z Skew-T diagram.

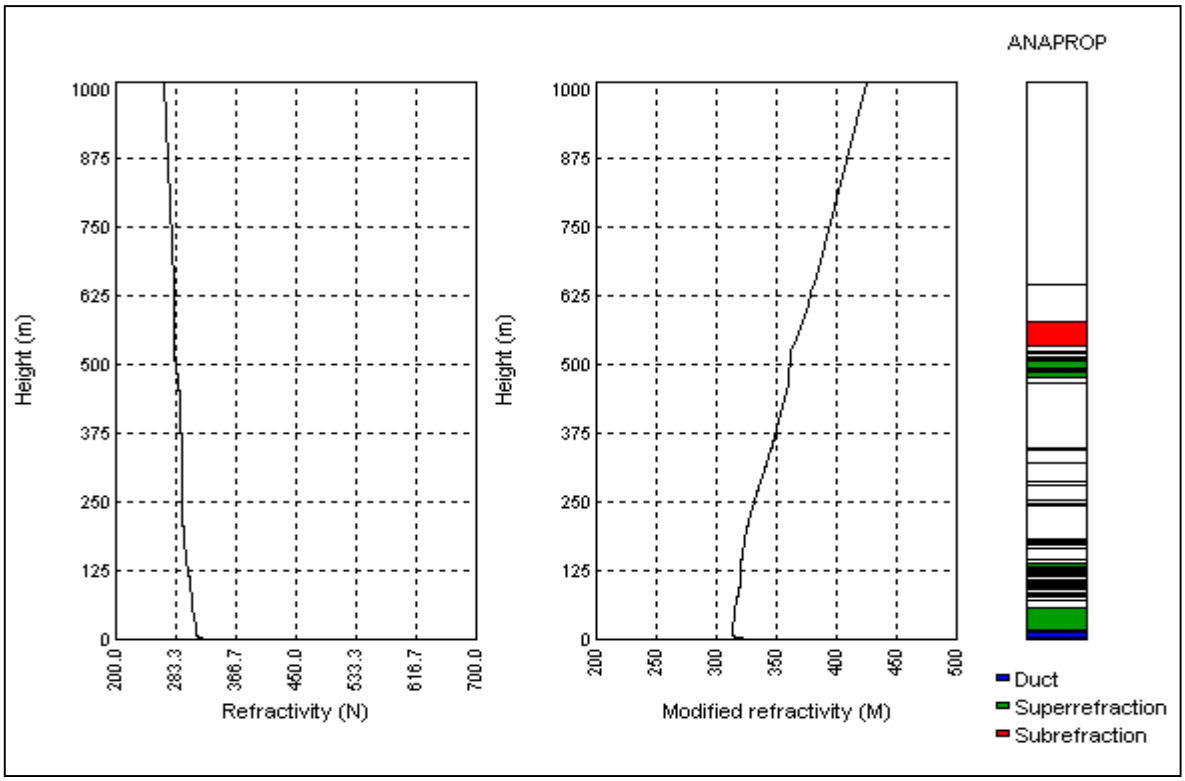

Figure 23. 10 Apr 1800Z Refractivity diagrams for M and N from EEMS.

2. 29 April 2000

The general synopsis for 1200Z has a low 1005mb, centred 800nm east of the AOI, moving rapidly east, continuing to deepen (Fig 24 and 25). High 1018mb, centred over North Carolina extends a building ridge toward the region, so that a local area of high pressure lies over the AOI by 1800Z. The area initially lies in a slightly unstable NE'ly moderate flow that backs NW'ly and reduces to light by 1800Z (see Figs 26-29).

The synoptic pattern would be expected to produce an increasingly dry and stable profile in the upper and medium levels, due to ridging, with some remnant instability at LL due to the close proximity of the low-pressure system earlier in the day (see Fig 30).

Air at LL will be relatively cool and dry, as a result of its source region, making it unstable given the warmer SST.

In terms of the refractivity (see Fig 31), medium and upper levels are expected to produce super-refractive layers and possibly elevated ducting, due to adiabatic warming and subsidence, whilst at LL the dryness of the air will be expected to produce some surface based ducting.

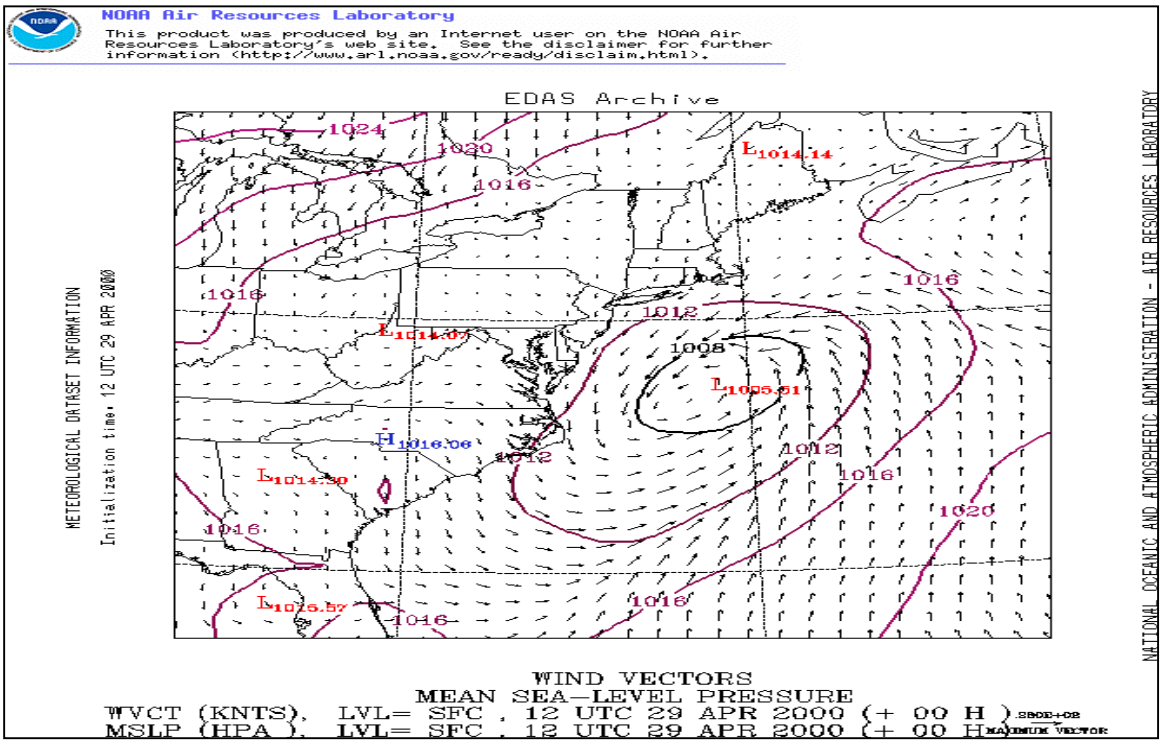

Figure 24. 29 Apr 1200Z.Synoptic chart at 4 mb spacing.

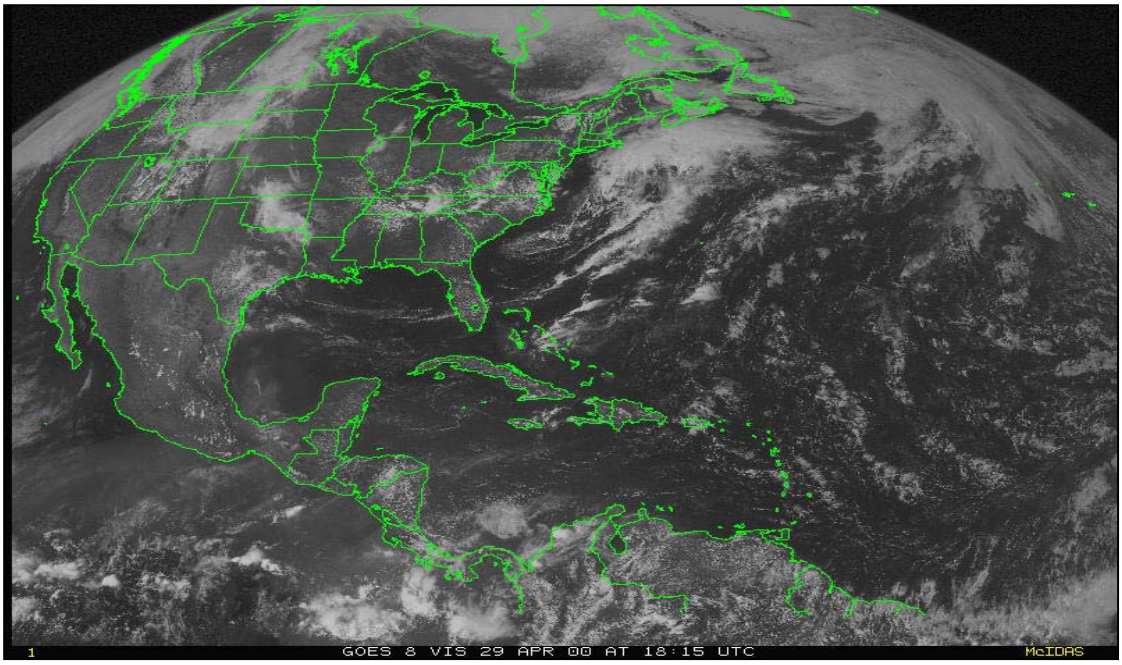

Figure 25. 29 Apr 1815Z GOES-E visible satellite image.

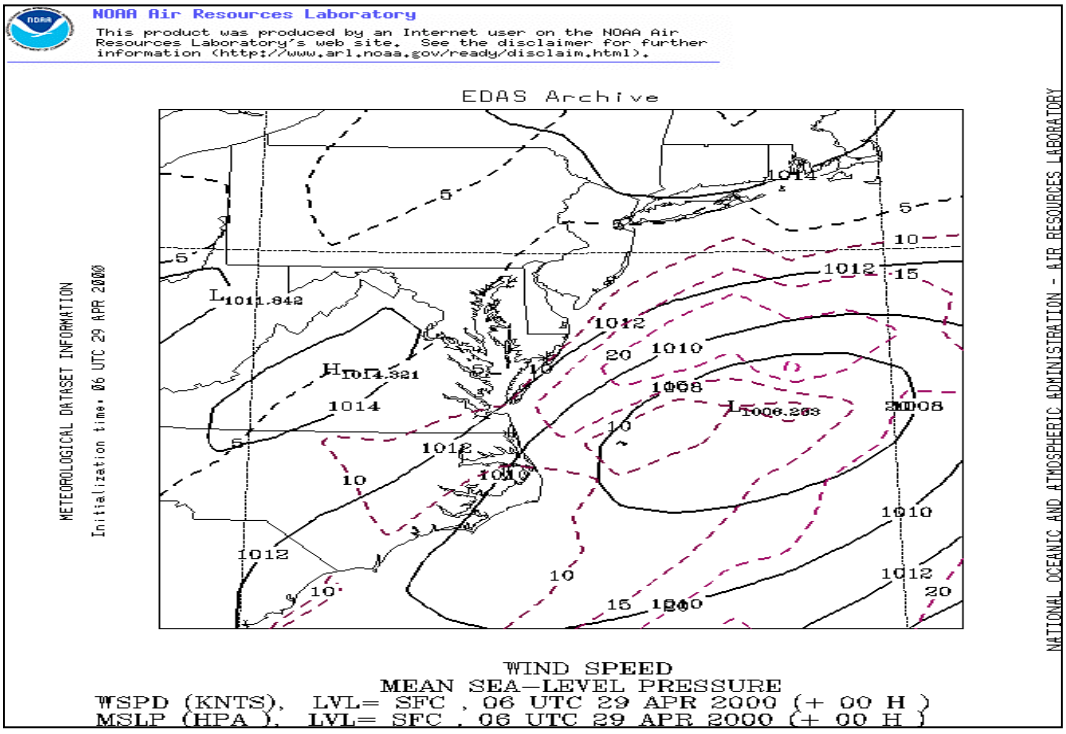

Figure 26. 29 Apr 0600Z. Synoptic chart at 2mb with wind speed.

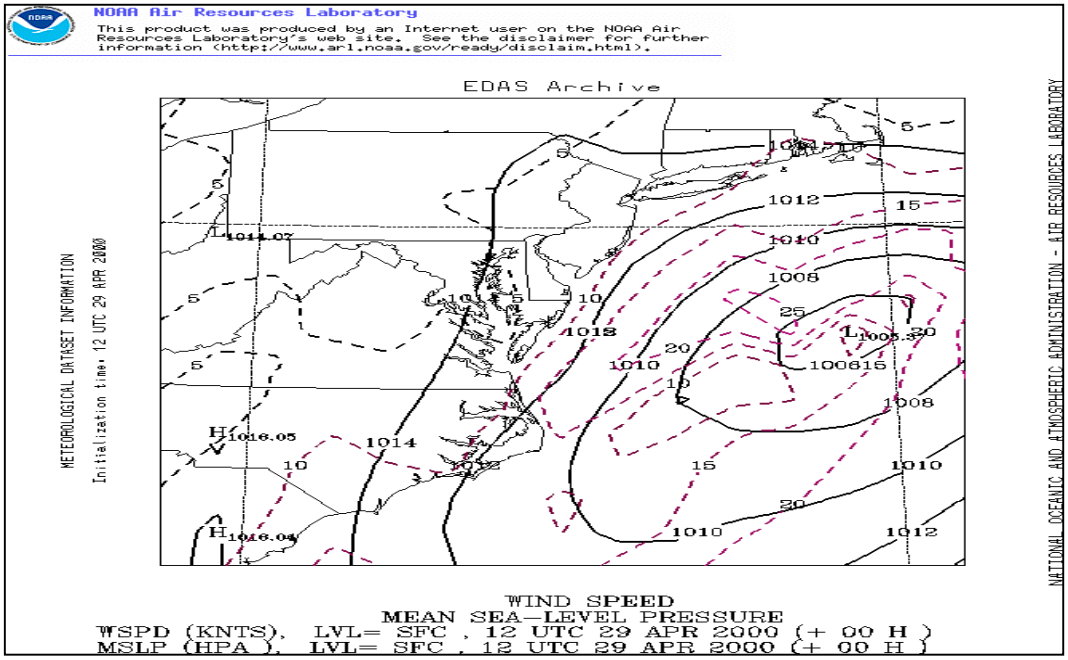

Figure 27. 29 Apr 1200Z. Synoptic chart at 2mb with wind speed.

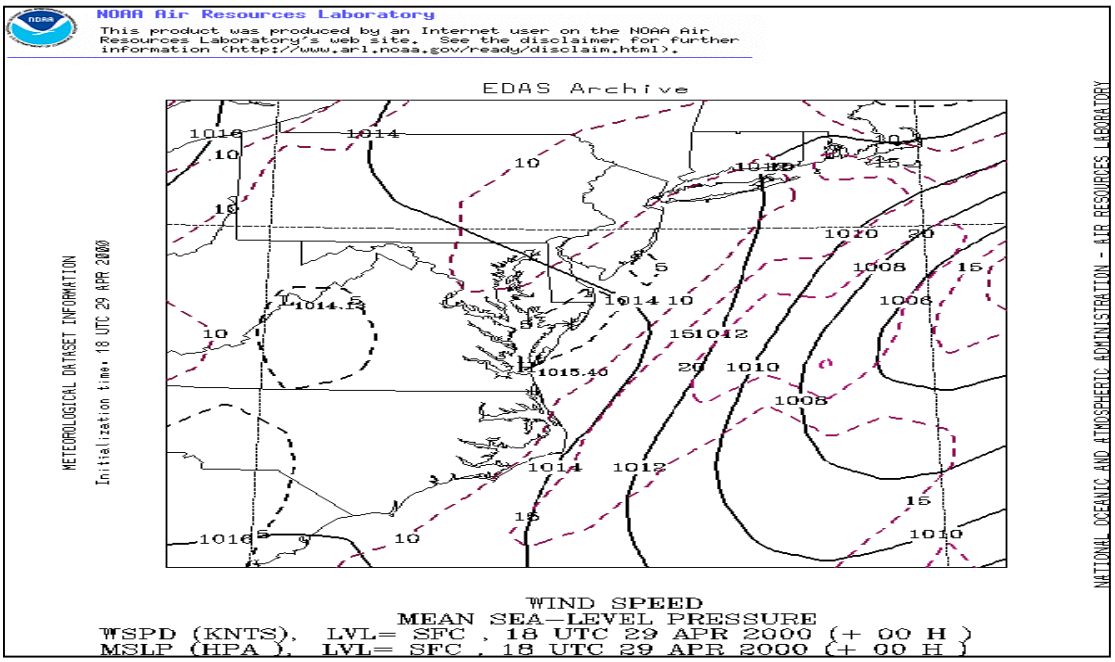

Figure 28. 29 Apr 1800Z. Synoptic chart at 2mb with wind speed.

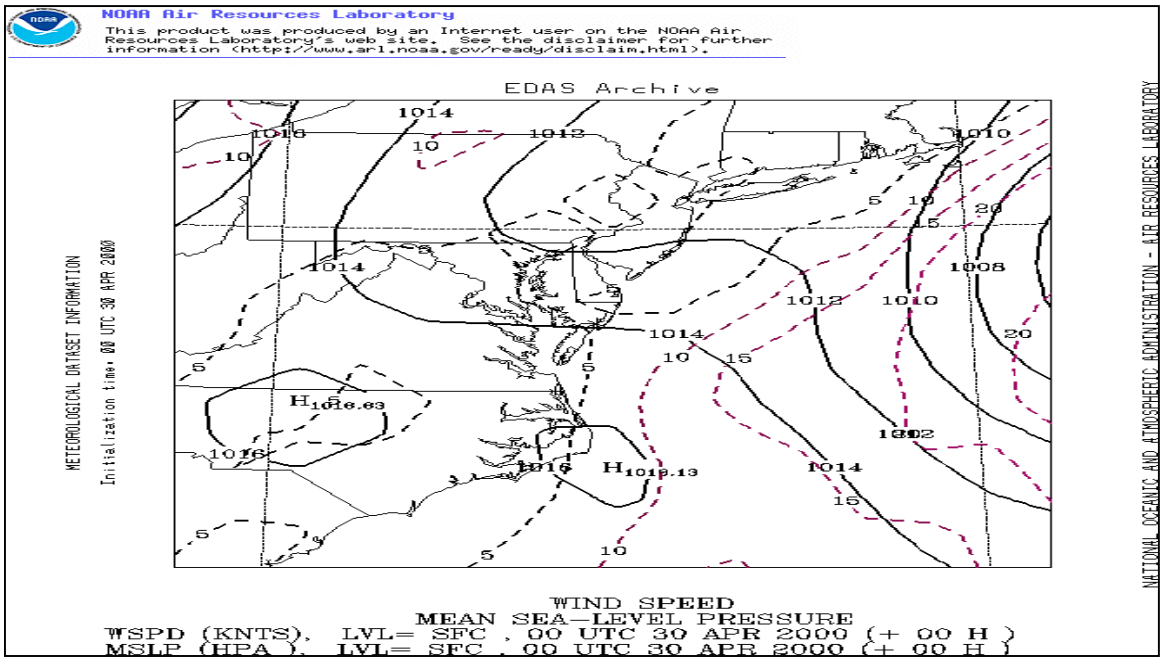

Figure 29. 29 Apr 1200Z. Synoptic chart at 2mb with wind speed.

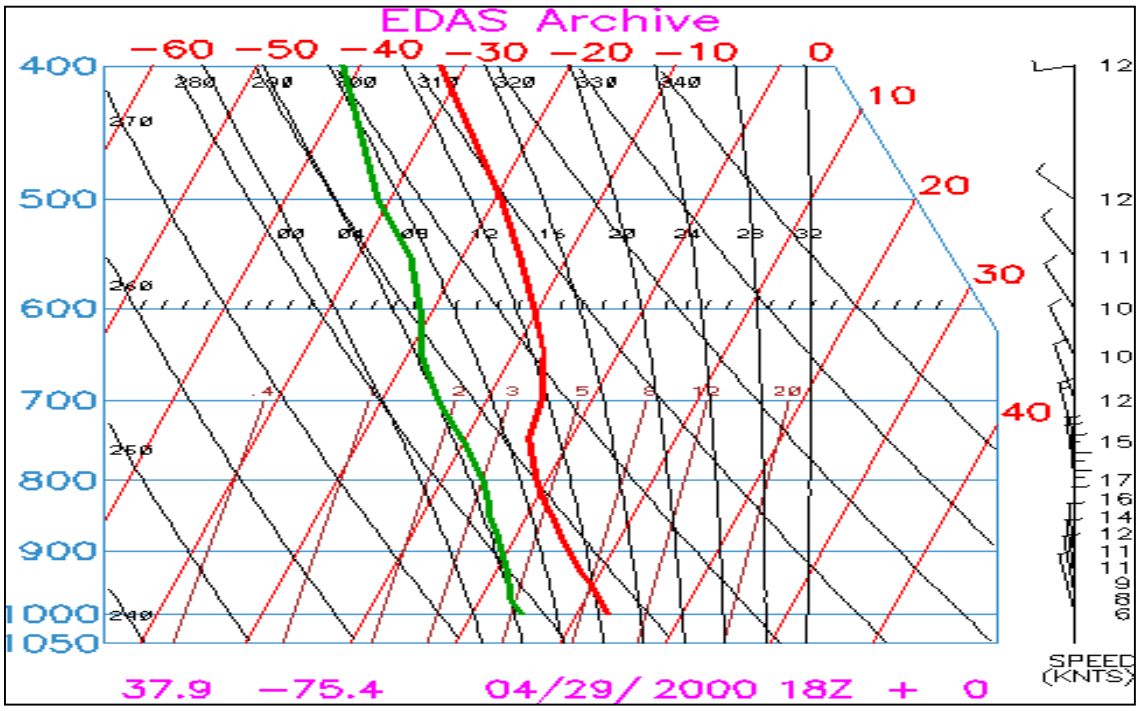

Figure 30. 29 Apr 1800Z Skew-T diagram.

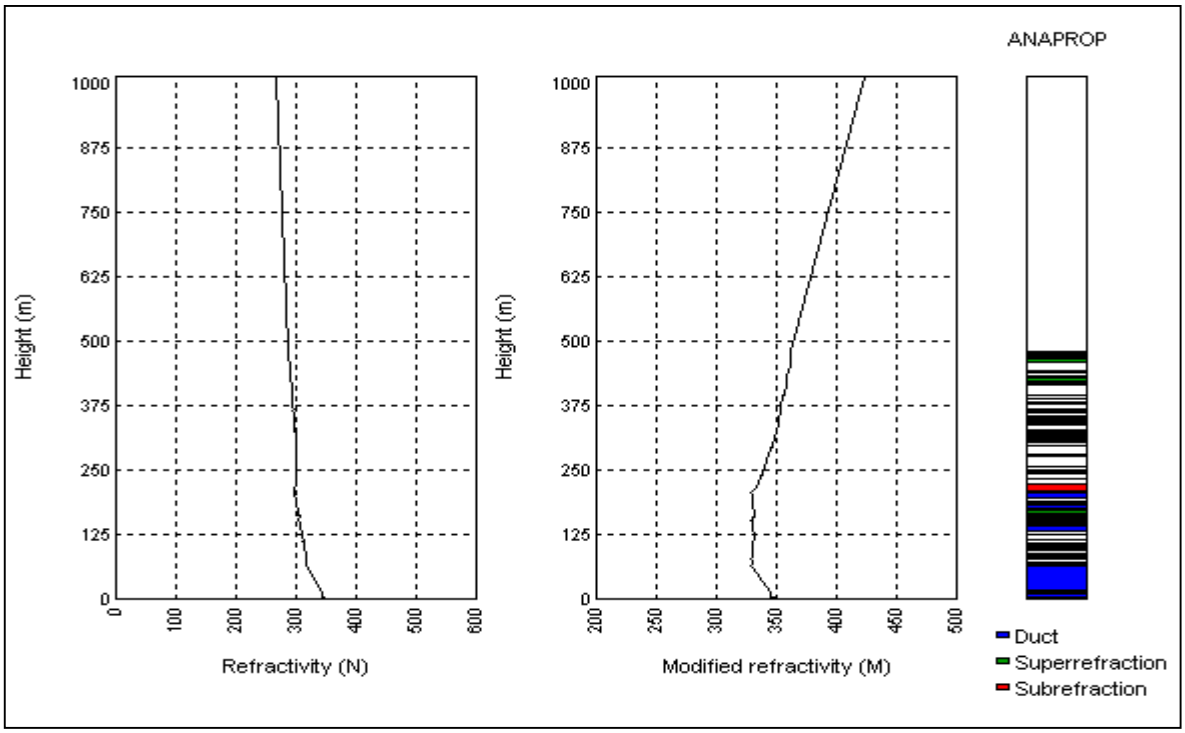

Figure 31. 29 Apr 1800Z. Refractivity diagram of M and N from EEMS.

3. 01 May 2000

The general situation is dominated by a high 1023mb, centred 200nm southeast of the AOI, which moves fairly quickly to the southeast as a frontal system moves in toward the area from the northwest (see Figs 32 and 33). The frontal system to the northwest moves slowly lying approximately 250nm to the northwest by 1800Z. The region is initially characterised by subsidence associated with the high pressure, which is slowly eroded and reduced in strength steadily throughout the day.

Surface winds over the area are initially light westerly, backing and increasing steadily throughout the day, ahead of the frontal system, to become fresh southwesterly by 1800Z (see Figs 34-37).

The main synoptic influence on the vertical profile (Fig 38) is initially the high pressure, producing subsidence and adiabatic warming. As the frontal system advances from the northwest, cloud layers at the medium and upper level are expected to begin moistening the profile. At the surface, the airflow is dry and relatively warm, conditions conducive to the formation of a relatively strong evaporative duct and possible surface ducting (see Fig 39) as the wind strength increases later in the day, resulting in a deeper mixed layer. A number of super-refractive layers and possible elevated ducts would be expected earlier in the day, due to the subsidence associated with the early ridging conditions. These features would be expected to degrade as the front, moves closer, causing a general moistening and areas of ascent.

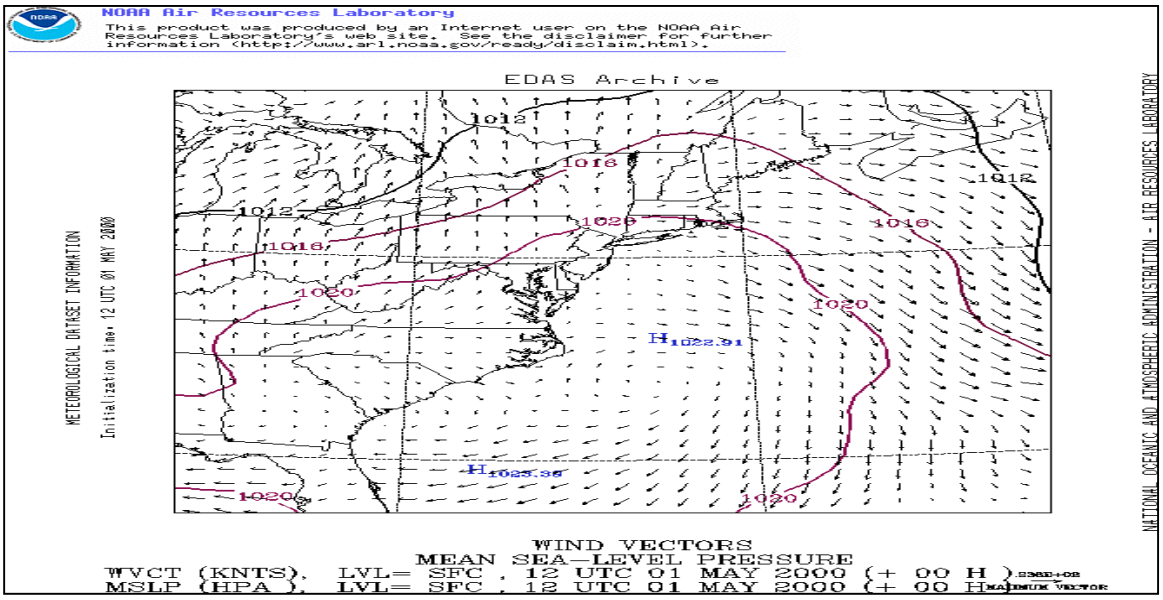

Figure 32. 01 May 1200Z. Synoptic chart at 4mb spacing.

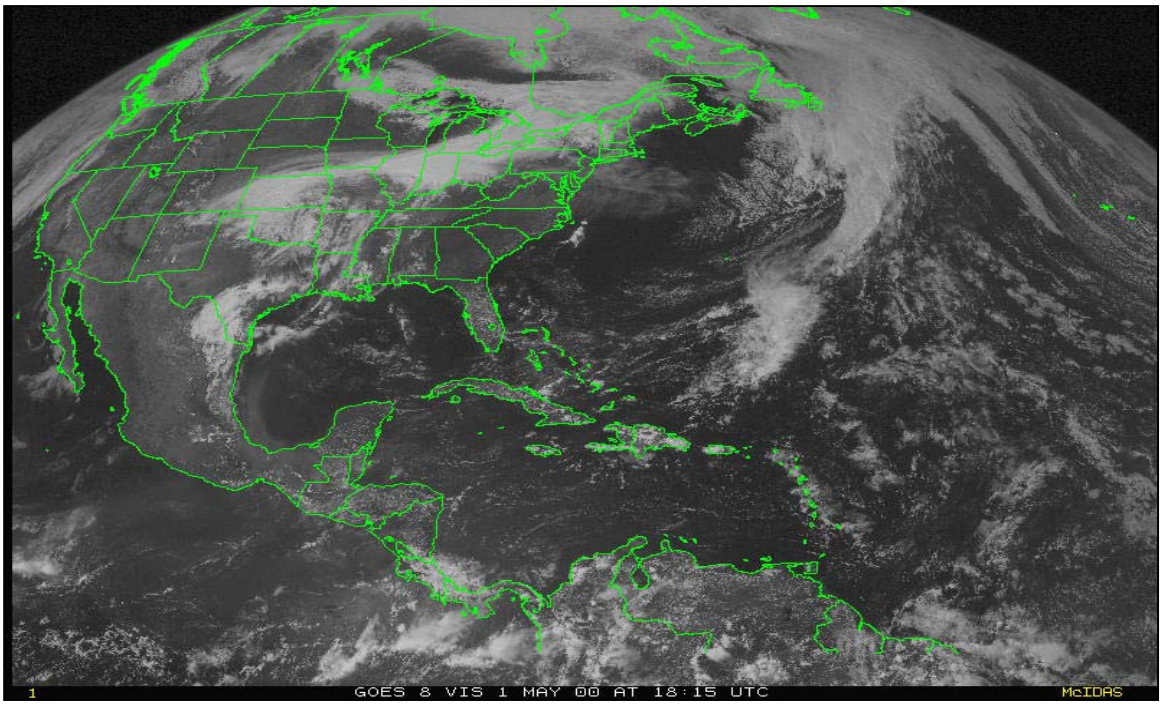

Figure 33. 01 May 1815Z. GOES-E visible satellite image.

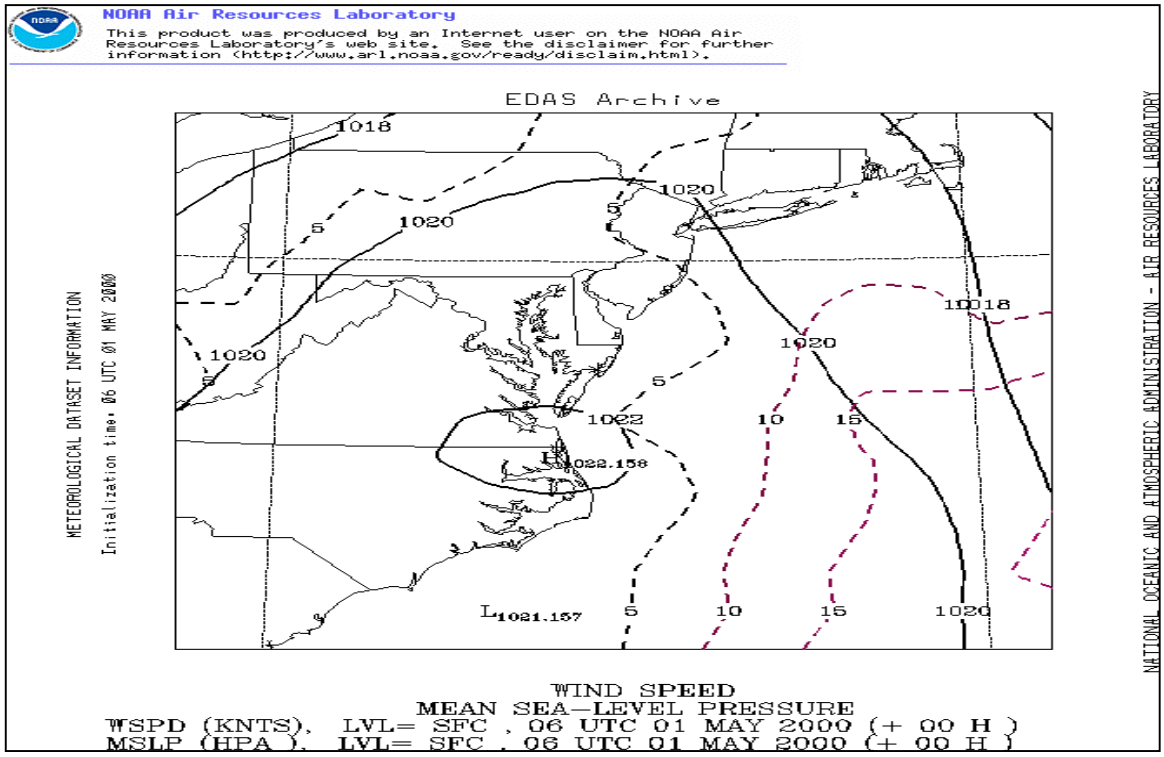

Figure 34. 01 May 0600Z. Synoptic chart at 2mb with wind speed.

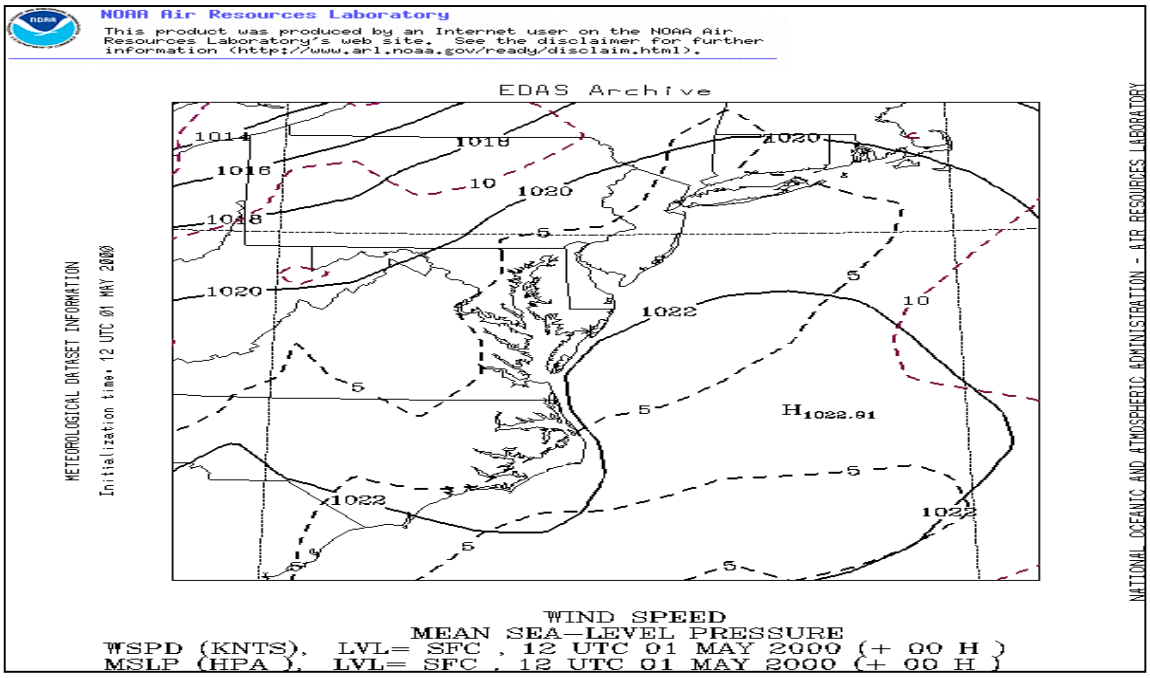

Figure 35. 01 May 1200Z. Synoptic chart at 2mb with wind speed.

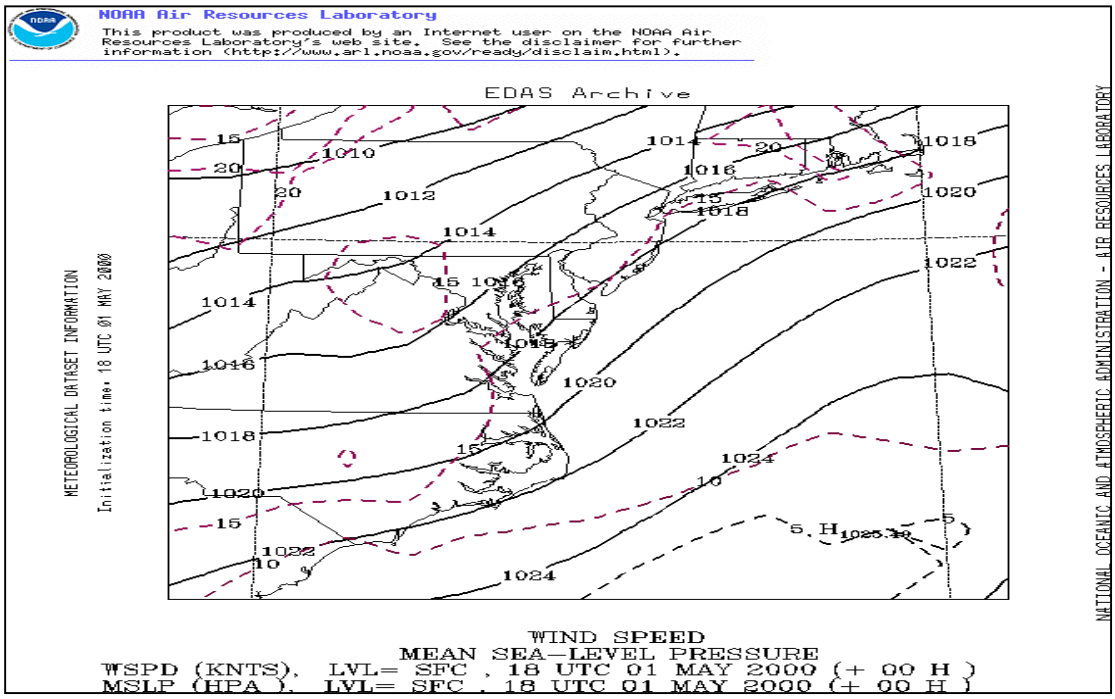

Figure 36. 01 May 1800Z. Synoptic chart at 2mb with wind speed.

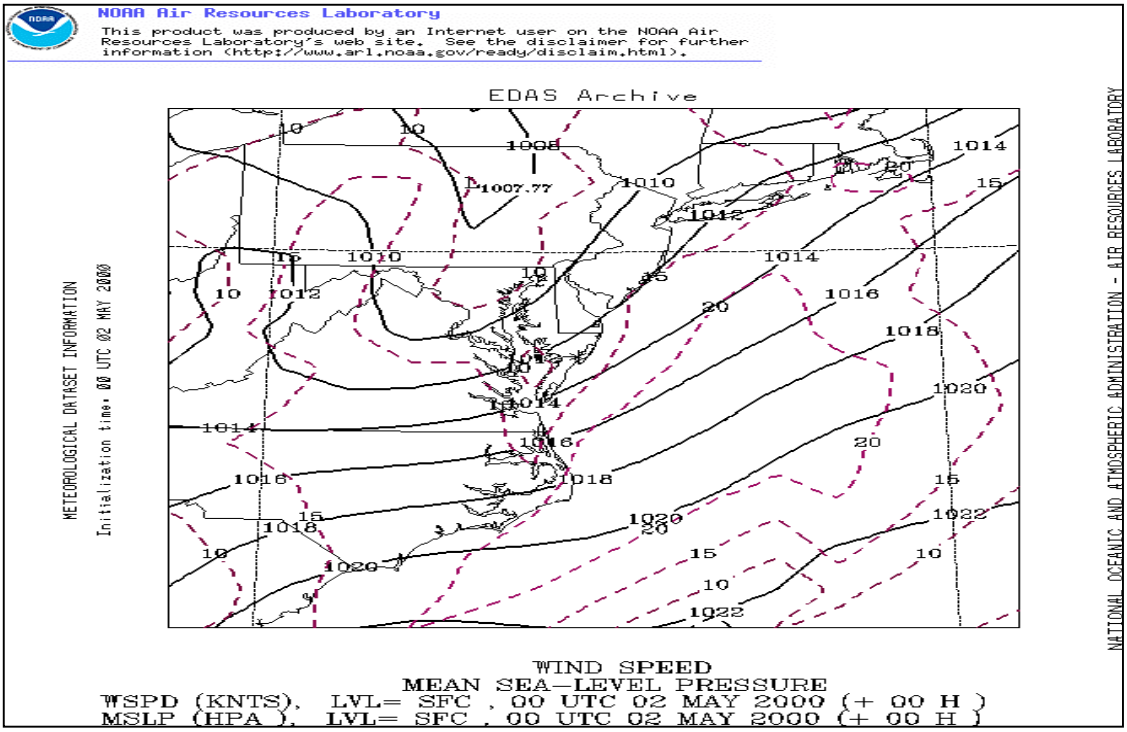

Figure 37. 02 May 0000Z. Synoptic chart at 2mb with wind speed.

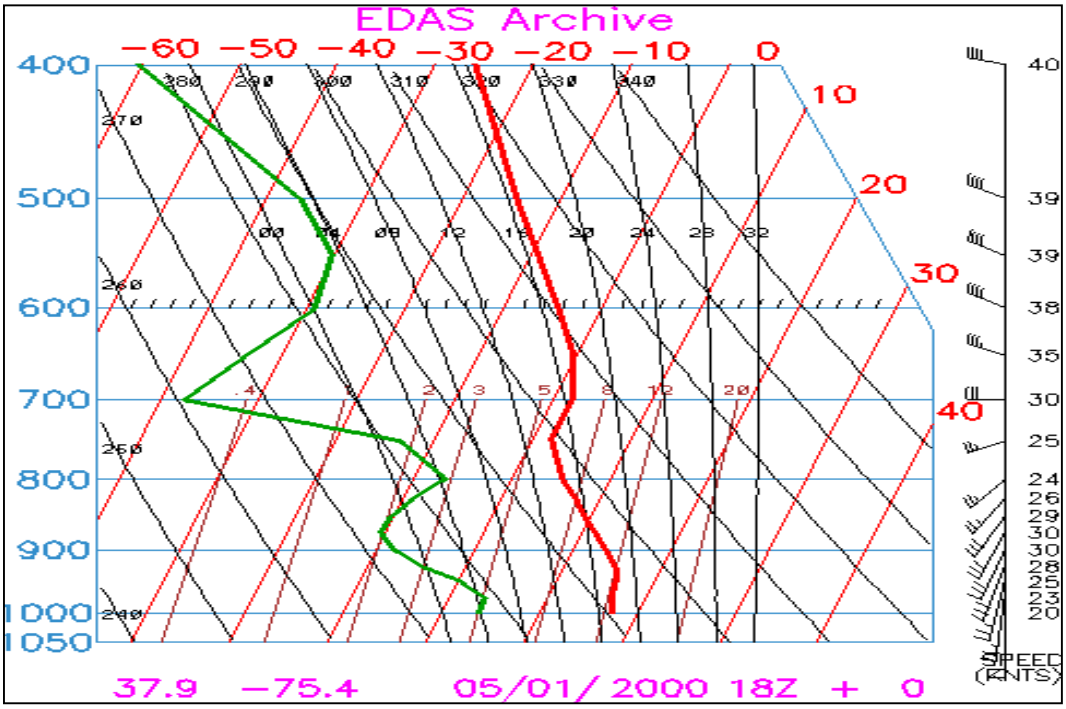

Figure 38. 01 May 1800Z. Skew-T diagram.

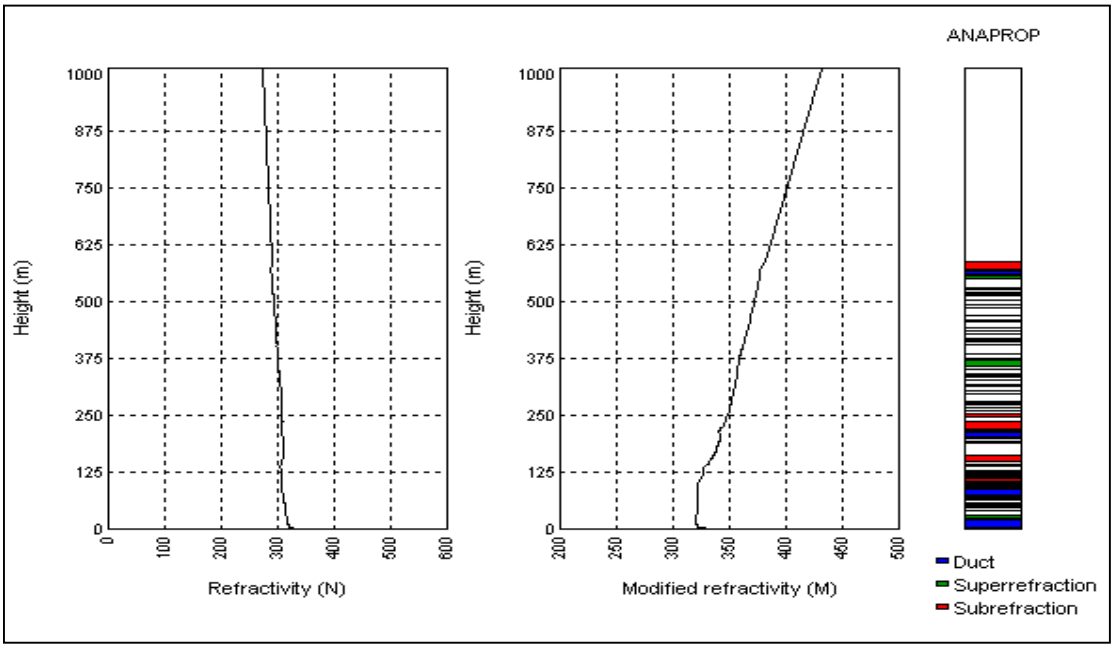

*

Figure 39. 01 May 1800Z. Refractivity diagram of M and N from EEMS

4. 03 May 2000

The general synoptic situation on this day is a cold front lying to the southeast of the area, which is moving steadily to the southeast and away from the AOI (Figs 40 and 41). High 1029mb centred over New England extends a ridge southwest over the AOI, which steadily builds during the day as the cold front progresses to the east.

Winds are initially light and variable, due to the location within the centre of the high, becoming mainly easterly and moderate by the end of the period (see Figs 42-45).

A stable, dry profile throughout the majority of the atmosphere would be expected (see Fig 46) as the ridge builds and general descent becomes dominant. Adiabatic warming associated with the descent will give super-refractive layers and possible elevated ducts, which may descend close to the surface, allowing a surface based duct to develop (Fig 47).

The surface flow initially originates from the northeast, producing some potential instability in the lower layers, though the lack of wind and the sea track will limit the development of a strong evaporation duct.

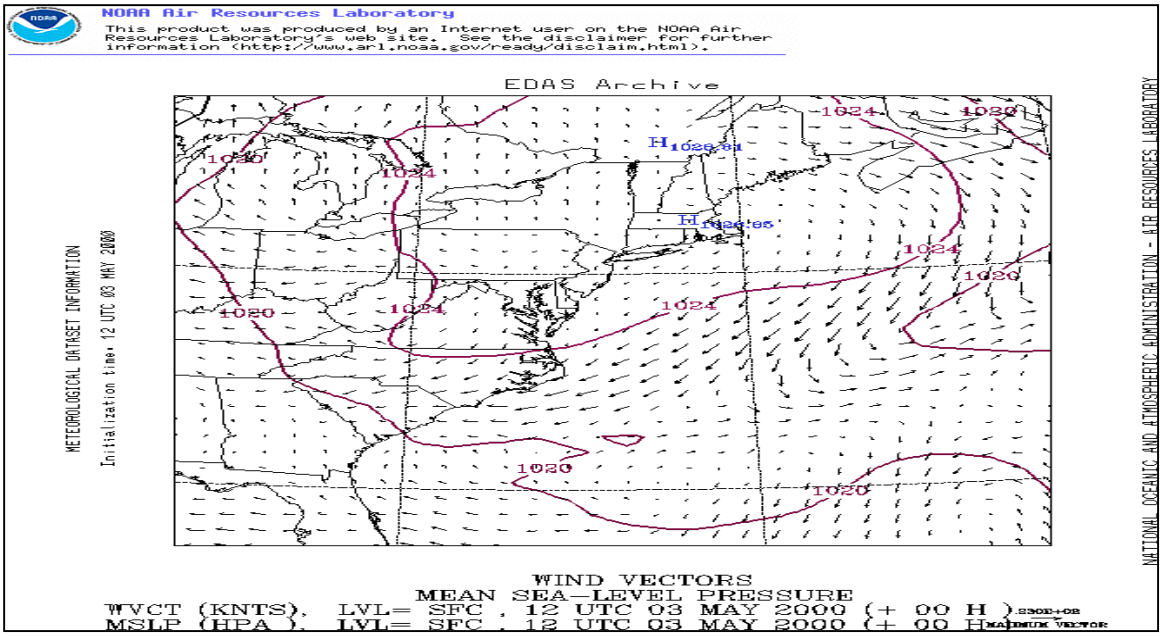

Figure 40. 03 May 1200Z. Synoptic chart at 4mb spacing.

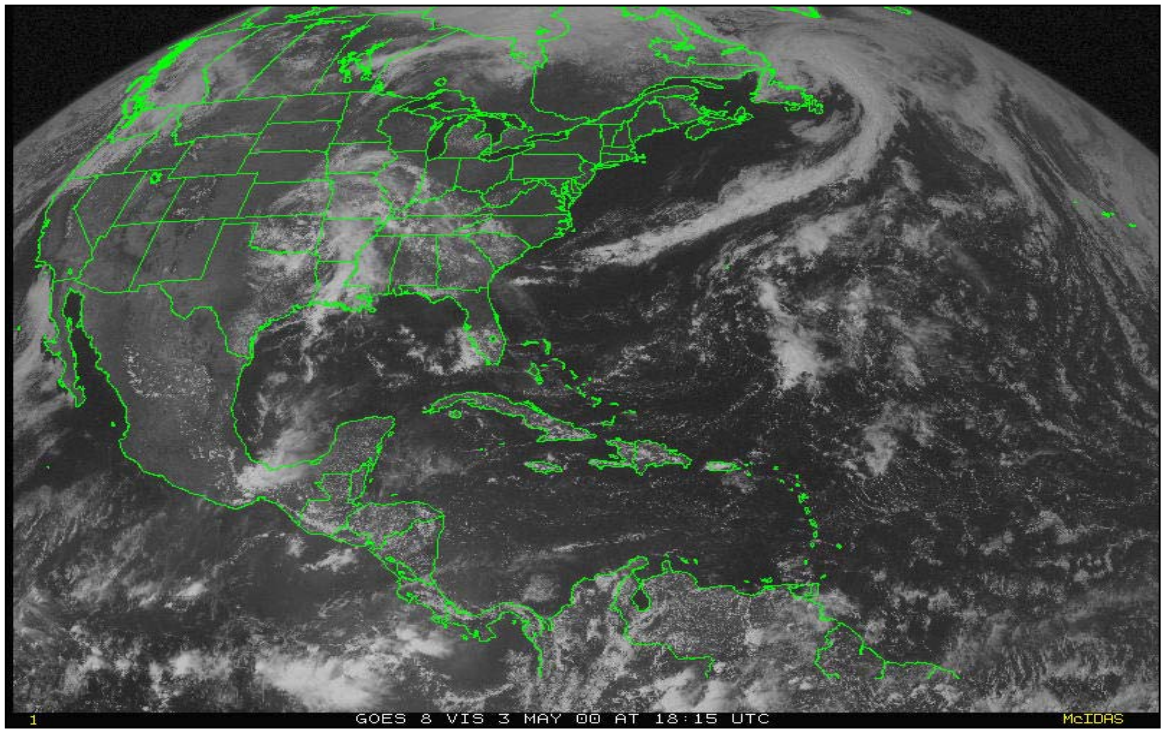

Figure 41. 03 May 1815Z. GOES-E visible satellite image.

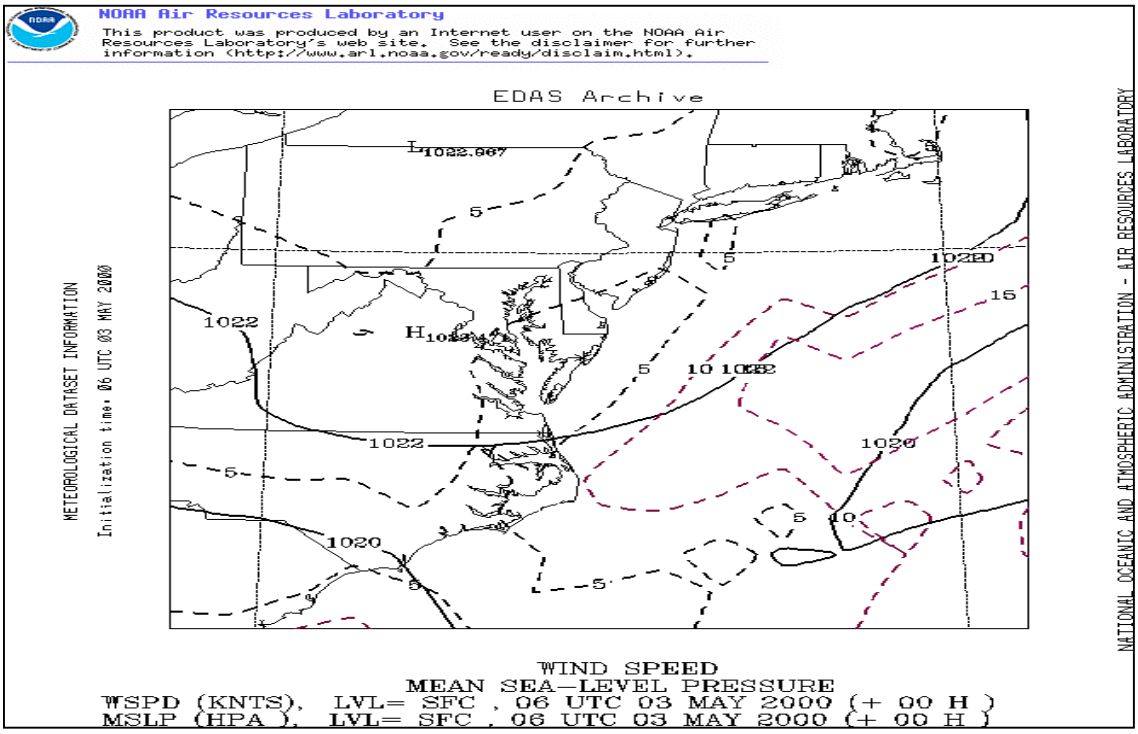

Figure 42. 03 May 0600Z. Synoptic chart at 2mb with wind speed.

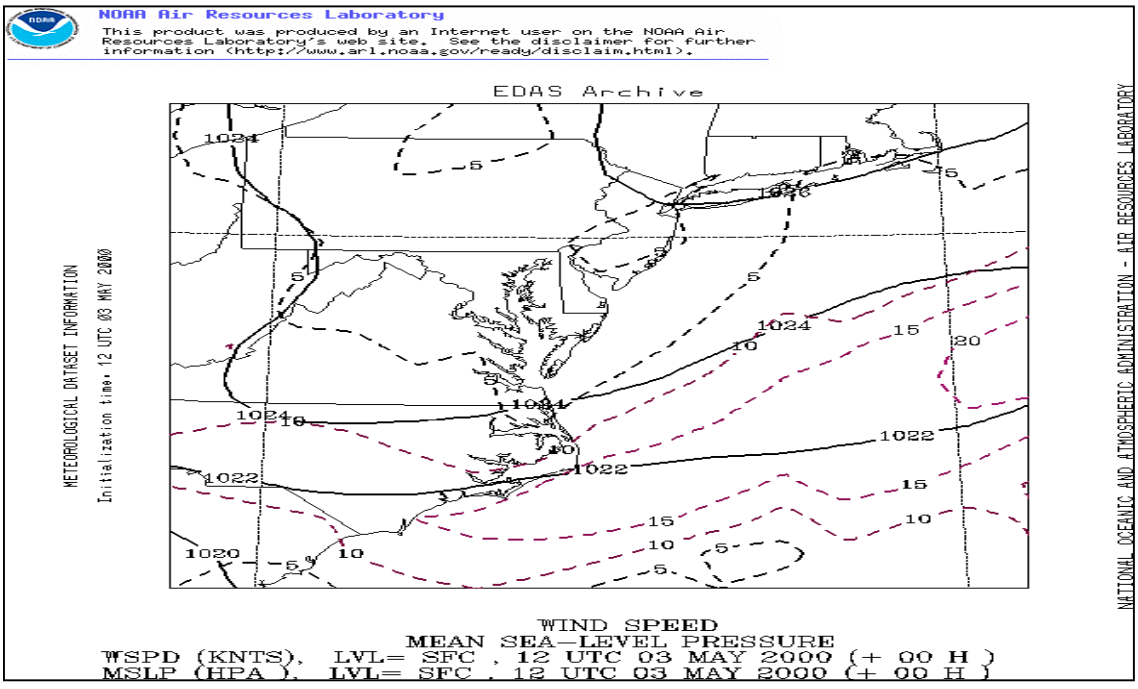

Figure 43. 03 May 1200Z. Synoptic chart at 2mb with wind speed.

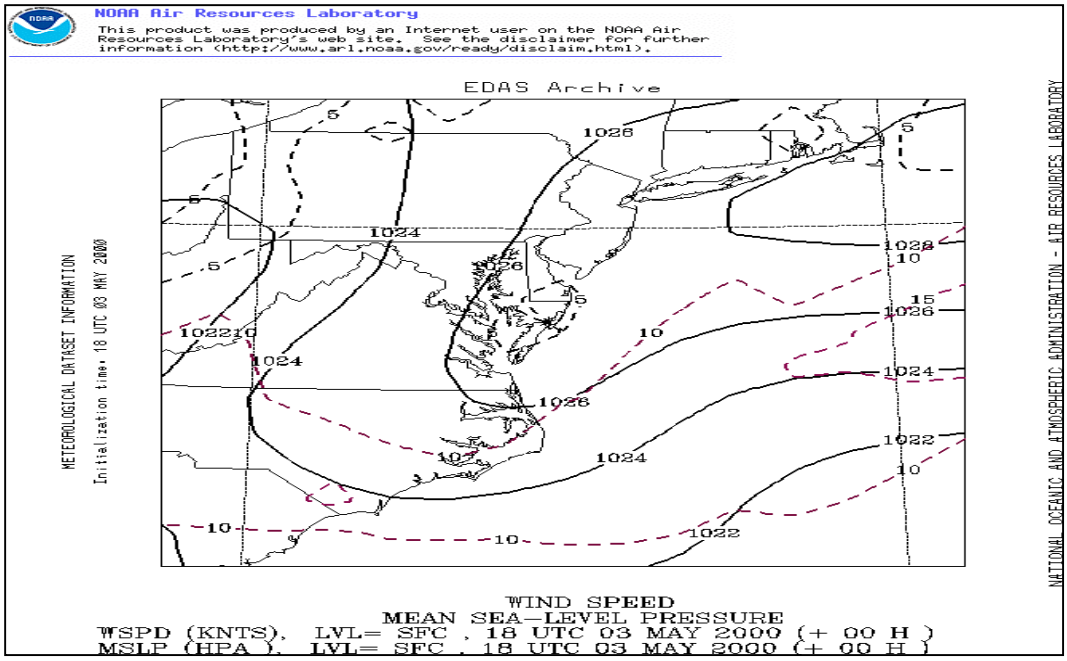

Figure 44. 03 May 1800Z. Synoptic chart at 2mb with wind speed.

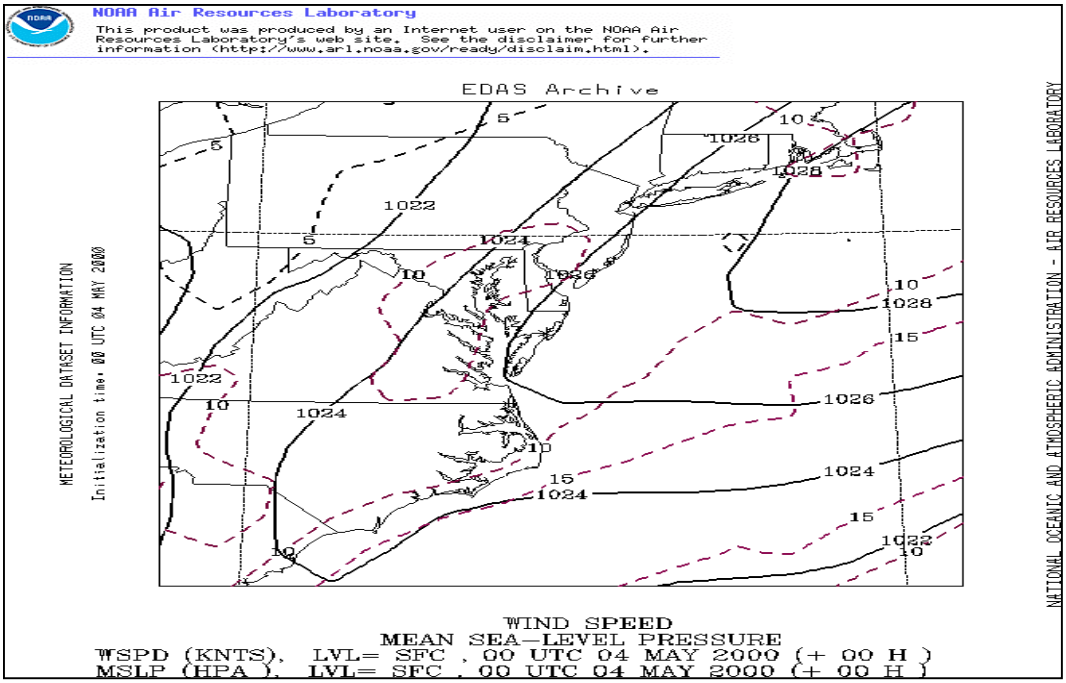

Figure 45. 04 May 0000Z. Synoptic chart at 2mb with wind speed.

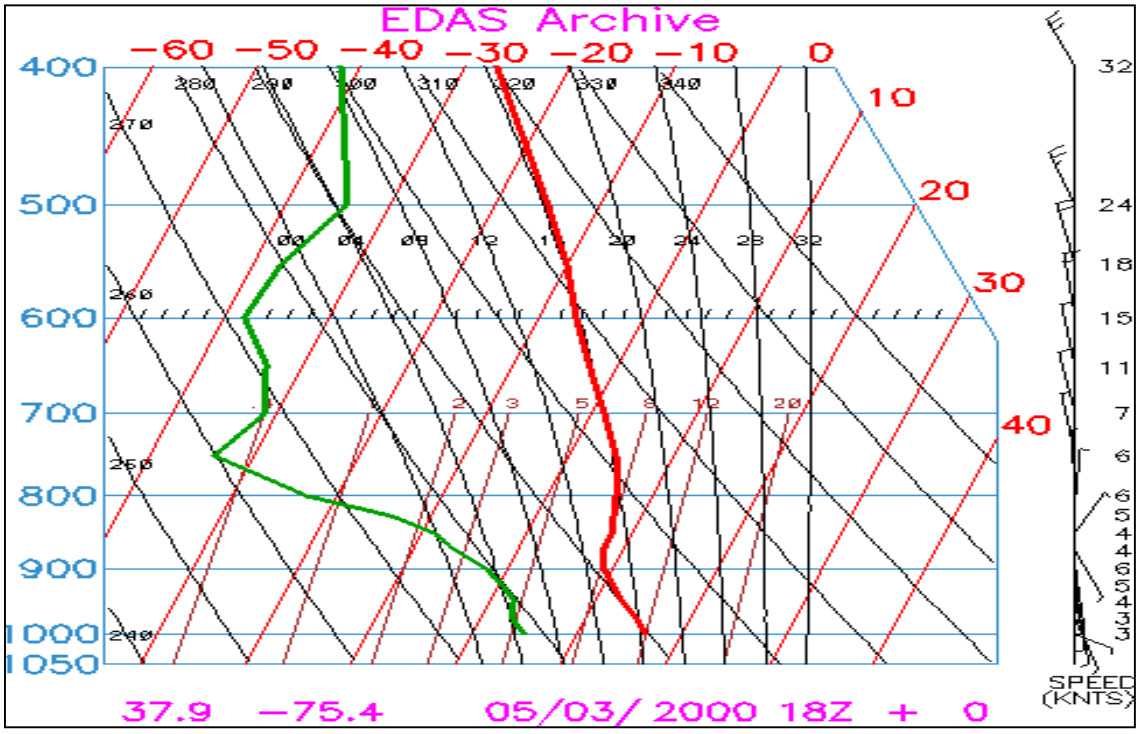

Figure 46. 03 May 1800Z. Skew-T diagram.

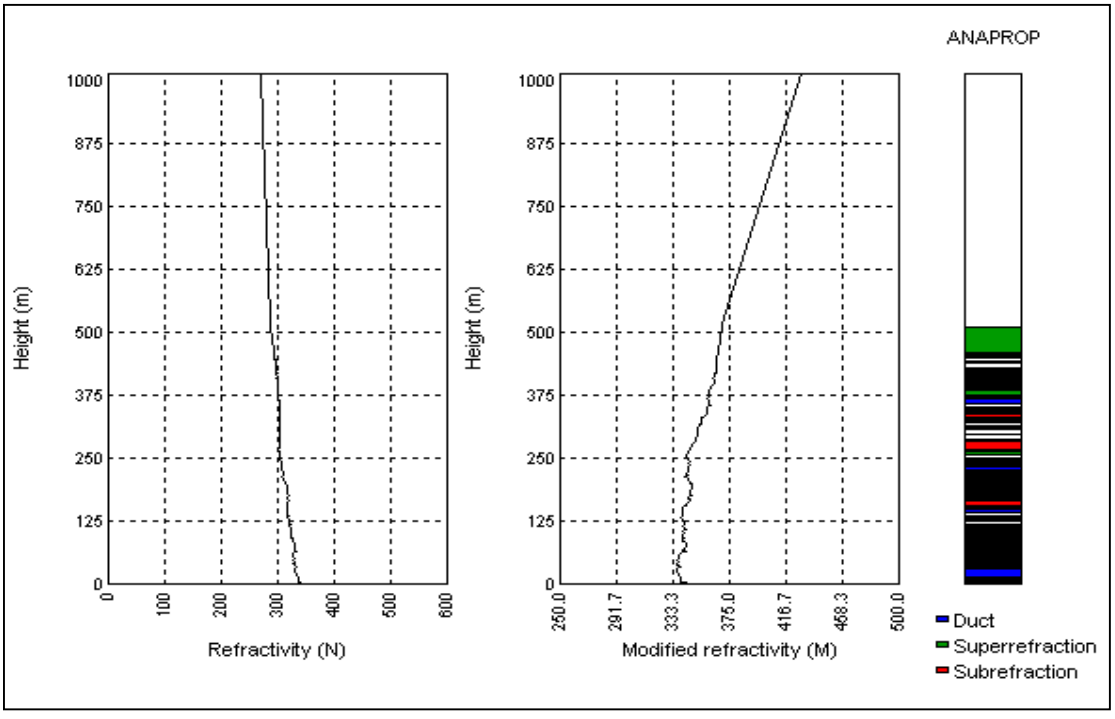

Figure 47. 03 May 1800Z. Refractivity diagram of M and N from EEMS.

THIS PAGE INTENTIONALLY LEFT BLANK

X. PROPAGATION EFFECTS ANALYSES

A. PROPAGATION MODEL (EEMS/AREPS) INPUTS

1. Environmental Inputs

Both rocketsonde and bulk evaporation duct model refractivity profiles (calculated from the NPS flux buoy data) described the atmosphere for the selected periods that relate observed propagation factors to the observed atmosphere. Several steps, not normal operational procedures, were deemed necessary to merge the two descriptors. First, each of the four rocketsonde soundings from the four days of 10th and 29th April, 1st and 3rd May were edited using a tested MATLAB algorithm designed to remove invalid lines from the sounding file. This was necessary to create a file readable by the environmental program within each propagation model (ascending soundings, duplicate pressure levels, soundings below sea level, etc. were corrected).

The edited profiles were formatted and stored for use as the input file for the EEMS/AREPS environmental programs. Because of the importance of EEMS/AREPS to the results of this study, the procedures used to prepare the data and the procedures used in obtaining results will be identified as they are within the application of EEMS/AREPS.

2. EEMS

The advanced or "In-depth" mode of EEMS was used throughout this study. The rocketsonde profiles were loaded into the "environment" section as M versus height profiles. The meteorological inputs of SST (float), air temperature, relative humidity, wind speed, and atmospheric pressure were all input to calculate the evaporation duct using correct station height data for the NPS buoy. This duct was then appended to the rocketsonde profile, using the option within EEMS, which merges the evaporation duct with the upper air profile.

Once complete a research set-up was used to input the transmitter parameters, frequencies and platform details into the model, which were then saved for multiple runs.

The model was then run at specific frequencies and heights to produce a number of coverage, propagation factor and loss curve diagrams.

3. AREPS

First, the "custom columns" feature of the environmental program was used to create individual M-unit versus height profile which were then saved in an .ENV file for use in AREPS. Once complete, two methods were then used to assess the effect of the evaporation duct:

- Firstly, the meteorological data was input and the Paulus-Jenske evaporation model option checked, which appends this calculated duct to the rocketsonde profile.
- Secondly, the surface data was input and the Naval Postgraduate School evaporation duct model option checked. This model is not appended to the upper air profile, but merely appends a standard atmosphere above the duct.

Once each type of run was set-up, again using the research mode, the appropriate, transmitter data was input and the frequency selected. A series of runs were then made using different combinations of height and frequency to simulate the MPMS II data.

4. RF System Inputs

As already discussed the research/in-depth modes of each model were used to recreate the MPMS II system using the parameters listed in Table 4. In order to make the "one-for-one" comparison of the AREPS output with the MPMS II measurements, the principle of reciprocity was applied. During the propagation tests all transmitters for the MPMS II system were aboard the *R/V Sealion*, and varied in height from 1 to 10m (3 to 33 ft) and the receivers were on the shore. The S-band (3.7 GHz) receiver was at 18.3 m (61 ft) and the X-band (9.3 GHz) receiver at 31.4 m (104 ft). The principle of reciprocity allows the one-way propagation loss and propagation factor to be computed while assuming the transmitter and receivers are in the opposite placement. That is, both EEMS and AREPS computed propagation loss with the transmitters on shore at 18.3 m (61 ft) for S-band, and at 31.4 m (104 ft) for X-band, and the receiver varying in position from 1 to 10 m (3 to 33 ft).

The EEMS and AREPS propagation loss fields were "sliced" at the 1.8 m (6 ft), 6.4 m (21 ft) and 9.1 m (30 ft) altitudes using the "propagation loss vs. range" output option. The 1.8 m height was selected to correspond to the terminal phase of a typical sea-skimming anti-ship cruise missile. The 6.4 m and 9.1 m heights were somewhat arbitrary, intended to sample the remaining part of the column evaluated by the MPMS II. Neither, EEMS or AREPS could produce a three-dimensional propagation loss or propagation factor field that could be directly compared with the three-dimensional field provided by the MPMS II system. However, two-dimensional slices from EEMS and AREPS and MPMS II could be created for comparison. The propagation loss data and free-space reference data from EEMS and AREPS were then saved to files for comparison to the MPMS II files. The AREPS propagation factor coverage diagrams presented in the next two chapters were produced by saving the propagation loss data to an output file, converting the data to propagation factor, and plotting as a contour diagram using MATLAB.

B. MPMS II DATA

The MPMS II data was provided by NSWC-DD, courtesy of Janet Stapleton. These data consisted of three-dimensional data arrays containing height, range and propagation loss. As neither EEMS nor AREPS could match the output method of MPMS II, it was necessary to reduce the data to individual two-dimensional slices. Range versus propagation factor vectors were extracted from the 6, 21 and 30 ft array rows. MATLAB was then used to display the MPMS II loss curves against the computed EEMS and AREPS loss curves.

THIS PAGE INTENTIONALLY LEFT BLANK

XI. PROPAGATION MODEL RESULTS VERSUS MPMS II

A. INTRODUCTION

The following section details the results from propagation model predictions using available METOC data with the EEMS and AREPS TDA', as previously described in Chapter X. The presented results address the modeling of the atmosphere influence (with EEMS and AREPS), the predicted and observed propagation effects in terms of coverage diagrams and loss curves, and the frequency affected (S-, and X-band) by the atmospheric influences. The same atmosphere input was used in all cases even though the bulk models used to derive the profile and the profile merging approaches differed.

Results are presented separately for each day and include:

- EEMS propagation coverage diagrams for 0-80nm and to 0-1000ft for S and X bands.
- EEMS propagation coverage diagrams for 0-40nm and 0-35ft for S and X bands (low-level, for direct comparison with MPMS II results).
- MPMS II propagation coverage diagrams for 0-40nm and 0-35ft for S and X bands.
- Propagation loss curves showing results from EEMS, S and X bands at 6, 21 and 30ft.
- AREPS propagation coverage diagrams for 0-80nm and 0-1000ft for S and X bands, using both the Paulus-Jenske evaporation duct calculation with rocketsonde data appended, and the NPS evaporation duct model only.
- Combination propagation loss curves for EEMS, AREPS (PJ), AREPS (NPS), MPMS II measured data, free space, and standard propagation curves for each model.

A discussion of the results from EEMS is the first presented for each day, comparing model performance against actual measured results, from MPMS II, with particular reference to frequency. A discussion of performance results for AREPS using the Paulus-Jenske ED model merged with the rocketsonde profile, AREPS (PJ), and AREPS with the NPS ED model with no merging with a rocketsonde derived profile, AREPS (NPS), follows the discussion of EEMS performance results. Finally, discussion of combined results, EEMS, AREPS (PJ) and AREPS (NPS) completes the performance discussion. An important consideration in the analyses/interpretation will be to evaluate the need for the AREPS (NPS) to have the ED-upper level profile merging. It is

important to emphasise that the premise of this thesis is to simulate model performance under operational type scenarios. The presented errors and critique are not intended as an indictment of model performance. The fact that both EEMS and AREPS both fail on occasions to replicate the MPMS II observations could have less to do with the abilities of the models, than with the spatial and temporal complexities of environment, and the method by which it has been sampled and analysed.

For reference purposes Figure 48 shows the main features of the propagation loss curve, the interference, diffraction and troposcatter zones.

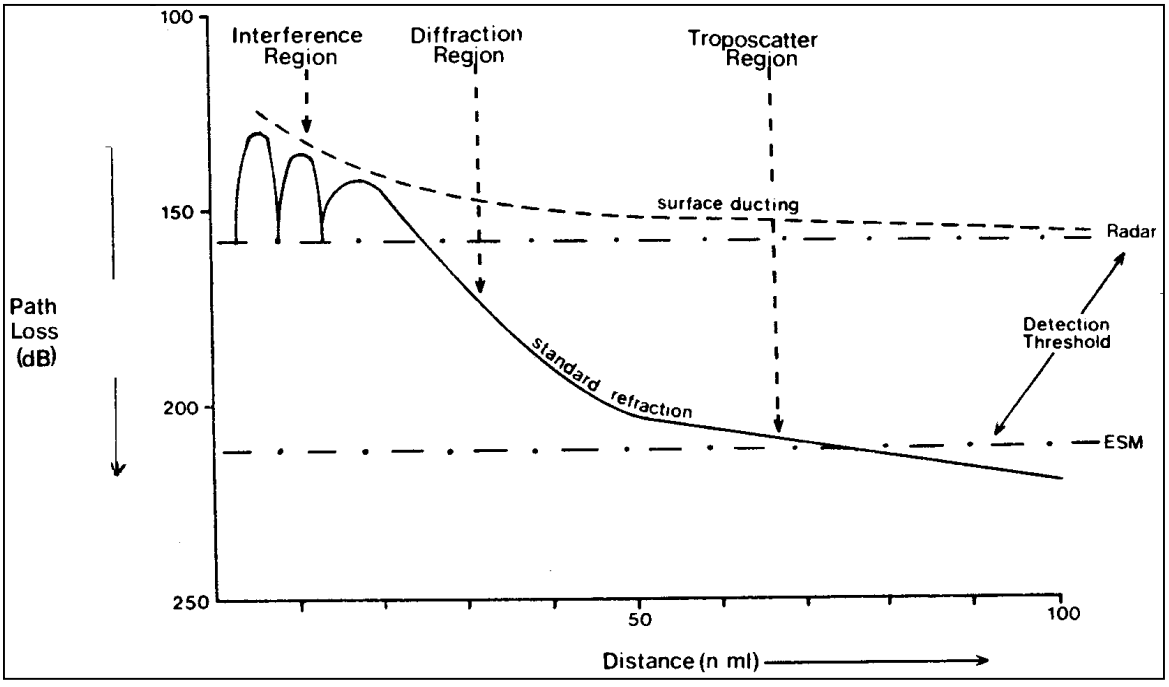

Figure 48. Path loss curve for a near-surface transmission path.

B. DISCUSSION OF RESULTS

1. 10 April 2000. S Band

The 10th April had little evidence of the existence of a surface based duct. It was, however, characterised by fairly strong humidity gradient above the surface, resulting in above average propagation due to the evaporation duct (ED). Although there was no marked strong surface based ducting (SBD) there was super refraction above the ED (see Fig 23 in Chap IX).

The coverage diagrams for S-Band, from EEMS and AREPS (PJ), Figs 49-50 and 51-52 show small range extensions due to the ED and the overlying super-refractive layer with stronger horizontal energy propagation in the near surface zone. Both models predict conditions of above average radar propagation range, by virtue of the calculated ED height (EEMS, 11.4m and AREPS (NPS), 8.2m). AREPS (PJ), however, qualifies as an average radar weather category, by virtue of a calculated 6m evaporation duct. It is noted that another difference, besides different bulk models for the evaporation duct, between these two AREPS predictions is that AREPS NPS only has the evaporation duct as an influencing factor while AREPS PJ has the Paulus-Jenske evaporation duct merged with the rocketsonde profile.

At low-levels, it can be seen that the MPMS II (observed) loss (Fig 53) results show a clear interference pattern with distinct nodes and anti-nodes (seen as alternating zones of high and low loss), which are also evident in the EEMS modelled results, but at slightly different locations (Figs 49 and 50). The comparison of propagation loss curves demonstrates significant differences in the modelled propagation at low-levels (see Fig 54). At ranges less than 8 nm, and at both 21 and 30ft, AREPS (PJ) and EEMS show significant interference patterns in the near field, with the EEMS pattern being significantly more pronounced. At distances greater than 8nm, EEMS and AREPS (PJ) are in close agreement (within 3dB at 30ft) although this difference widens with altitude (4-6dB at 21ft). EEMS agrees best with observed results (MPMS II), although by 35nm it over-estimates the loss by 10-12dB, too much with respect to most operational criteria. AREPS (NPS), which includes effects of ED only, diverges very quickly from the MPMS

II results (and also the EEMS and AREPS (PJ) model predictions), over-predicting the loss by 15-18dB at 10nm and 30-35dB by 35nm.

Closer to the surface, at the 6ft height, all three model predicted losses diverge even further, with EEMS again agreeing best with the observed (MPMS II), The low level relatively good performance of EEMS modelled propagation loss does not apply to ranges within the near field interference pattern but almost coincides with the MPMS II loss patterns after 10nm., albeit slightly smoother. In this longer-range region, AREPS (PJ) predicts greater losses of 13-15dB, whilst AREPS (NPS) over predicts even greater losses of 10-12dB.

2. 10 April 2000. X Band

At this higher frequency, the effects of different evaporation duct (ED) bulk models within the propagation models are much more apparent (in Figs 55-58), as expected since higher frequencies are more sensitive to the evaporation duct. The EEMS bulk model specifies an ED, which will trap nearly all of the X band energy, whilst the NPS model specifies an ED, which is close to having a significant effect on X-band. The Paul-Jenske model specifies a weaker ED, which, in turn, has the least effect on X-band, ducting the least energy. The respective coverage diagrams clearly demonstrate this specified duct strength versus effect factor. The EEMS generated coverage diagrams (Fig 55 and 56) show multi-path interference patterns with significant node and anti-node patterns, a significant anti-node occurs at 18nm with a reciprocal node at 26nm. Neither of the AREPS (PJ or NPS) produced coverage diagrams (Figs 57 and 58) containing such features. The observed (MPMS II) coverage diagram for X-band (Fig 59) also indicates significant multi-path interference patterns throughout. A significant anti-node occurs at 20nm and an anti-node at 25-28nm. The MPMS II pattern contains several weaker such multi-path patterns throughout the diagrams at a number of different heights.

The generated propagation loss diagram (Fig 60) reveal that the EEMS model has a much more complex interference pattern than AREPS (PJ and NPS), Fig YY, and diverges most from the MPMS II loss curve, this becoming most pronounced at 6ft. Further, it is clear that the MPMS II profile also exhibits considerable multi-path interference structure. The MPMS II amplitude extrema are not as pronounced as in the

EEMS generated loss curves, or at the same locations. This is expected, as always, because MPMS II curves reflect sample averages. EEMS does however converge with MPMS II by 35nm.

Neither AREPS (NPS nor PJ) runs exhibit the interference patterns observed in the MPMS II data, but do more closely follow the mean of the loss curve out to 20nm, apart from a significant null at 8nm. By 35nm AREPS (PJ) is 8-10dB under-predicting at 30ft and 18-20dB at 6ft. AREPS (NPS) fares much better, almost exactly flowing the mean curve at 21 and 30ft, and only being 3-5dB too low at 6ft.

3. 29 April 2000. S Band

The primary influencing refractivity feature for this case was a strong surface based duct (Fig 31 in Chapter IX). Both EEMS and AREPS (PJ) address the surface-based duct influence by including the rocketsonde profile, but with differences in the merging of it with the ED. Both these models are expected to perform better than AREPS (NPS). Referring to the coverage diagrams for EEMS and AREPS (PJ) (Figs 61 and 63), both account for the surface based ducting and have a number of skip zones throughout the range up to a height of approximately 200ft. AREPS (NPS) (Fig 64), by virtue of considering only the ED, cannot replicate the surface-based ducting pattern, and would thus be expected to perform the poorest of each of the model runs. Interestingly, the MPMS II coverage diagram exhibits little evidence of ducting or multi-path interference patterns within the first 20nm of the run, indicating perhaps that the surface-based ducting strength reduces significantly toward the shore, as would be expected from the off-shore flow regime. Both AREPS (PJ) and EEMS are thus expected to under-predict the loss initially, whilst AREPS (NPS) will over-predict the loss.

Examining the propagation loss curves (Fig 66), they indeed demonstrate considerable multi-path interference patterns for both the EEMS and AREPS (PJ) runs. Both models predicts too low a loss at 35nm by up to 20-25dB at 6ft. AREPS (NPS) predicts too high loss 5nm and seaward, reaching an error of over 40dB by 30nm. This clearly shows the need to have a merging of the ED with profiles in order to get reasonable propagation predictions at longer ranges, beyond 10 nm.

Whilst both AREPS (PJ) and EEMS appear to have too much amplitude in interference patterns, a spatial smoothing of these loss curves would actually cause them to be relatively close out to 25nm. Further, an average of the smooth curves (MPMS II) would not be two different than the observed, out to 25 nm (Fig 66).

4. 29 April 2000. X Band

The coverage diagrams shown in Figs 67-69 show that X band is clearly strongly trapped, again in the lowest 200ft by the refractive profile. Both AREPS (PJ) and EEMS exhibit significant interference patterns and skip zones. AREPS (NPS) does not show the effects of the SBD (Fig 70), but by virtue of the calculated evaporation duct, 23ft (7.1m), is predicting some trapping of the X band energy. The MPMS II observed coverage diagram (Fig 71) shows an interference pattern between 15 and 30ft in the first 20nm, and then a stronger interference pattern at the surface from 20nm out, suggesting ducting is stronger as distance from the coast increases.

The loss curves generated by the EEMS and AREPS (PJ) models describe the MPMS II pattern well at both 21 and 30ft. Again, this applies to spatially smoothed since the nodes and anti-nodes are often too strong and in the wrong locations. At the lower level, at a height of 6ft, there are large operationally unacceptable differences in EEMS and AREPS (PJ) losses from those observed by MPMS II (up to 25-30dB). Further, the differences indicate that the models significantly under-estimate the loss. AREPS (NPS) ED influenced only model, whilst again, not exhibiting the interference pattern caused by the SBD, is actually as close to MPMS II as either of the other two full profile influenced models out to 20nm. At 20nm AREPS begins to significantly diverge by up to 30-35dB at 35nm.

5. 01 May 2000. S Band

The general refractive pattern for this day is a weak surface based duct (Fig 39, Chapter IX), shows a generally uniform (no trapping layer) profile with a fairly strong evaporation duct, giving an above average surface weather category, and super-refractive conditions at low-level. Both AREPS (PJ) and EEMS generated coverage diagrams (Figs 73-75) show extended ranges and interference patterns near the surface, indicative of

weak ducting/super-refraction. AREPS (NPS) generated coverage diagrams (Fig 76) exhibit near standard propagation patterns with little evidence of interference patterns above or near the surface.

The propagation loss curves, for all runs as shown in Fig 78, generally exhibit little evidence of interference patterns except for the now familiar EEMS generated features in the first 8nm. Beyond 8nm and at both 21 and 30ft, EEMS is within 3-4dB of the MPMS II results, which is quite acceptable for operational system performance application. Both AREPS (PJ and NPS) models over-predicted the loss by 5-6dB at 10nm and 13-18dB at 20nm. Again, these differences between observed and predicted are too large for most weapons system performance applications beyond 10 nm. Further, at 6ft, predicted versus observed differences are high for all models, with EEMS under-predicting the loss by 8-10dB and AREPS over-predicting it by 10-12dB.

6. 01 May 2000. X Band

As expected, generated and observed X-band coverage diagrams are considerably more complex than those at S band because the dominant feature was the ED to which X-band has more sensitivity (Figs 79-81). The MPMS II results exhibit an interference-pattern at low-level, lying from 10ft at the start of the run, rising to 35ft at 24nm (Fig 83) At the surface the general surface pattern is horizontally elongated, indicating enhanced propagation.

The EEMS generated coverage diagram is much more complex in the near field than those generated from both AREPS (PJ and NPS), much of this being due to the difference in the specified evaporation duct height. EEMS specified an evaporation duct of 41.6ft (12.8m), producing above average surface radar weather conditions, whereas AREPS (NPS) produces a duct of 25.35ft (7.8m) and AREPS (PJ), 19.5ft (6m). Both AREPS specified ED conditions were on the border of average to above-average RADAR weather conditions.

The propagation loss curves from MPMS II (Fig 84), display very significant interference patterns for the 21 and 30ft levels, but none for the 6ft level. The height dependence of interference pattern occurrence is reflected in the coverage diagrams, Fig

83, and is due to the most distinct interference pattern being elevated from the surface. This pattern is very reminiscent of the EEMS near field pattern. Beyond 8nm the EEMS generated loss curve tracks the MPMS II loss curve very well at 30ft, with 3-5dB. AREPS (NPS) generally under-predicts the loss until 30nm, at which point the curves crossover and the model then over-predicts.

At 21ft, the MPMS II observed loss profile shows some fade at 10-15nm, which none of the models manage to predict. Both EEMS and AREPS (PJ) begin to converge toward the MPMS II loss curve from 25nm onwards. AREPS (NPS) generally over-predicts the loss over the whole range, i.e. throughout the loss profile, which was surprising for the ED dominated case.

At 6ft, and out to 15nm, EEMS generated loss curve does not agree with MPMS II loss curve. However, the AREPS (PJ) is close to MPMS II throughout (within 3-5dB), which is acceptable agreement over such a long range. EEMS does agree with MPMS II until a distance of 25nm.

7. 03 May 2000. S Band

Refractivity profile conditions experienced during this day were the most complex of the four days chosen (Fig 47, Chap IX). For this reason, analyses and interpretations of predictions and comparisons based on this profile are expected to be the most challenging, and be the most error prone of the thesis set.

At the surface, conditions were unstable so mixing caused a smooth near-surface profile with an ED. However, above the surface layer, the profile had a trapping layer of approximately 100ft in width, above which had an associated surface-based duct. This duct was of sufficient thickness to affect both S and X band frequencies strongly, as evidenced by both the EEMS and AREPS (PJ) generated coverage diagrams (Figs 85-87). As with earlier cases with surface-based ducts, the AREPS (NPS) model cannot be expected to replicate observed interference patterns (Fig 88). The MPMS II observed coverage diagram (Fig 89) exhibits an anti-node at 16nm and a node at 27nm, both of which are also in evidence in the EEMS generated diagrams.

The resulting propagation loss curves (Fig 90), for heights of 21 and 30ft, for both EEMS and AREPS (PJ) exhibit very similar patterns, being within 3-5dB. Both models under-predicted the loss out to 25nm. EEMS then under-predicted the loss by 10 dB of the MPMS II observed loss from 25 to 40nm. AREPS (PJ) had very good agreement with MPMS II, being within 5dB over this range. Beyond 40nm, both models under-predicted the loss. AREPS (NPS) is generally in good agreement until 10-12nm, and then significantly over-predicts the loss from this point out. In general, at the lowest level, 6ft, AREPS (PJ) performed best, within 5 dB, and AREPS (NPS) did reasonably well over the whole range, whilst EEMS under-predicted by 10-15dB. The ED influenced AREPS (NPS) model does the best of all the model runs out to 15nm (Fig 90), but, again, significantly over-predicts after this distance since the influence of the surface-based duct is not accounted for.

8. 03 May 2000. X Band

At X band, strong effects of the SBD are again very ably demonstrated by both the EEMS and AREPS generated coverage diagrams (Figs 91-93). The MPMS II coverage diagram (Fig 95) also indicates these SBD effects, with extremely complex patterns of multi-path interference. As with earlier patterns, the MPMS II interference patterns strengthen with distance offshore, once more indicating that the strength and development of the duct significantly increases with offshore distance.

None of the model resulting X-band loss curves are in particularly good agreement with the MPMS II loss curve (Fig 96). AREPS (PJ) has the best agreement with MPMSII, but is 15-20 dB off in section. EEMS significantly over-predicted the loss, by 20-30dB from 10-15nm, before generally converging with distance from thereon. EEMS agreed best, of all the models, from 40-50nm. AREPS (NPS) does comparatively well out until 15nm, at which point it begins to significantly over-predicts the loss. The latter comparison result over a range distance, which is operationally significant, substantiates the decision to have the NPS ED model be the standard in AREPS. Again, this points out that a remaining step is for the AREPS (NPS) to have merging of ED and the upper air profile, in this case a rocketsonde derived profile.

C. PROPAGATION MODEL RESULTS

1. 10 April 2000. S Band

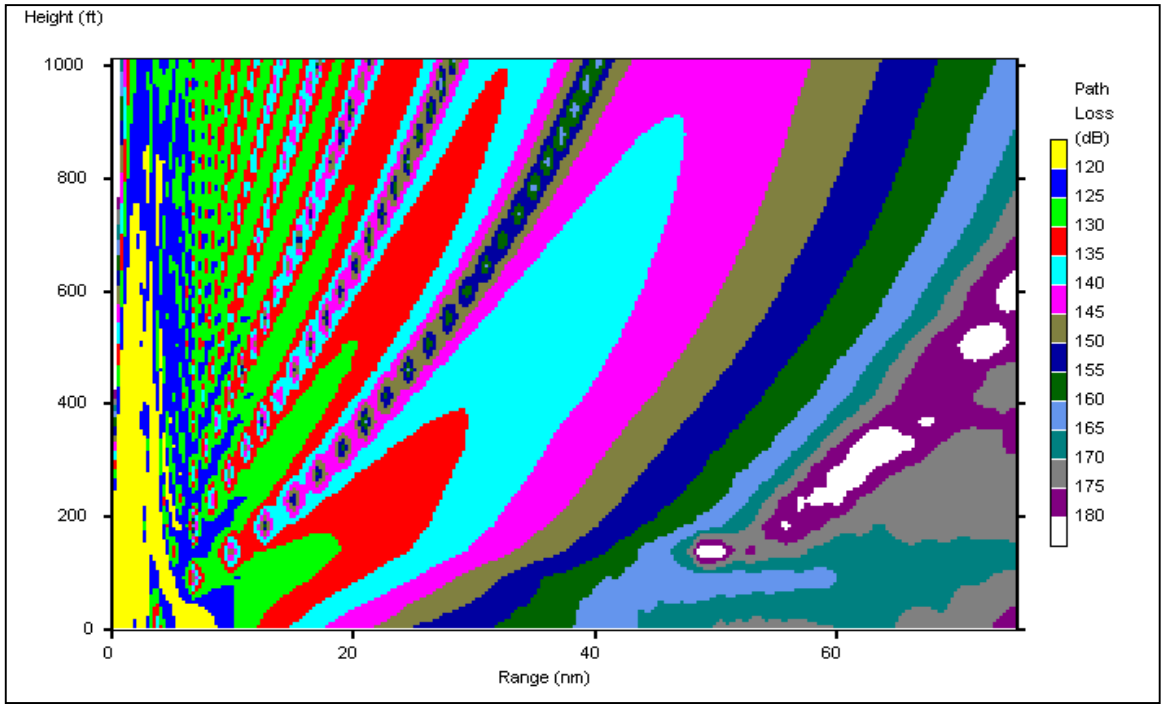

Figure 49. 10 Apr S Band coverage – EEMS.

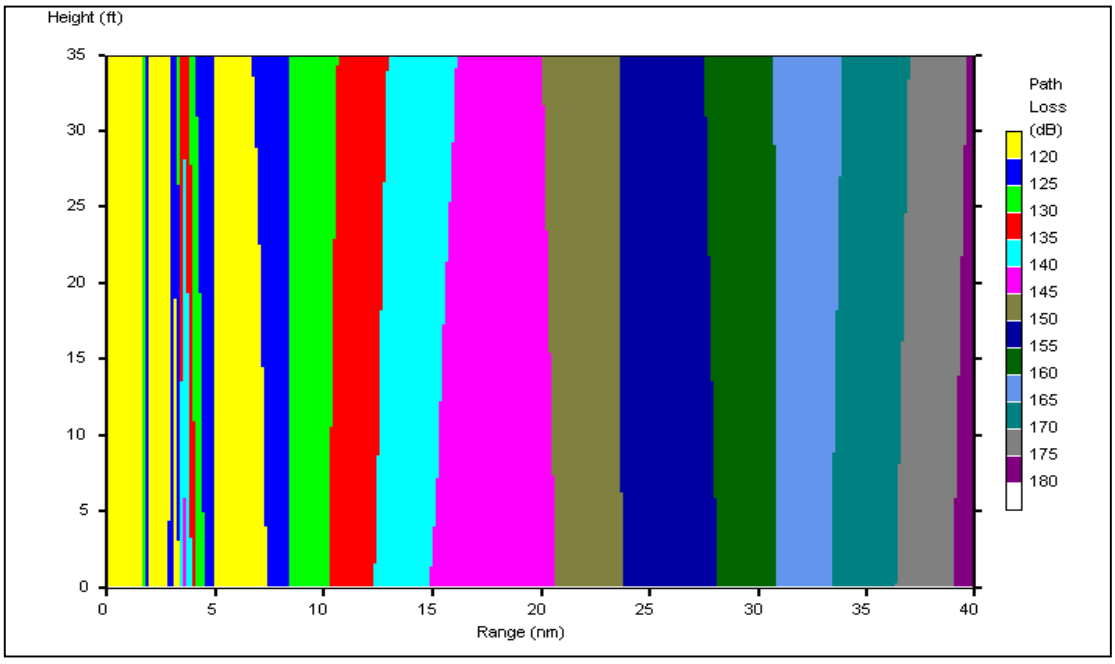

Figure 50. 10 Apr S Band low–level coverage – EEMS

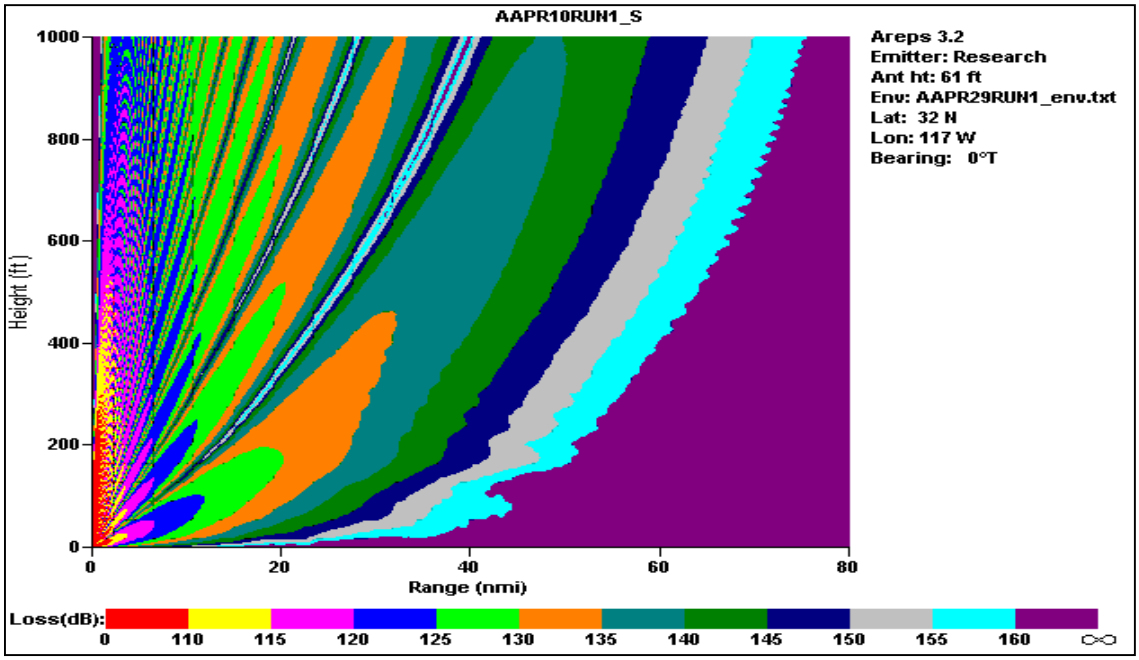

Figure 51. 10 Apr S Band. AREPS - Paulus Jenske

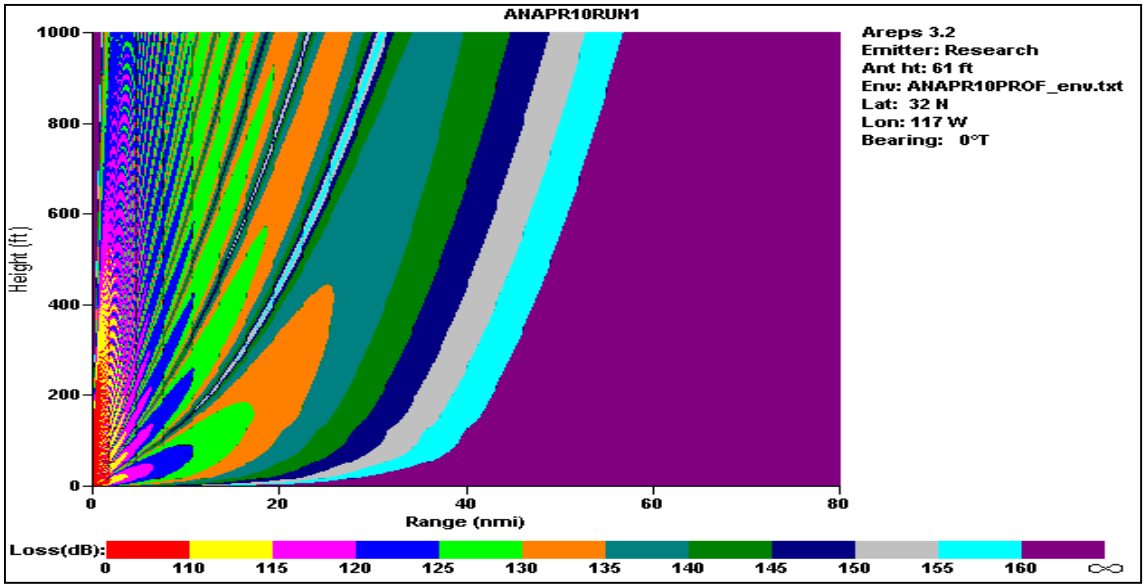

Figure 52. 10 Apr S Band. AREPS - NPS.

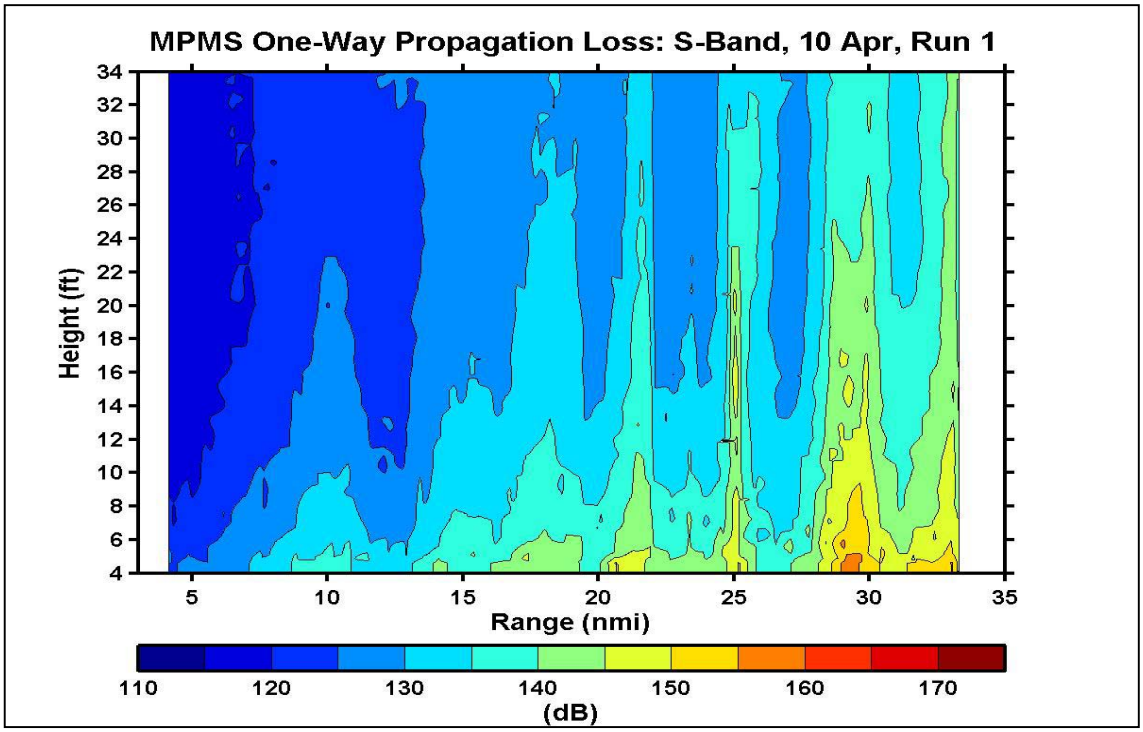

Figure 53. 10 Apr S Band, low-level coverage diagram – MPMS II.

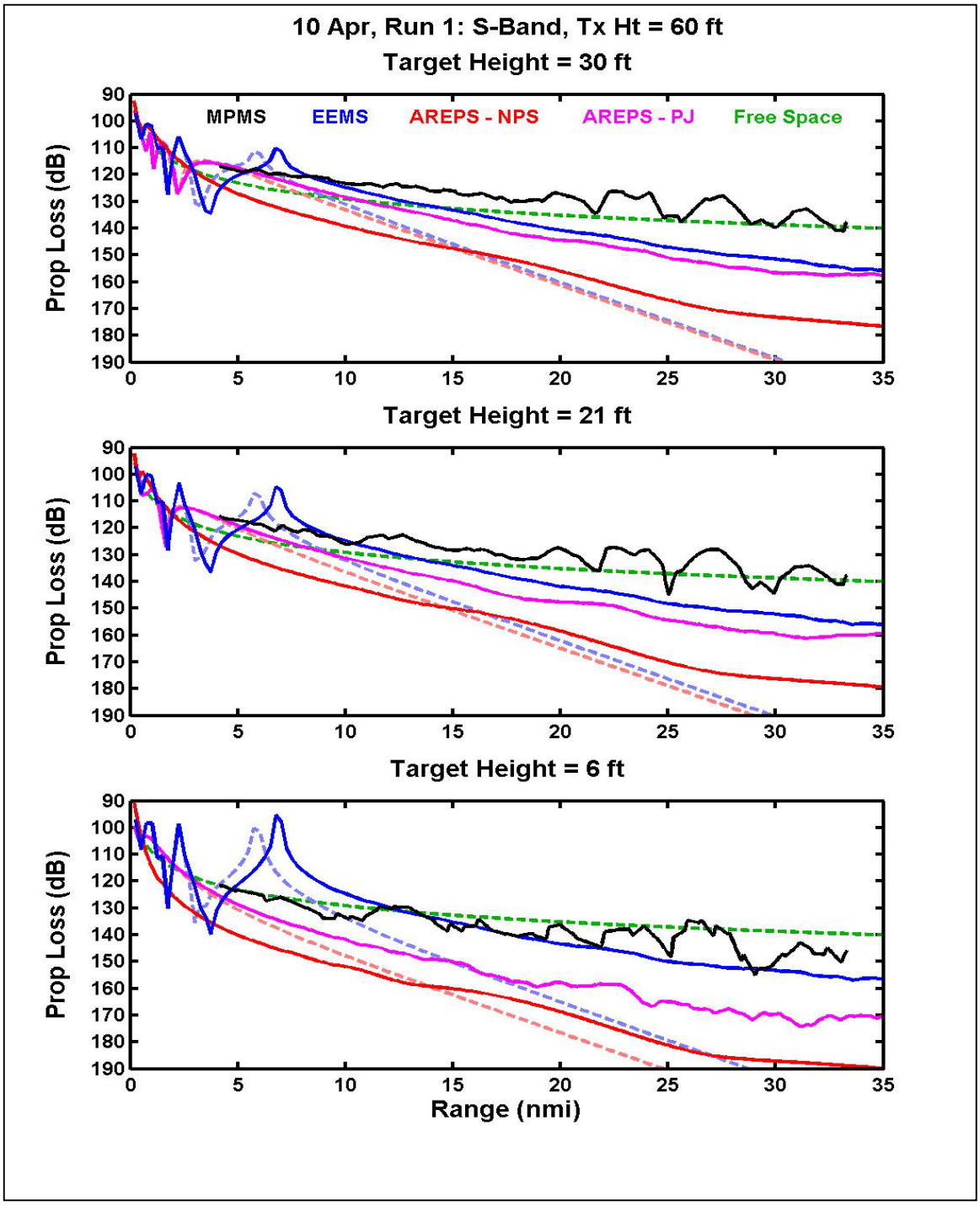

Figure 54. 10 Apr S Band. Propagation loss curves for EEMS, AREPS, MPMS II.

2. 10 April 2000. X Band

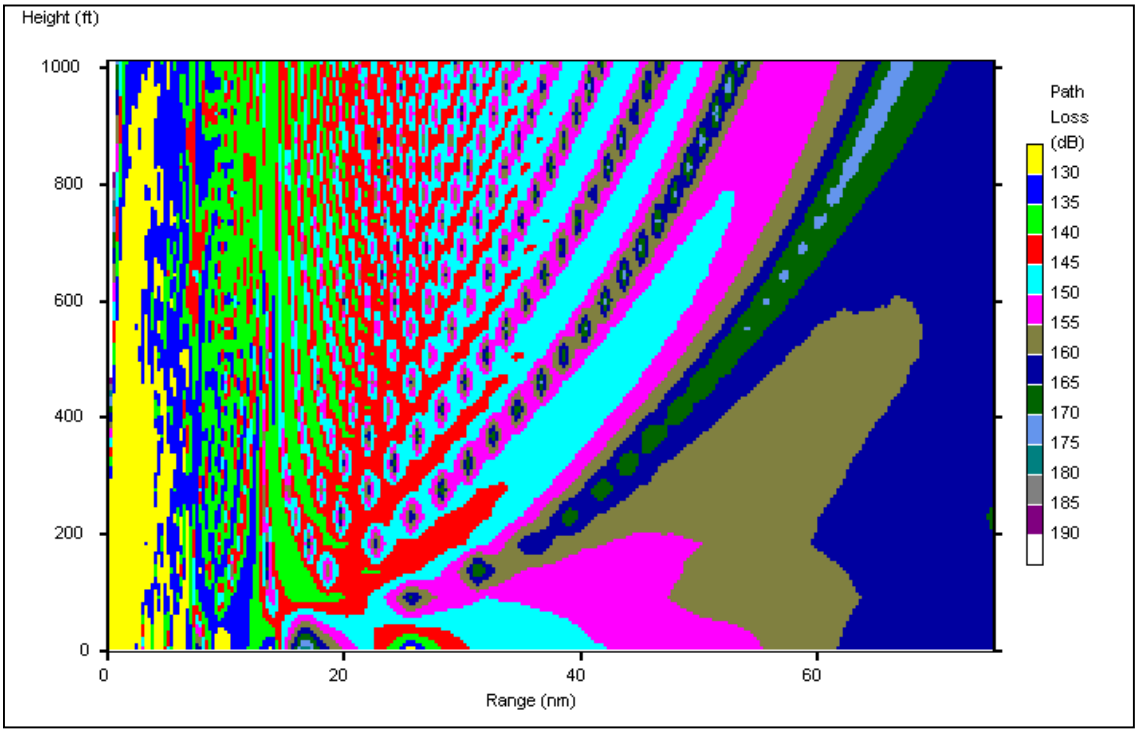

Figure 55. 10 Apr X Band coverage – EEMS.

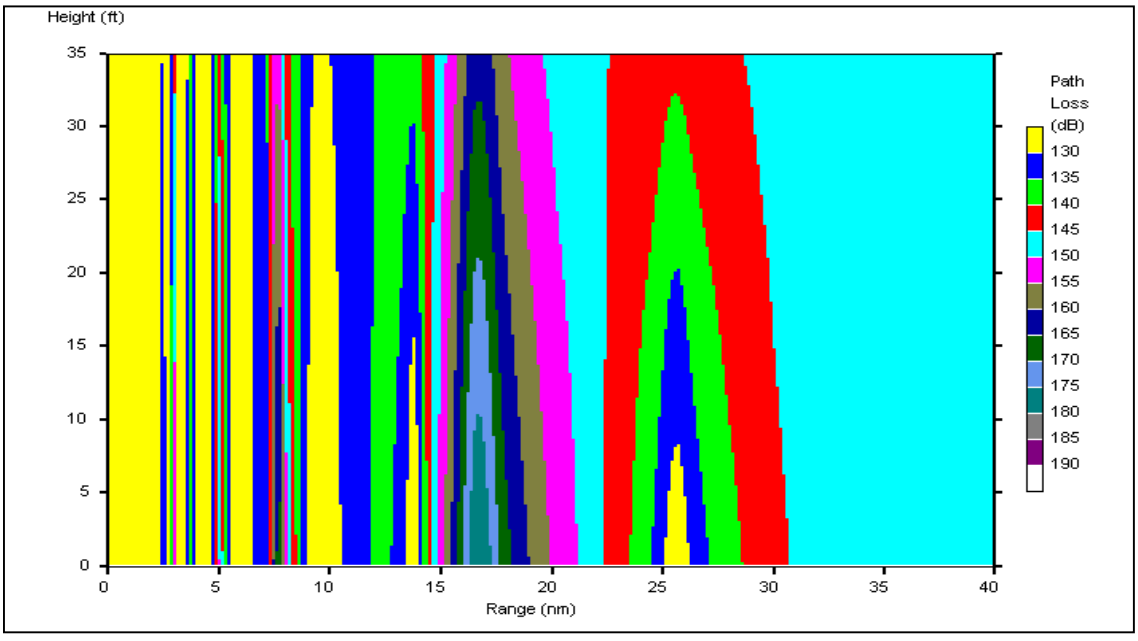

Figure 56. 10 Apr X Band low-level coverage - EEMS

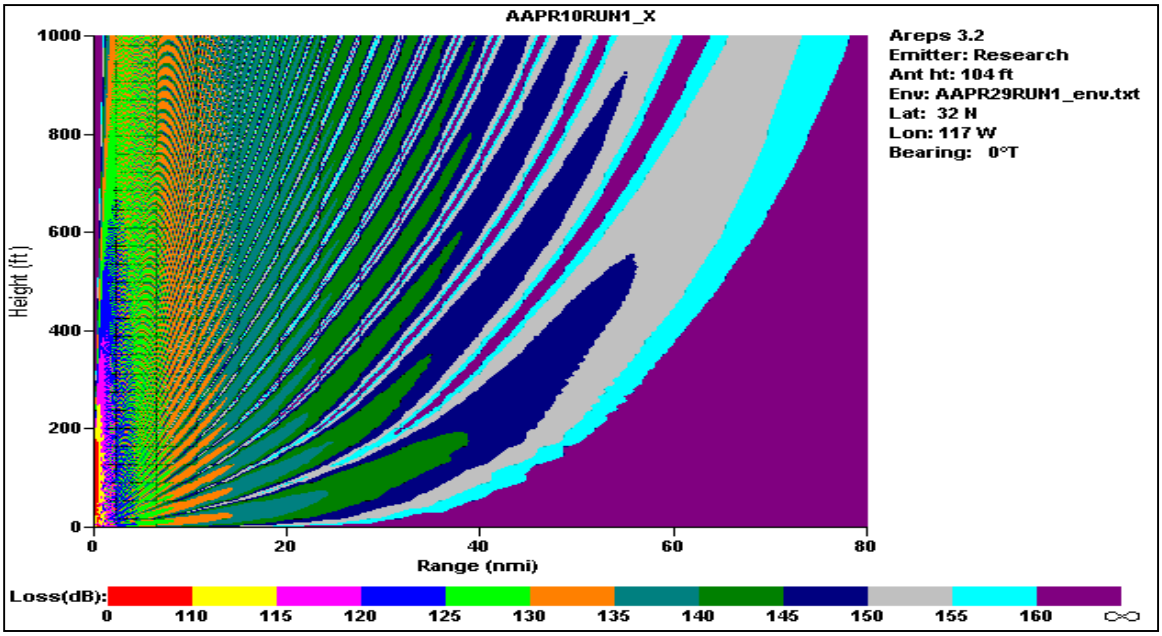

Figure 57. 10 Apr X Band. AREPS – Paulus-Jenske.

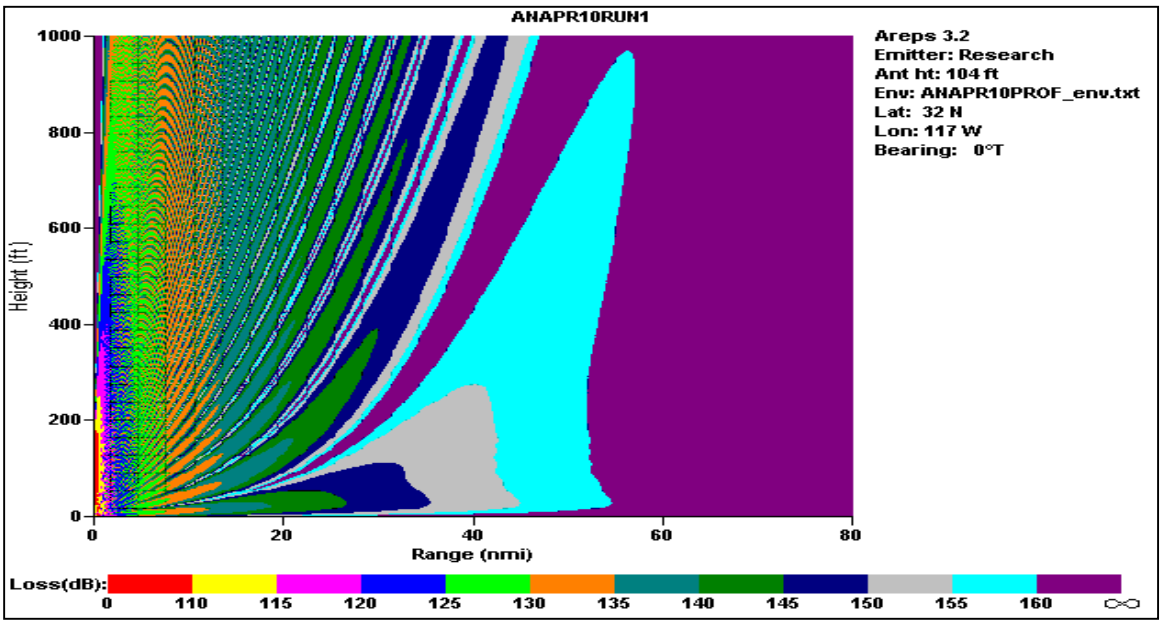

Figure 58. 10 Apr X Band. AREPS – NPS.

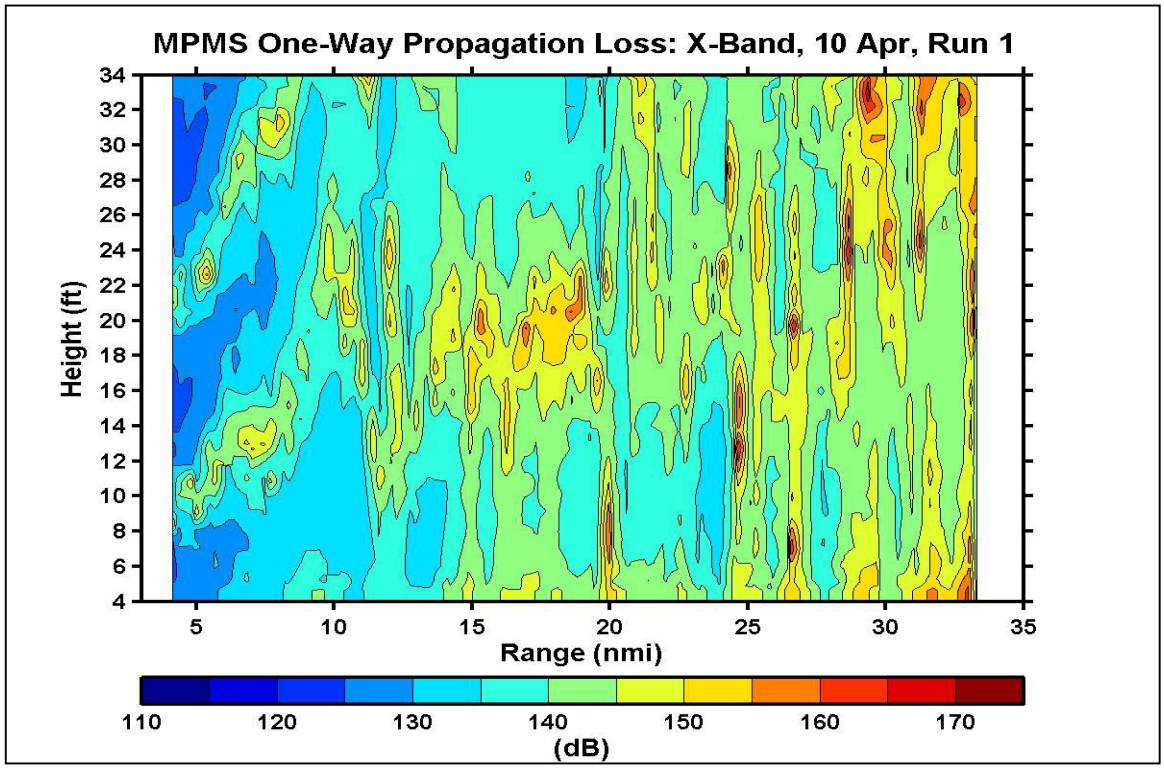

Figure 59. 10 Apr X Band low-level coverage – MPMS II.

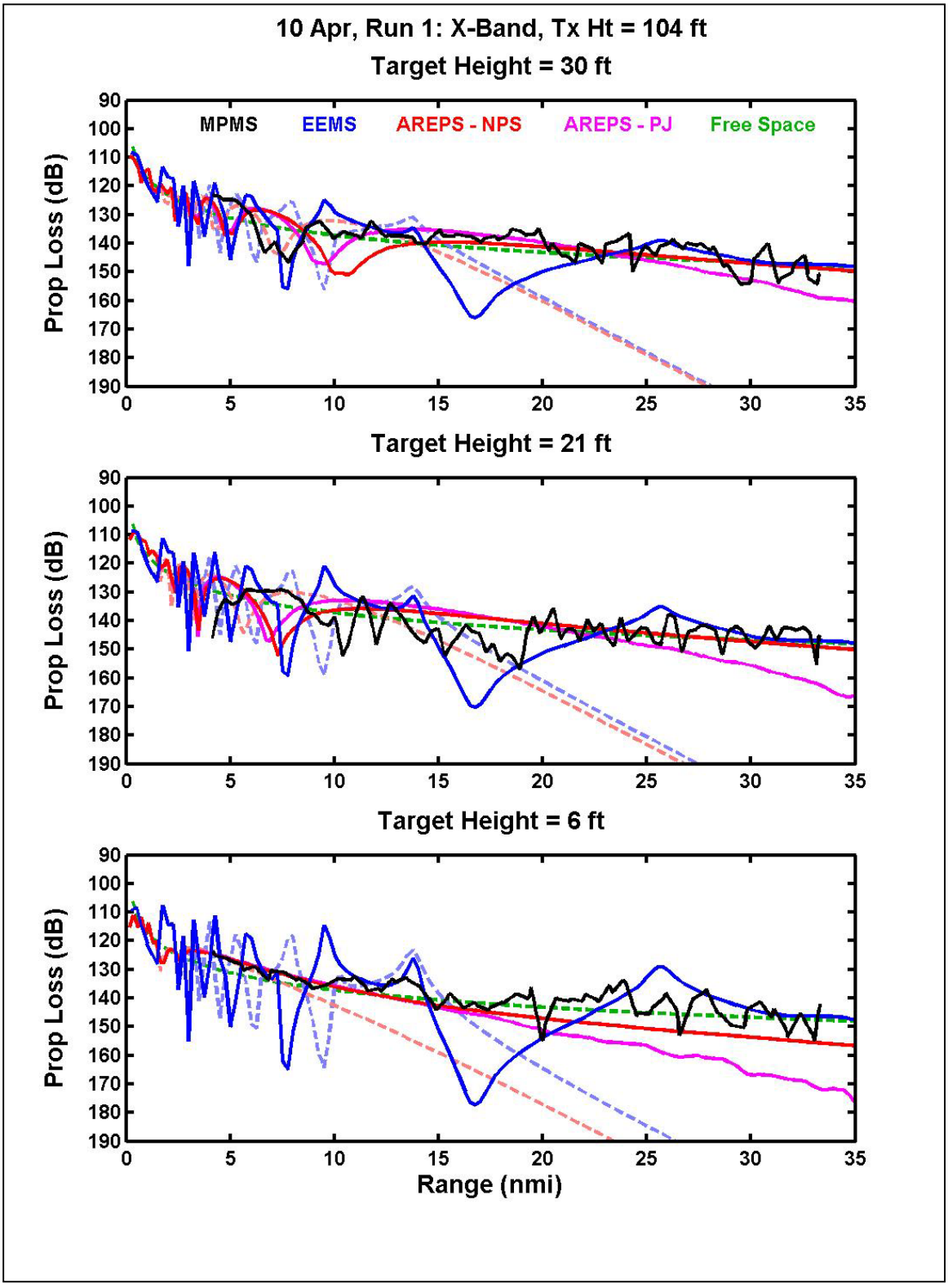

Figure 60. 10 Apr X Band. Propagation loss curves for EEMS, AREPS, MPMS II.

3. 29 April 2000. S Band

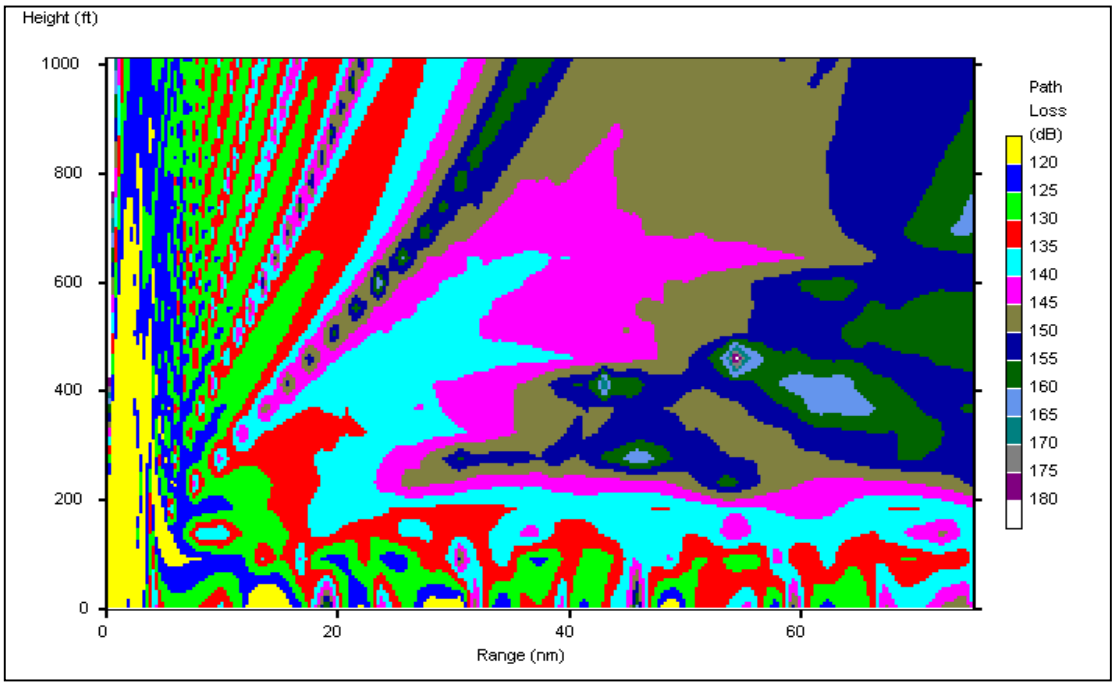

Figure 61. 29 Apr S Band coverage – EEMS.

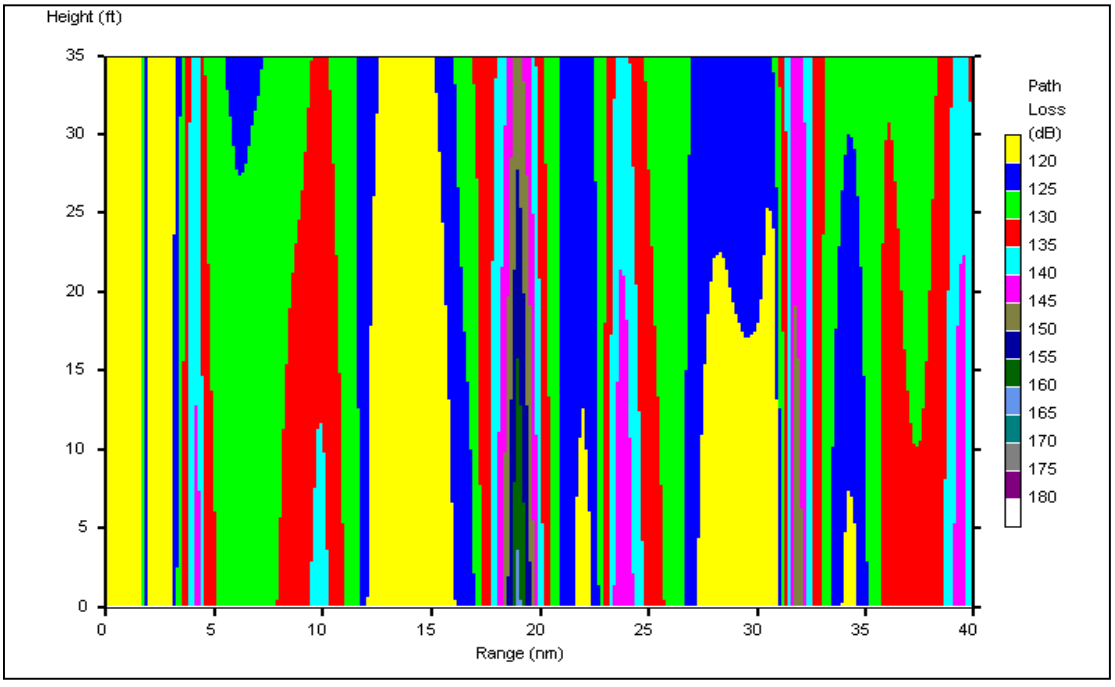

Figure 62. 29 Apr S Band. Low-level coverage – EEMS.

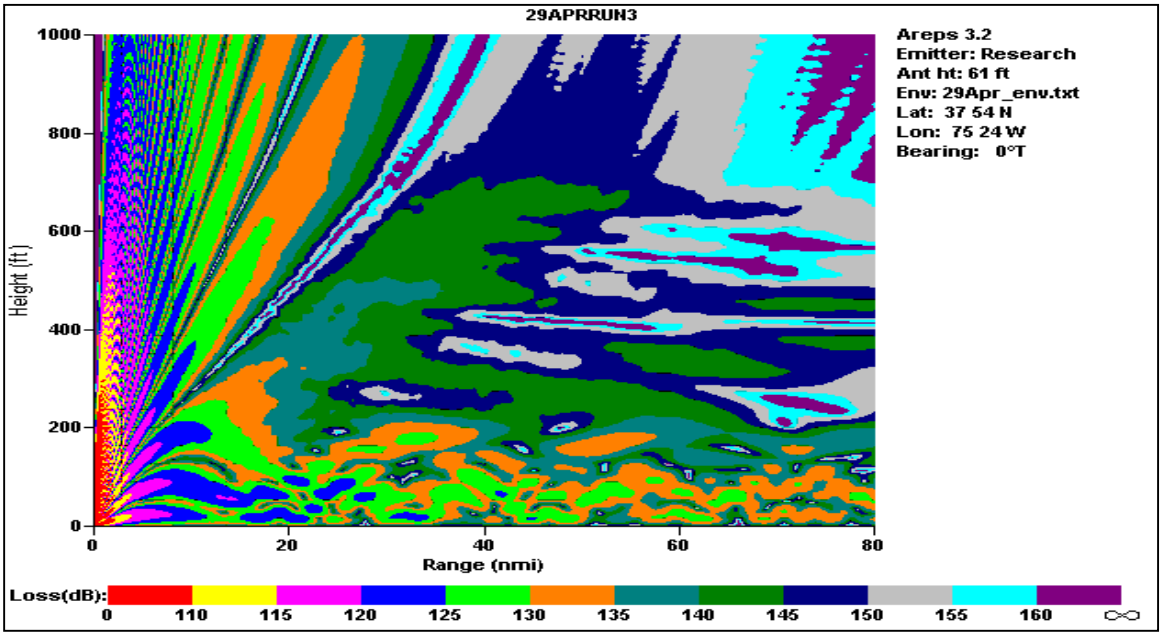

Figure 63. 29 Apr S Band. AREPS – Paulus-Jenske.

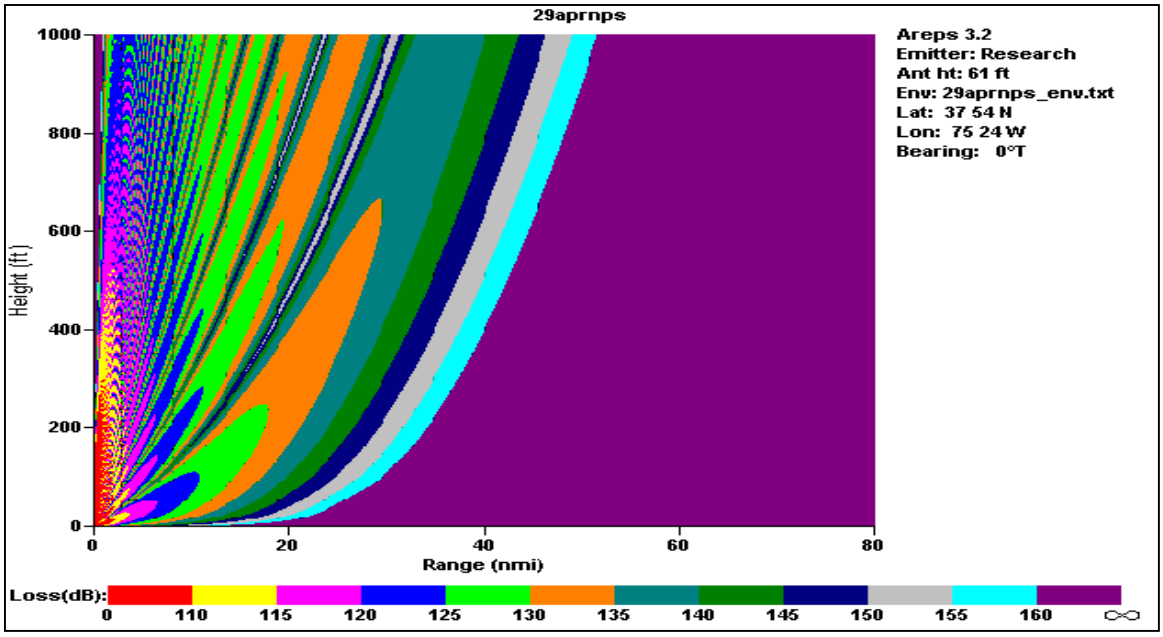

Figure 64. 29 Apr S Band. AREPS – NPS.

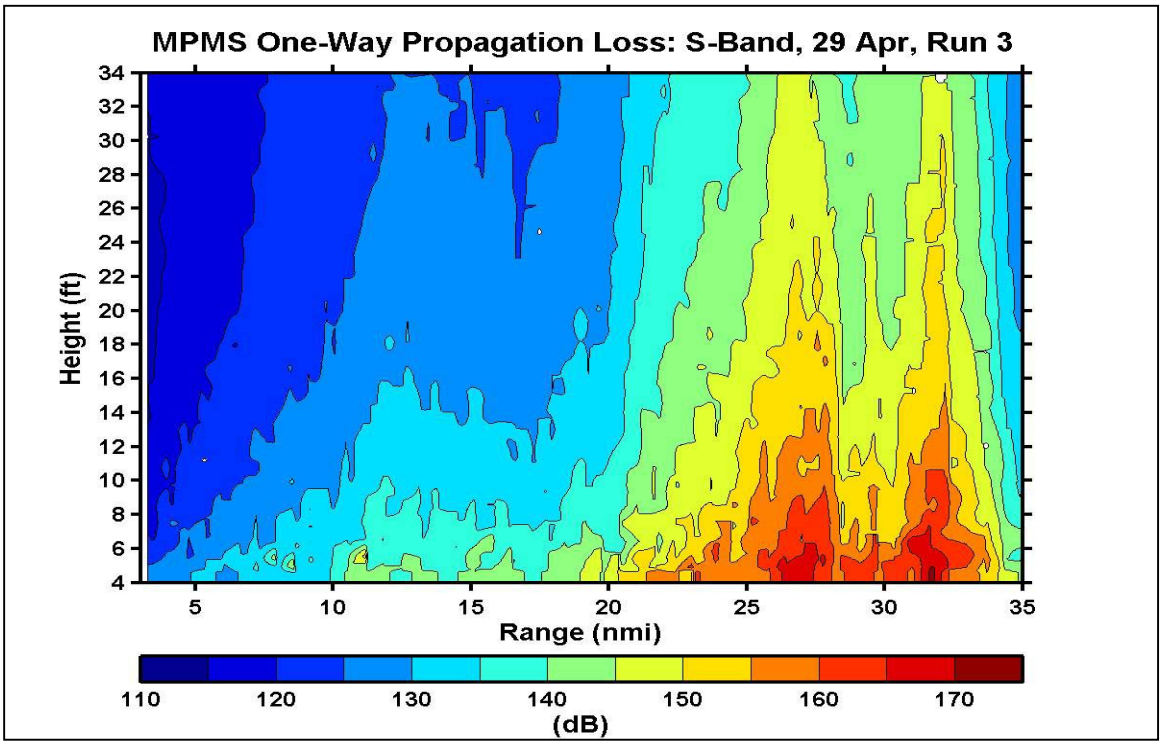

Figure 65. 29 Apr S Band. Low-level propagation factor – EEMS.

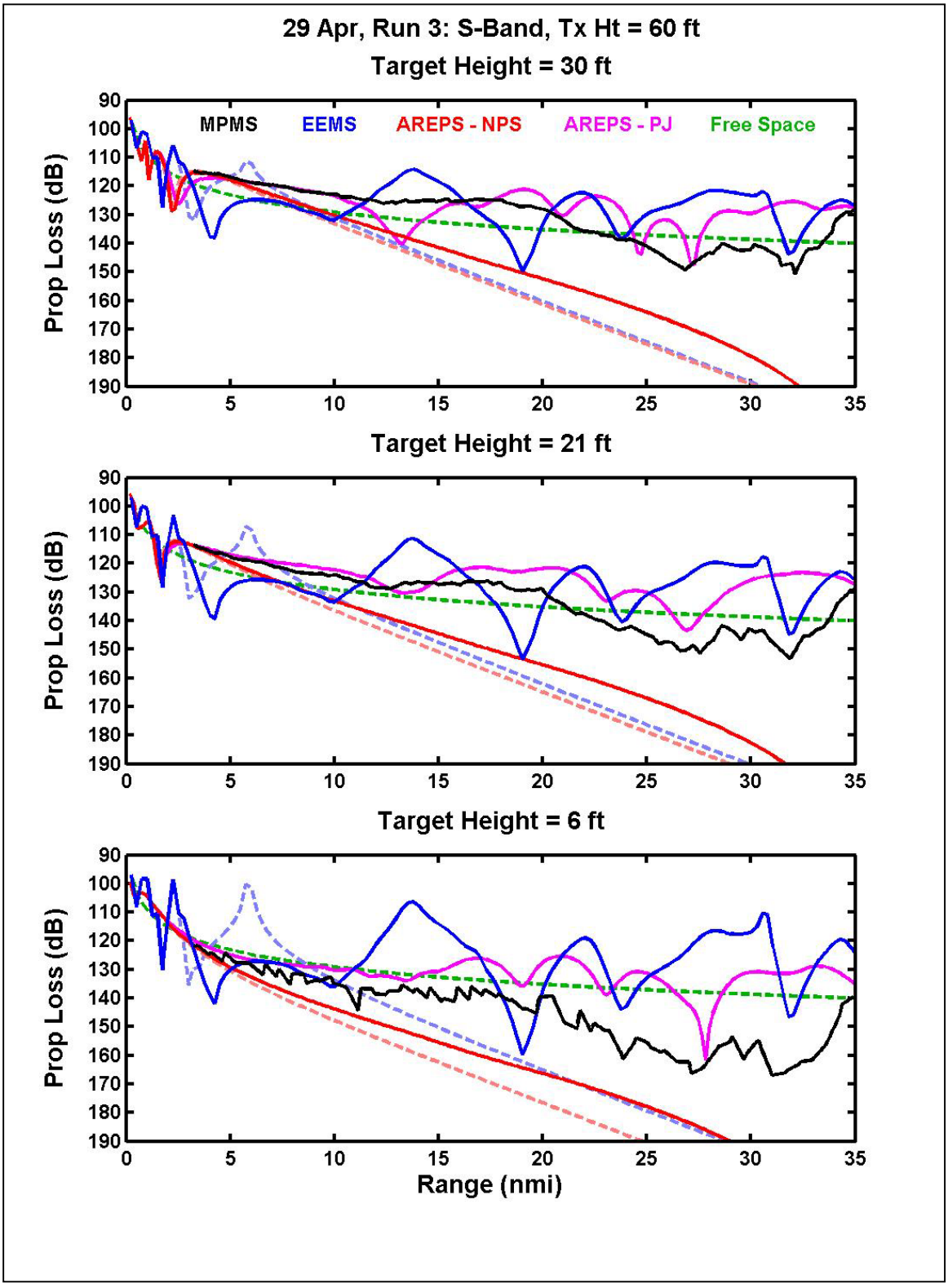

Figure 66. 29 Apr S Band. Propagation loss curves for EEMS, AREPS, MPMS II.

4. 29 April 2000. X Band

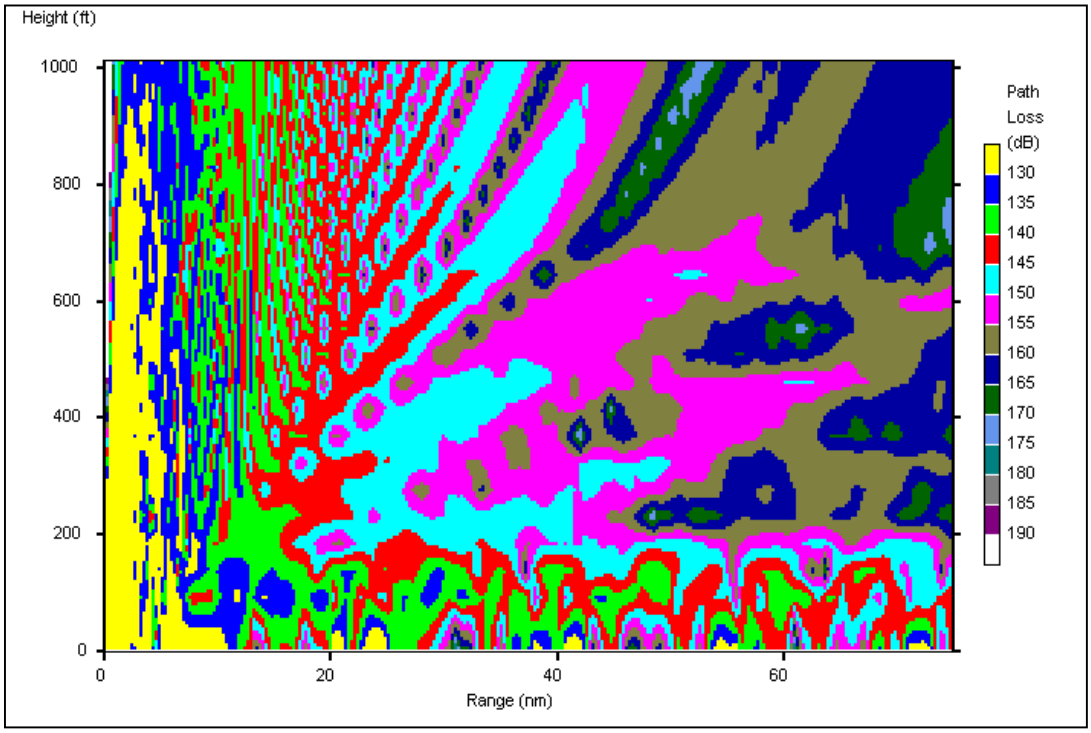

Figure 67. 29 Apr X Band. Coverage diagram – EEMS.

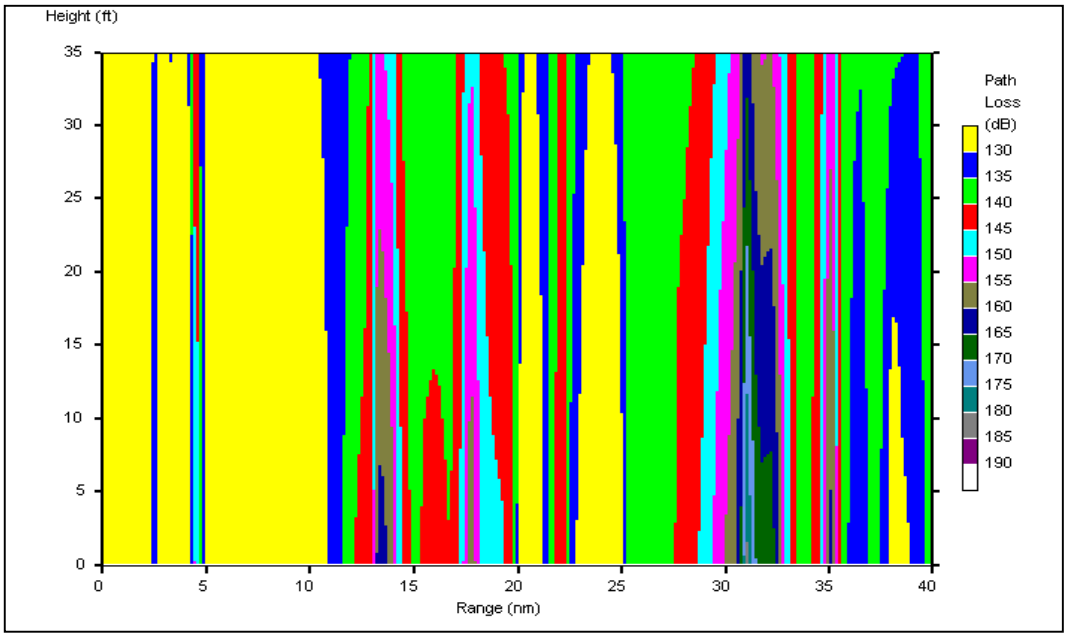

Figure 68. 29 Apr X Band. Low-level coverage - EEMS

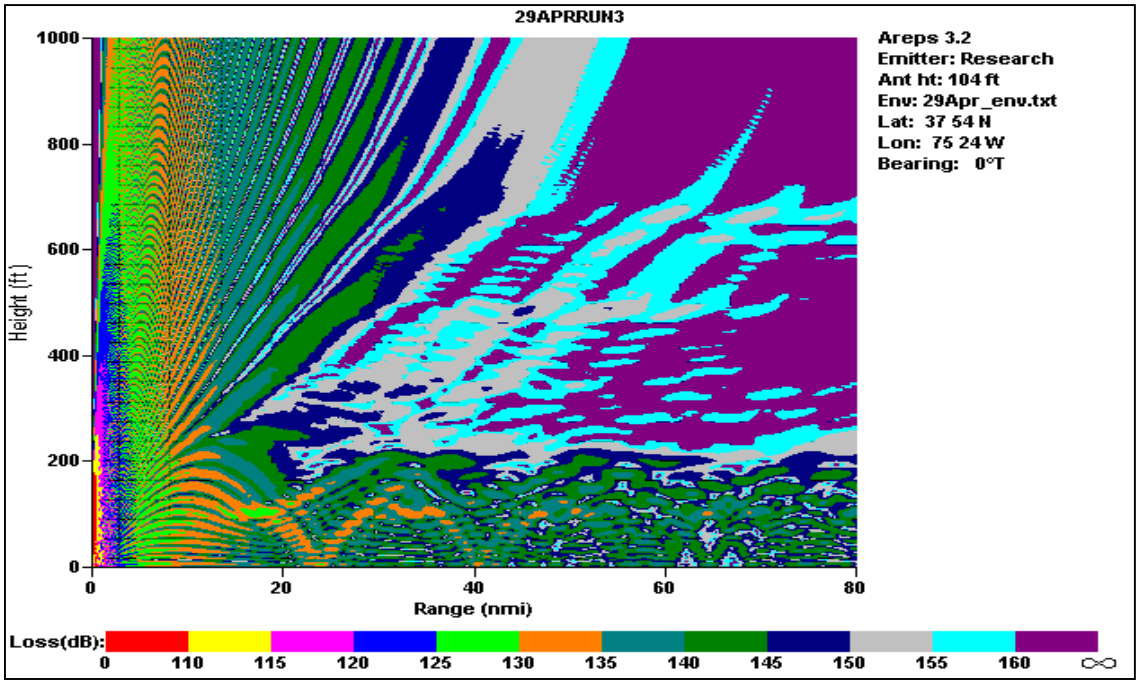

Figure 69. 29 Apr X Band. AREPS – Paulus-Jenske.

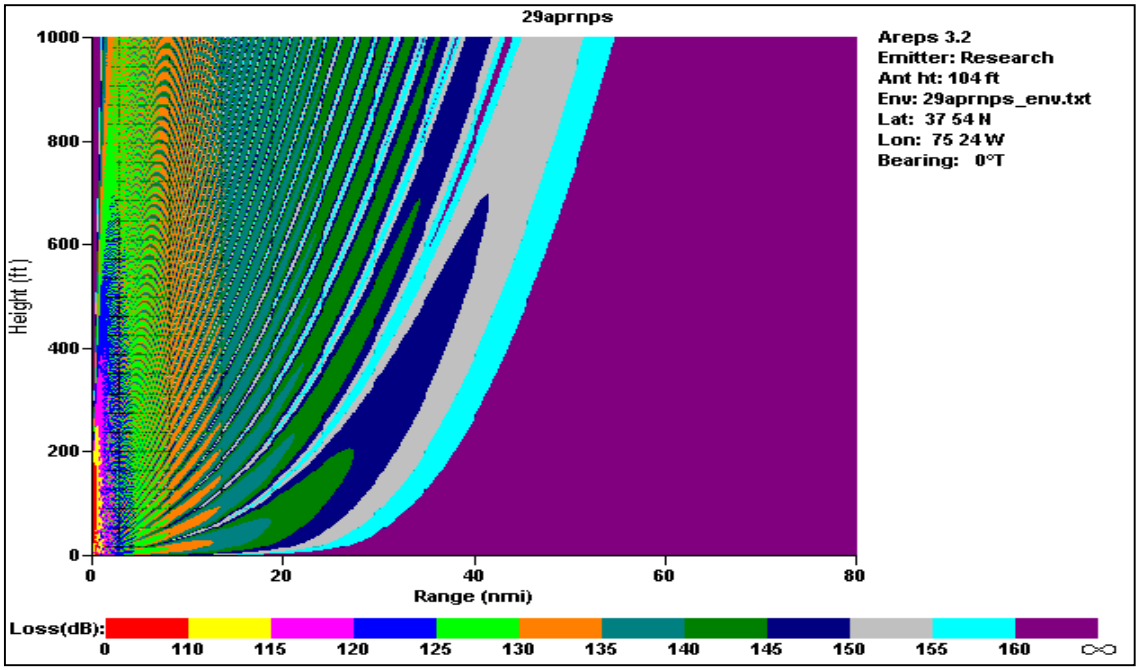

Figure 70. 29 Apr X Band. AREPS – NPS.

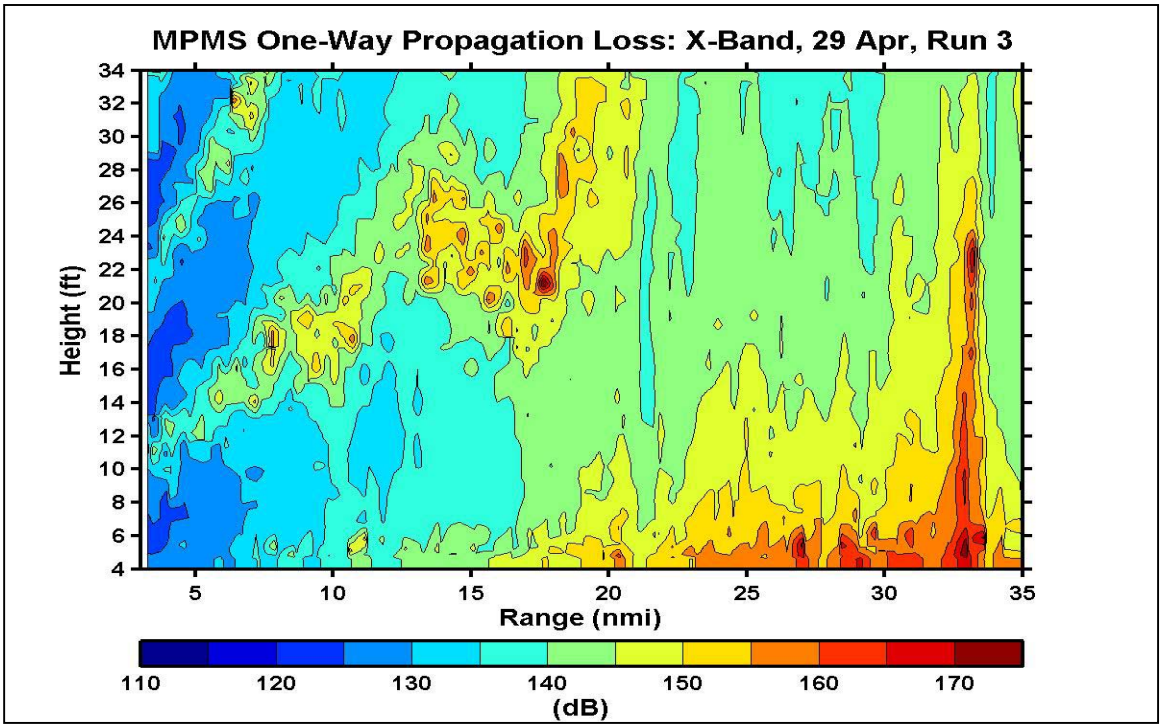

Figure 71. 29 Apr X Band. Low-level coverage diagram – MPMS II.

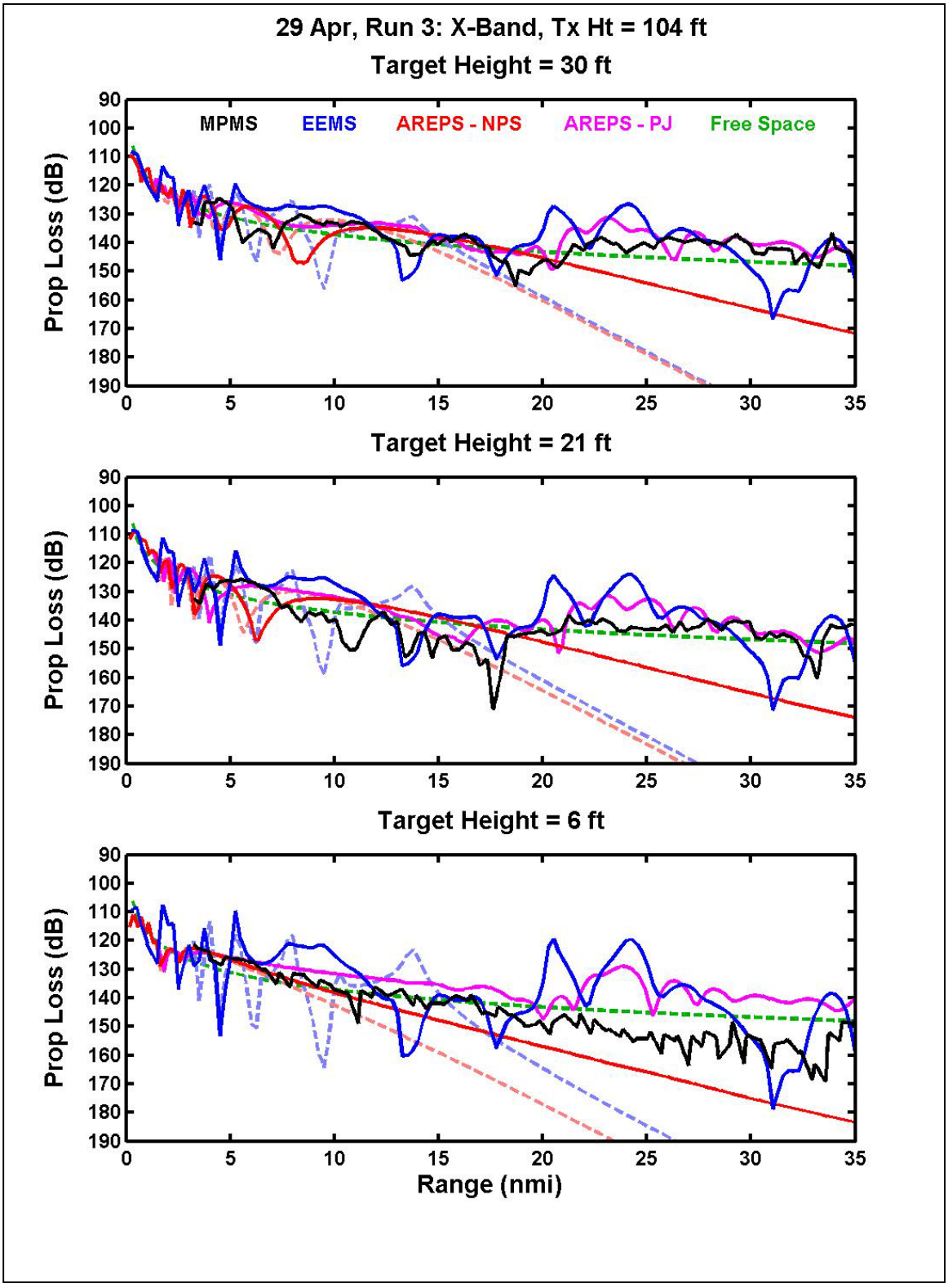

Figure 72. 29 Apr X Band. Propagation loss curves for EEMS, AREPS, MPMS II.

5. 01 May 2000. S Band

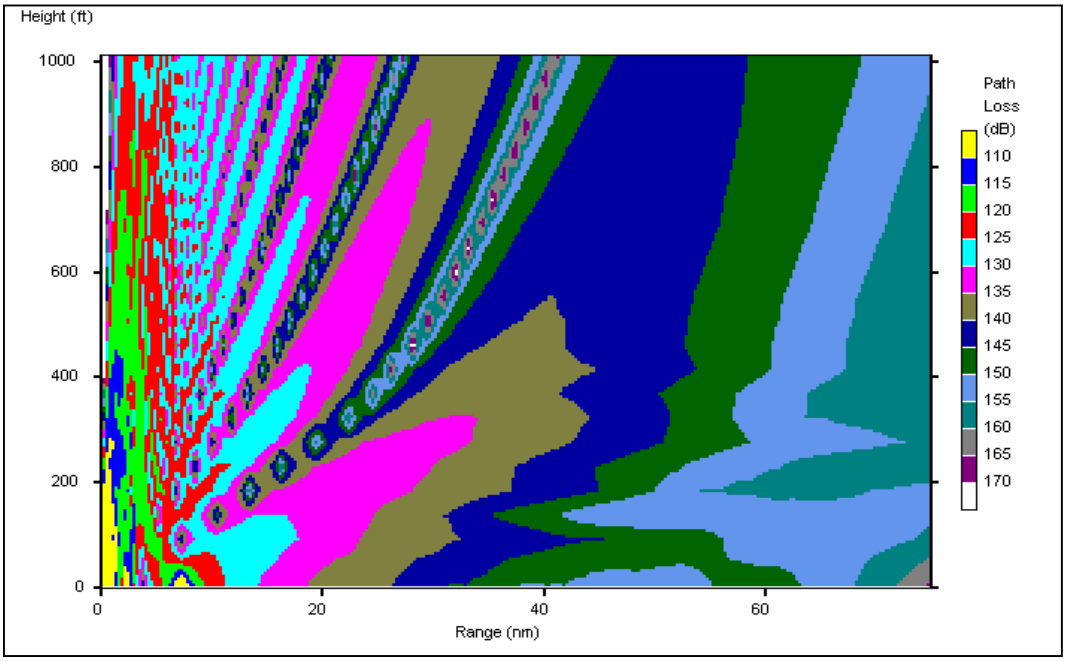

Figure 73. 01 May S Band. Coverage diagram – EEMS.

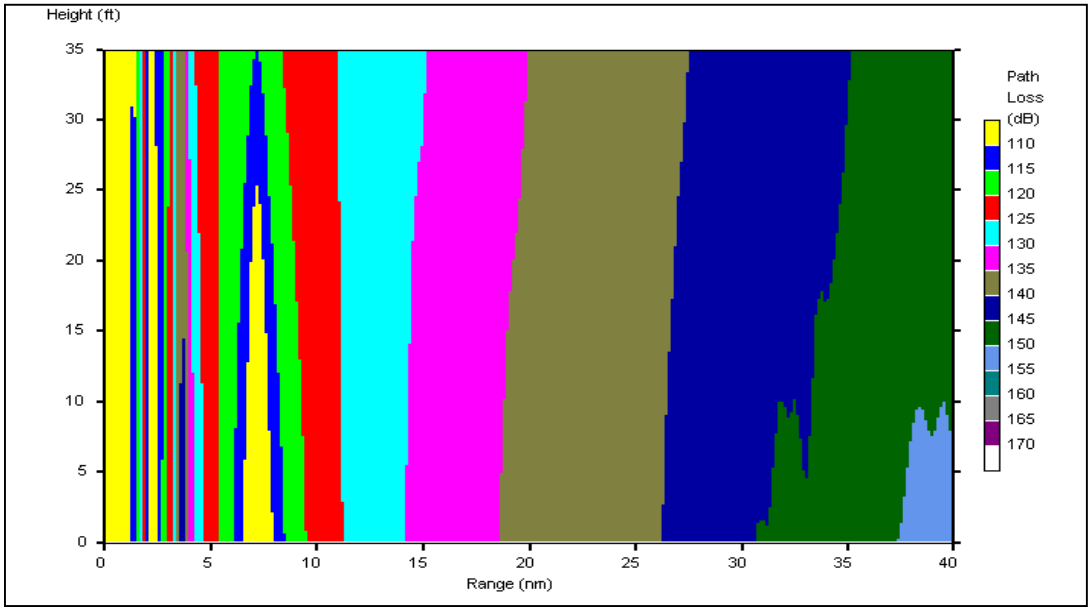

Figure 74. 01 May S Band. Low-level coverage - EEMS

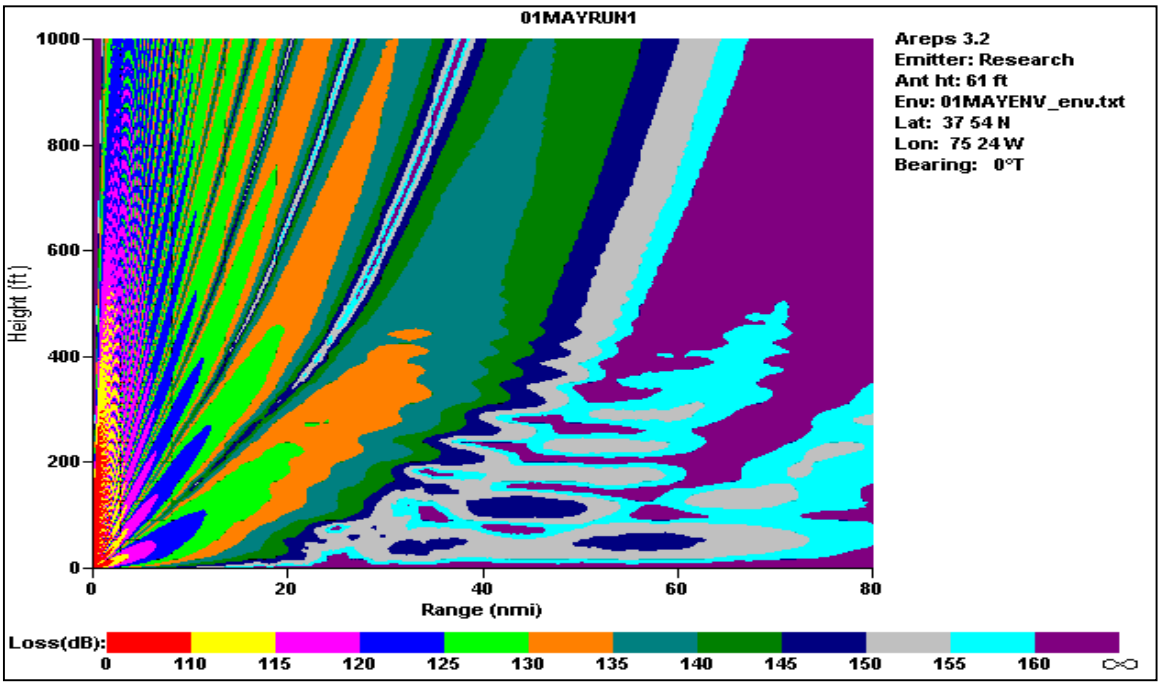

Figure 75. 01 May S Band. AREPS – Paulus-Jenske.

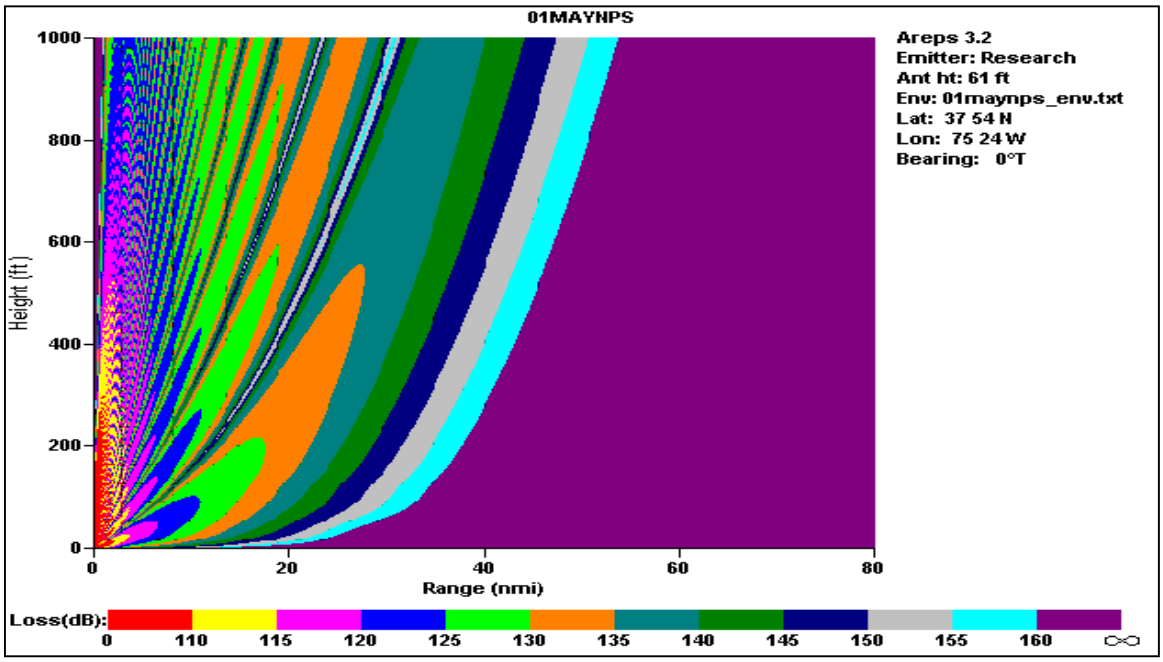

Figure 76. 01 May S Band. AREPS – NPS.

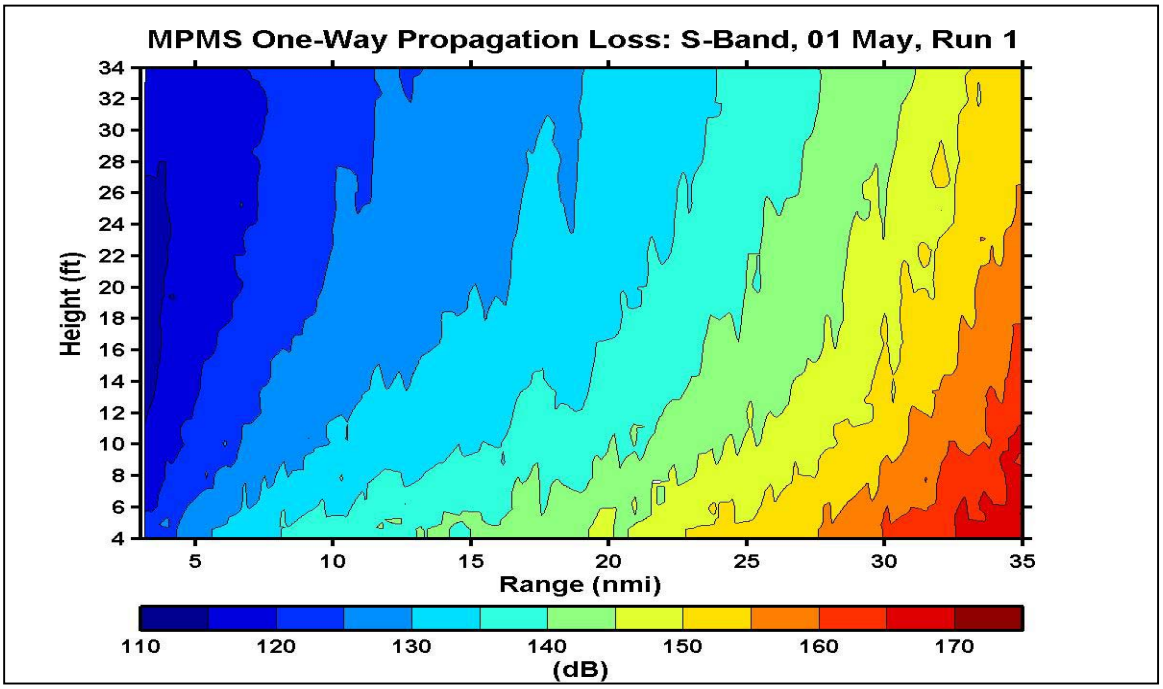

Figure 77. 01 May S Band. Low-level coverage diagram – MPMS II.

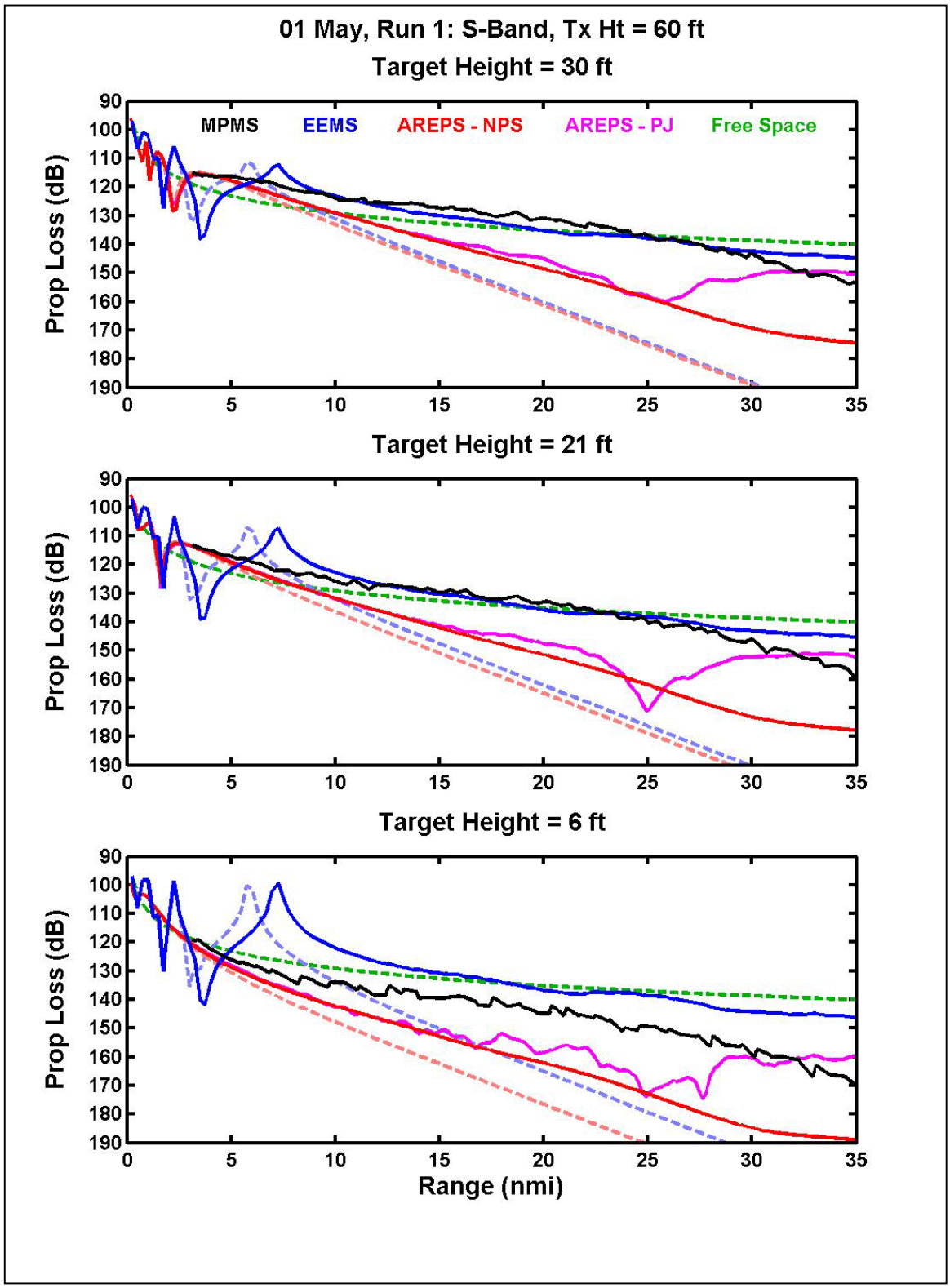

Figure 78. 01 May S Band. Propagation loss curves for EEMS, AREPS, MPMS II.

6. 01 May 2000. X Band

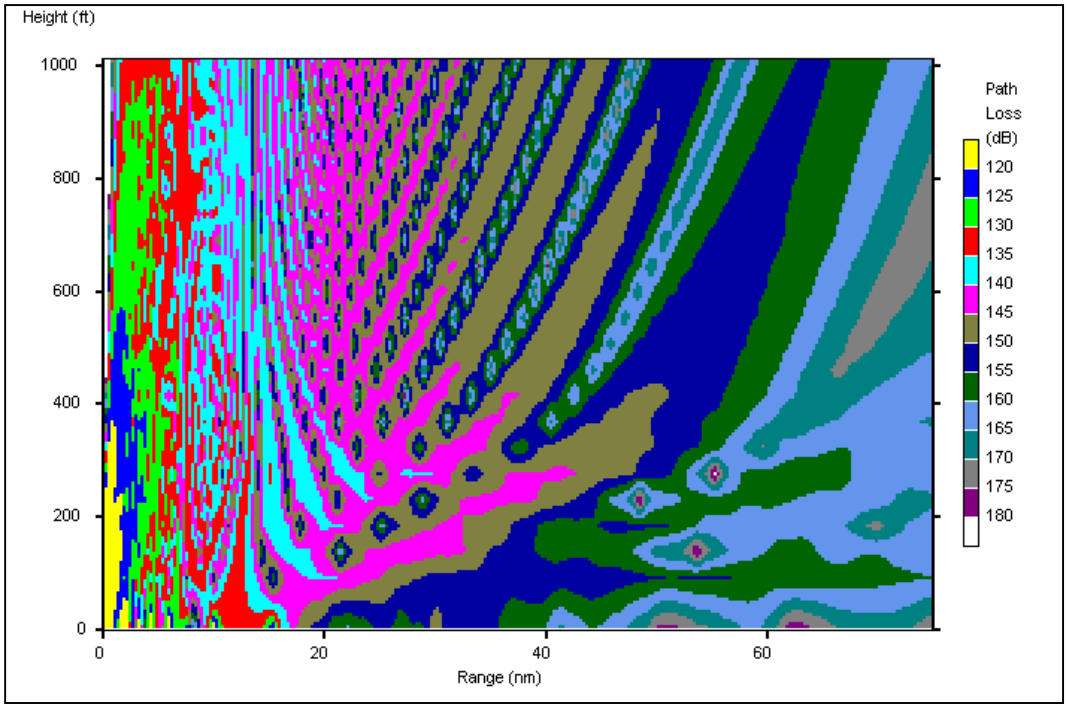

Figure 79. 01May X Band. Coverage diagram – EEMS.

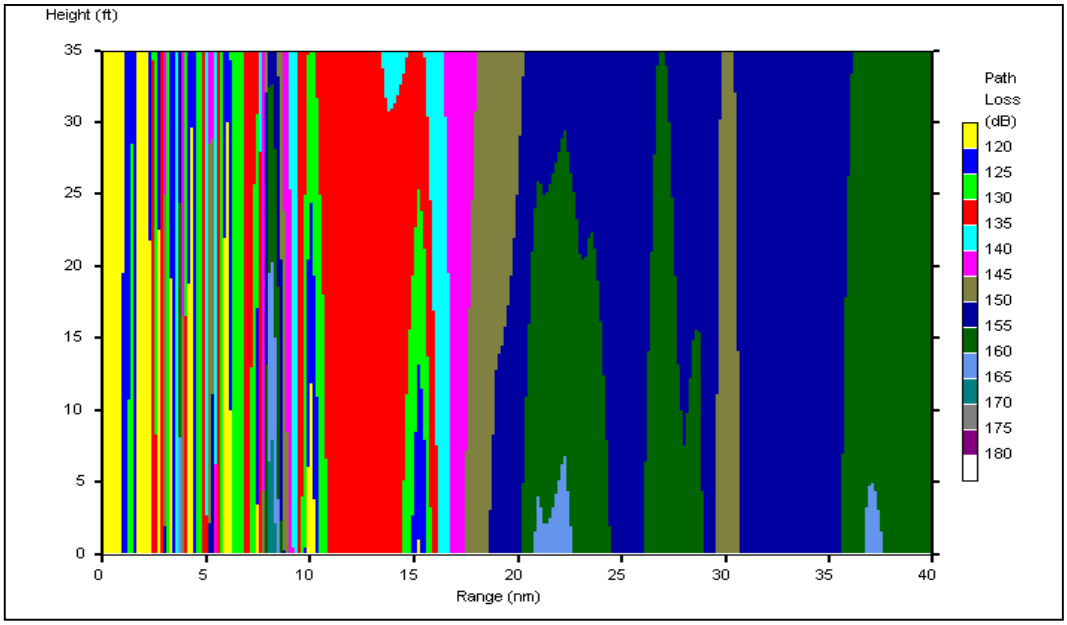

Figure 80. 01 May X Band. Low-level coverage - EEMS

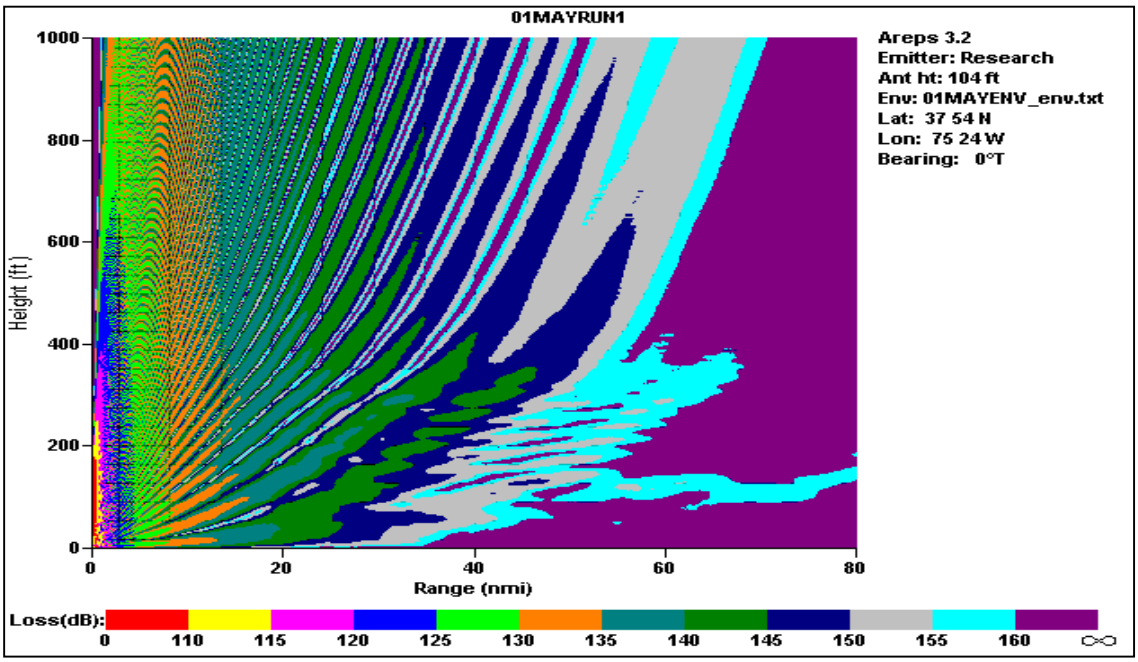

Figure 81. 01 May X Band. AREPS – Paulus-Jenske.

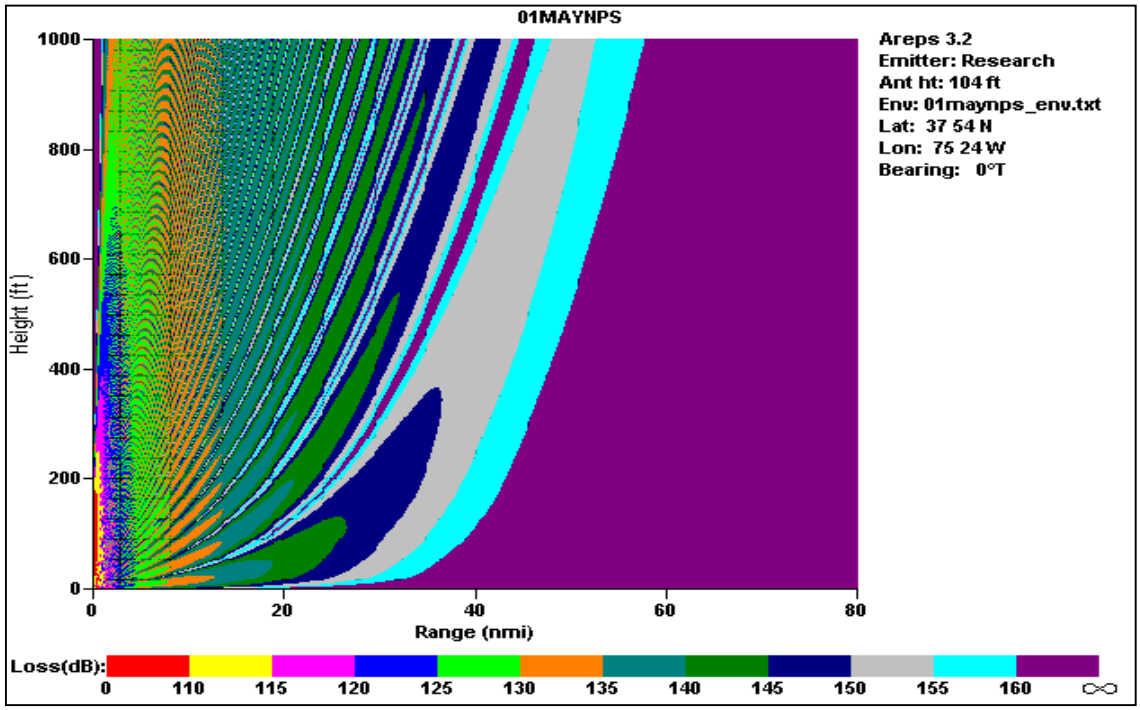

Figure 82. 01 May X Band. AREPS – NPS.

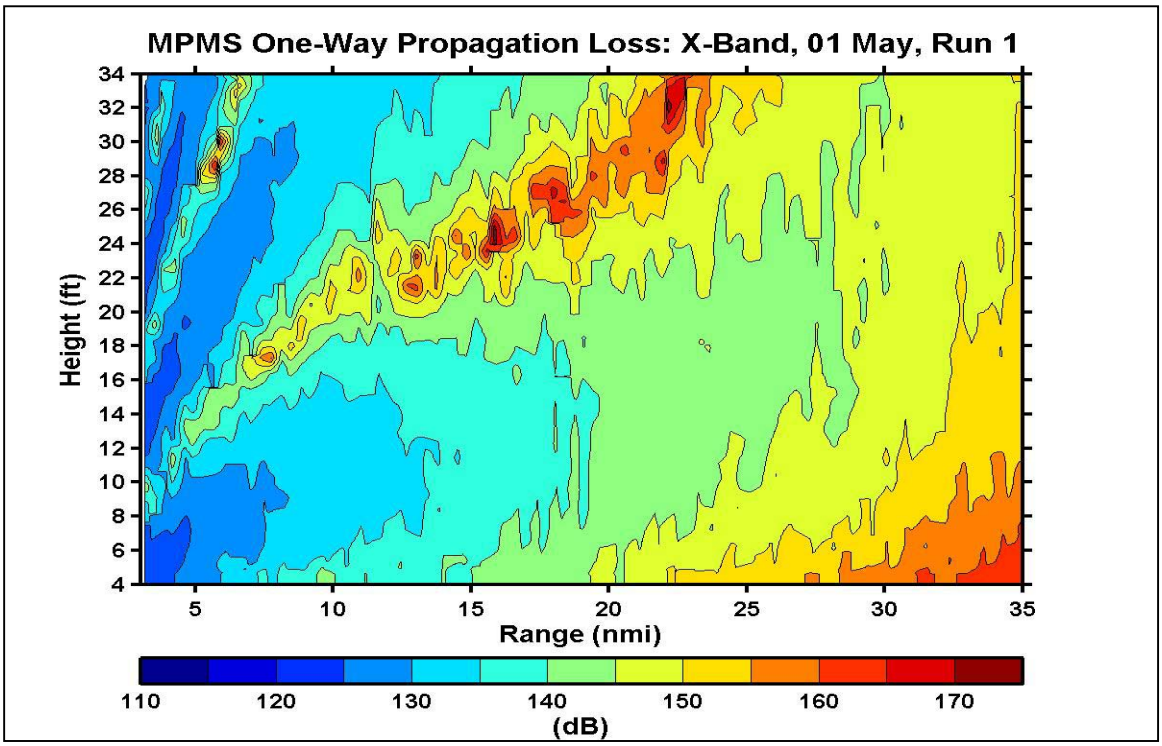

Figure 83. 01 May X Band. Low-level coverage diagram – MPMS II.

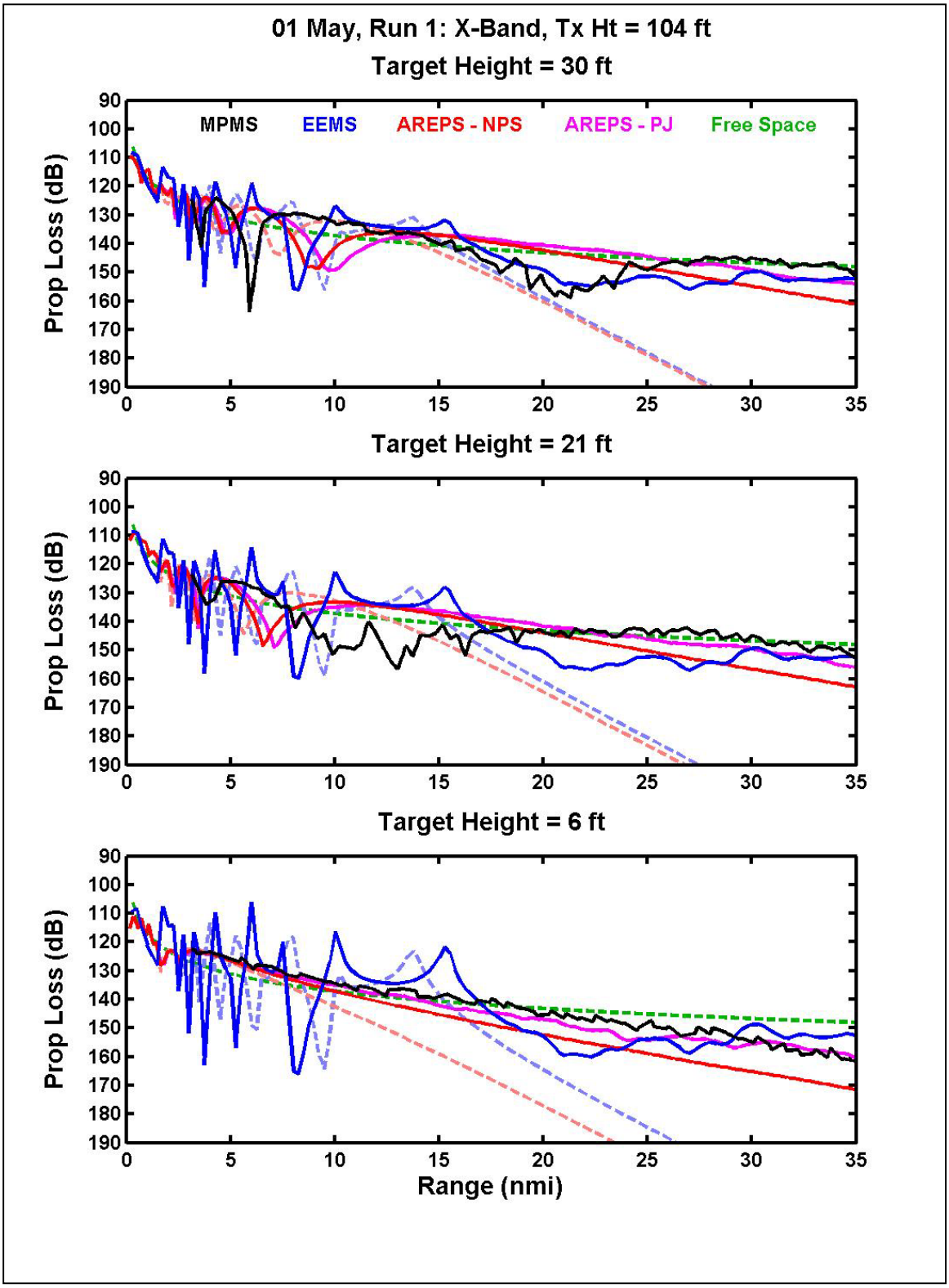

Figure 84. 01 May X Band. Propagation loss curves for EEMS, AREPS, MPMS II.

7. 03 May 2000. S Band

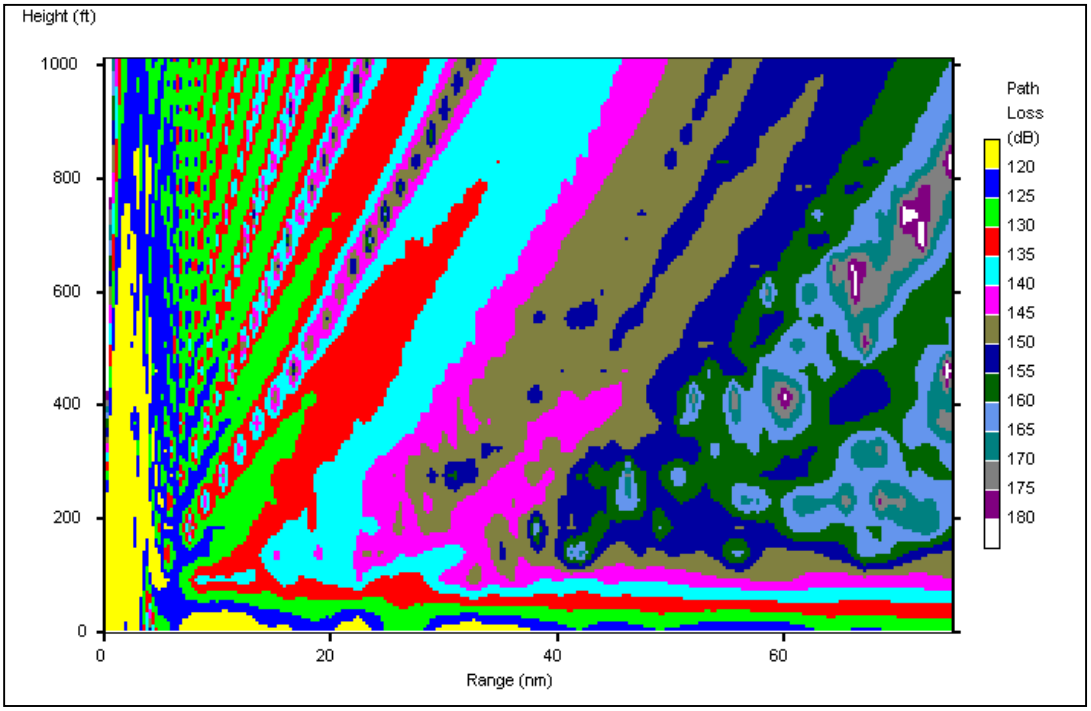

Figure 85. 03May S Band. Coverage diagram – EEMS.

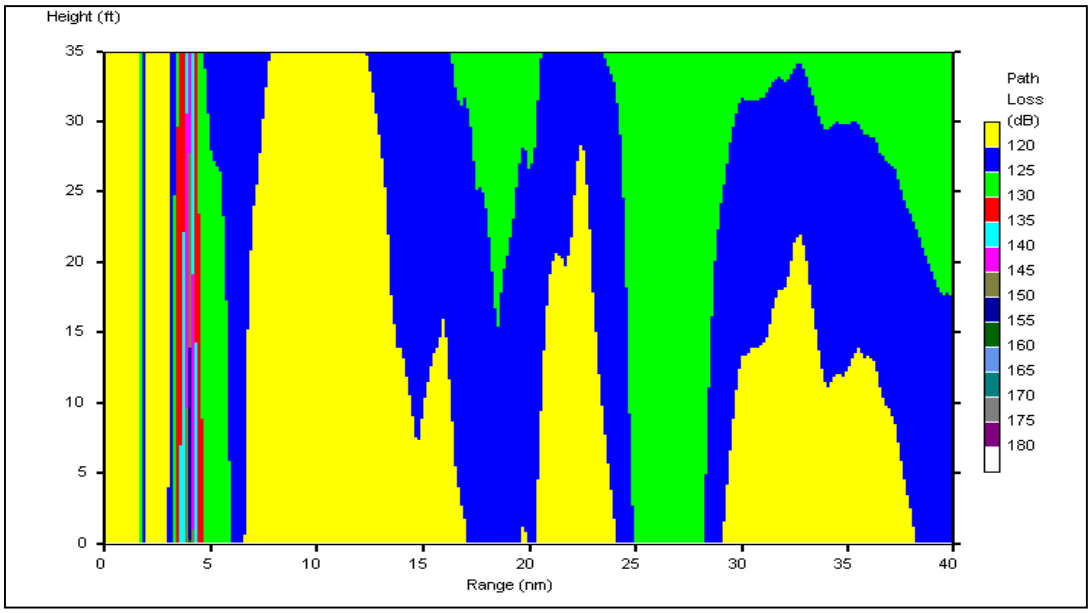

Figure 86. 03 May S Band. Low-level coverage - EEMS

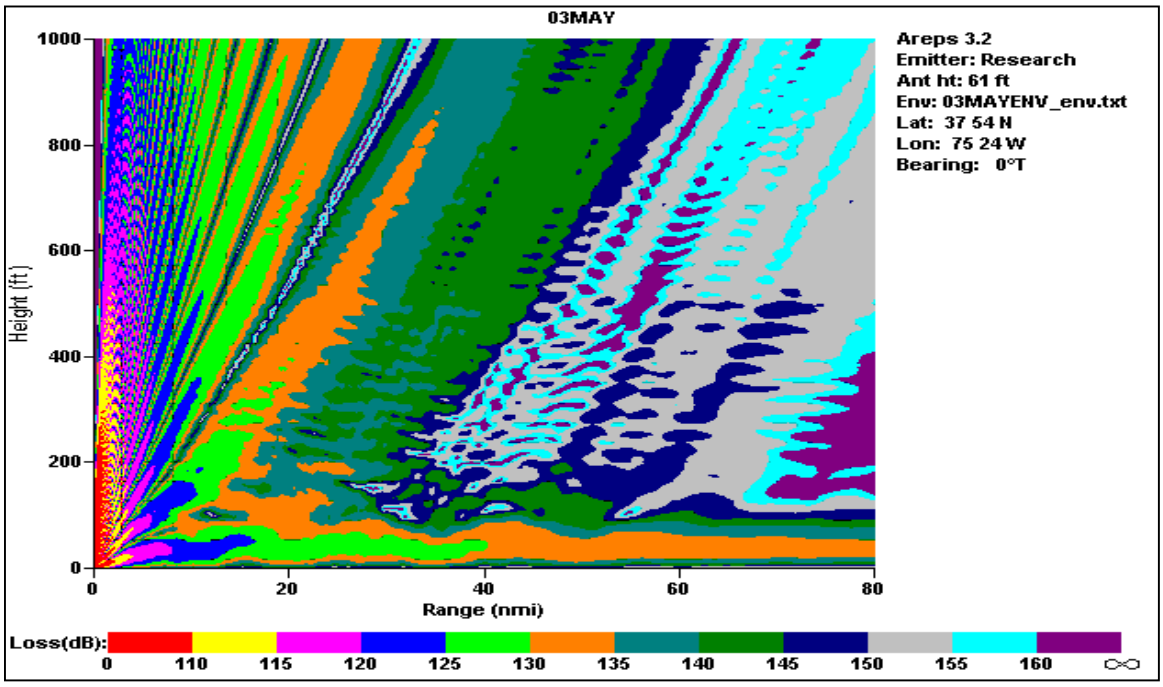

Figure 87. 03 May S Band. AREPS – Paulus-Jenske.

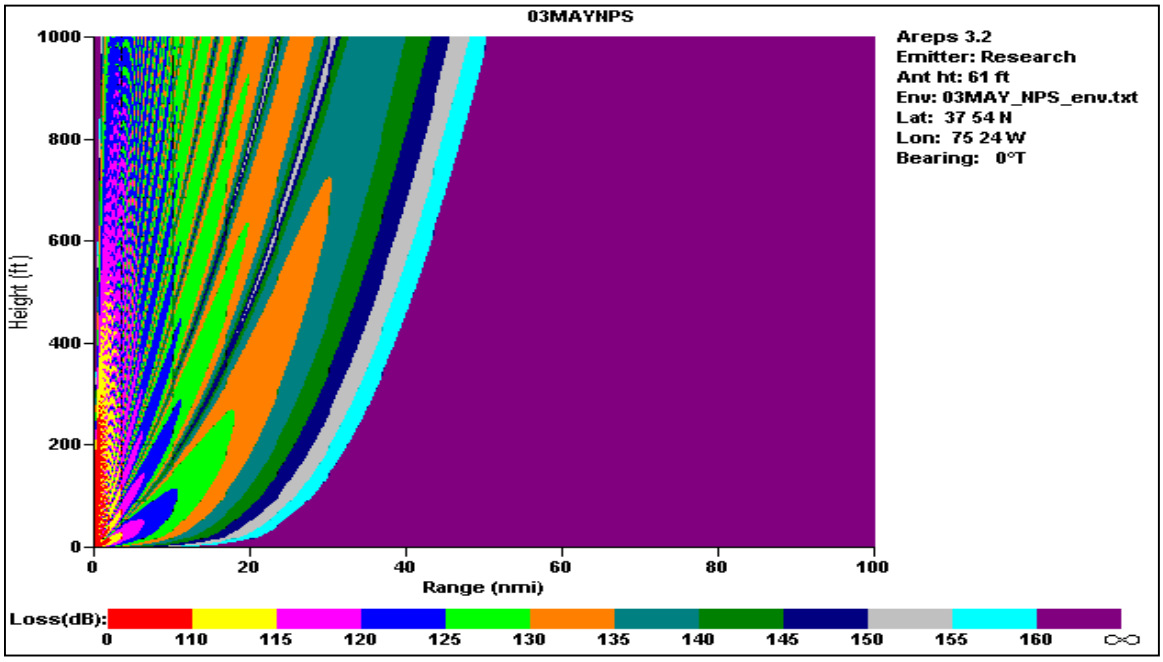

Figure 88. 03 May S Band. AREPS – NPS.

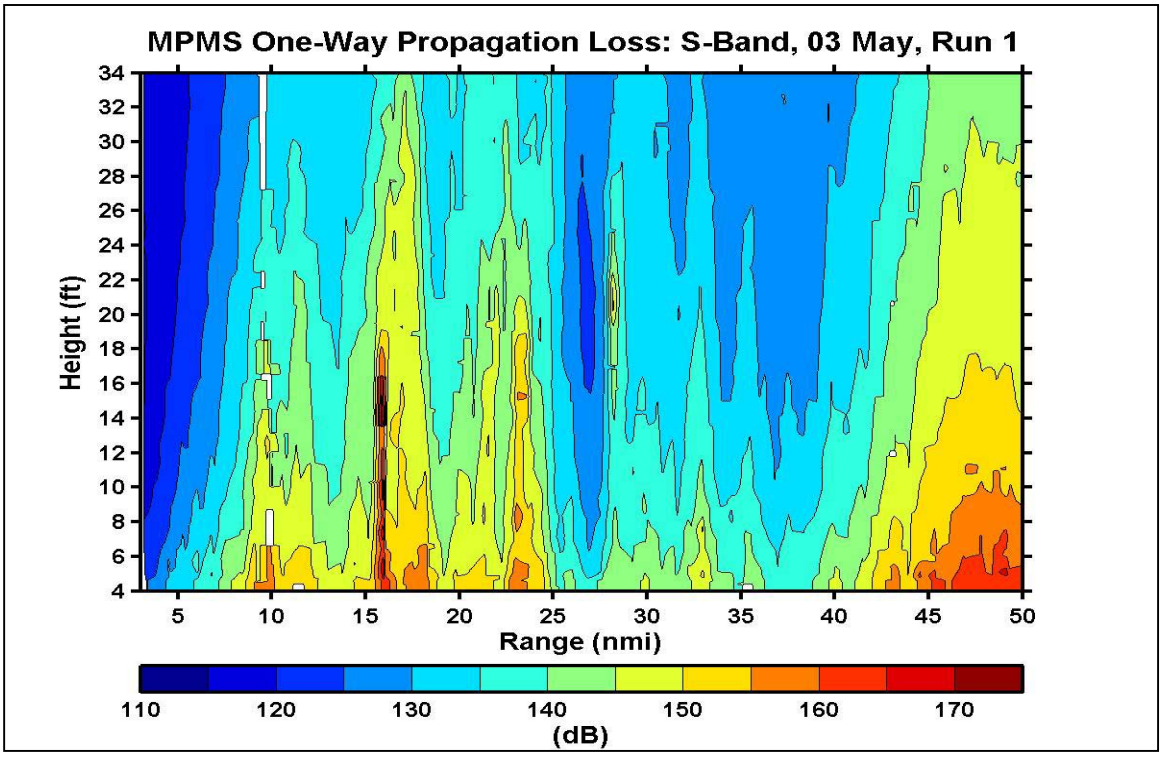

Figure 89. 03 May. S Band. Low-level coverage diagram – MPMS II.

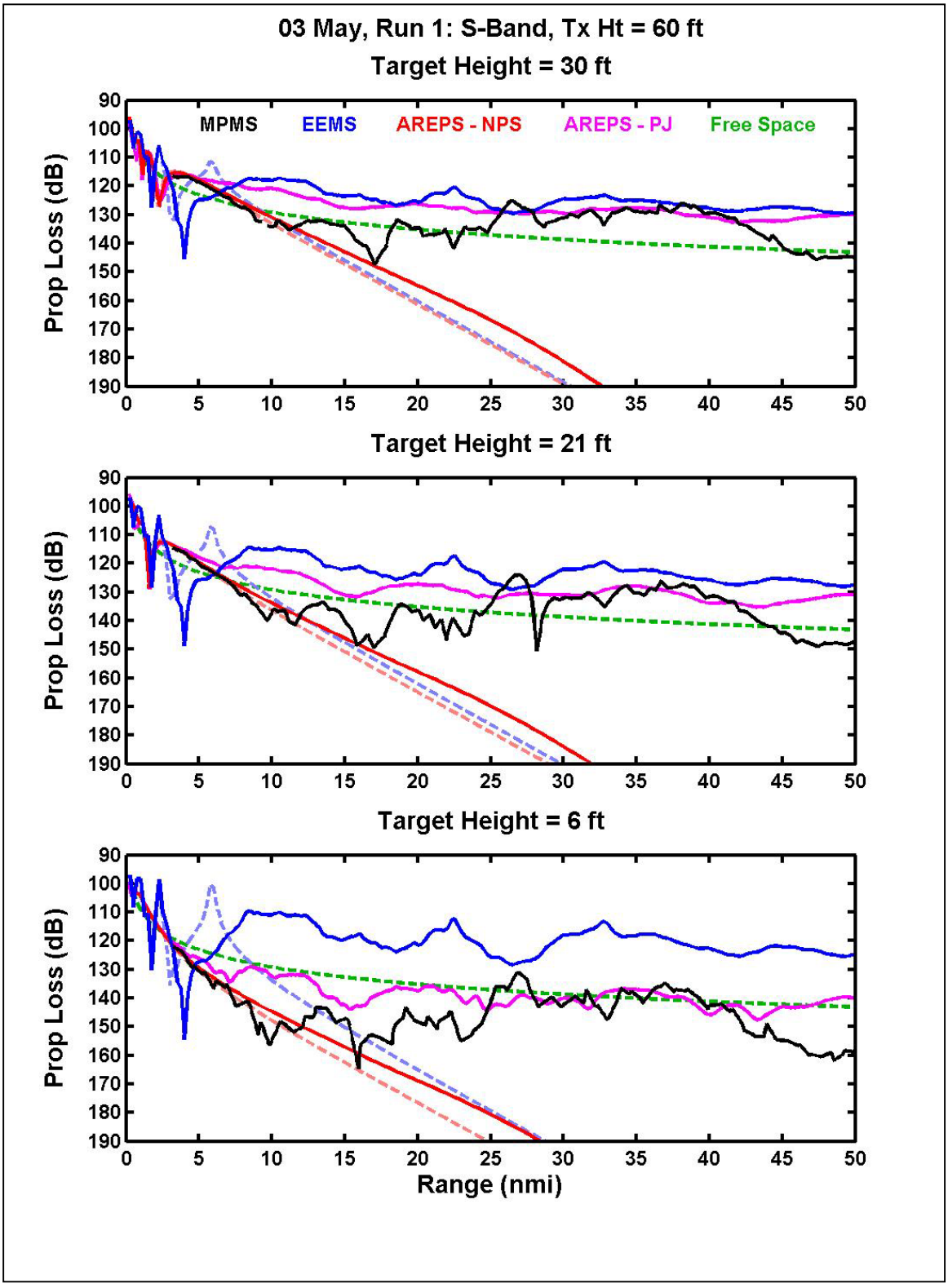

Figure 90. 03 May S Band. Propagation loss curves for EEMS, AREPS, MPMS II.

8. 03 May 2000. X Band

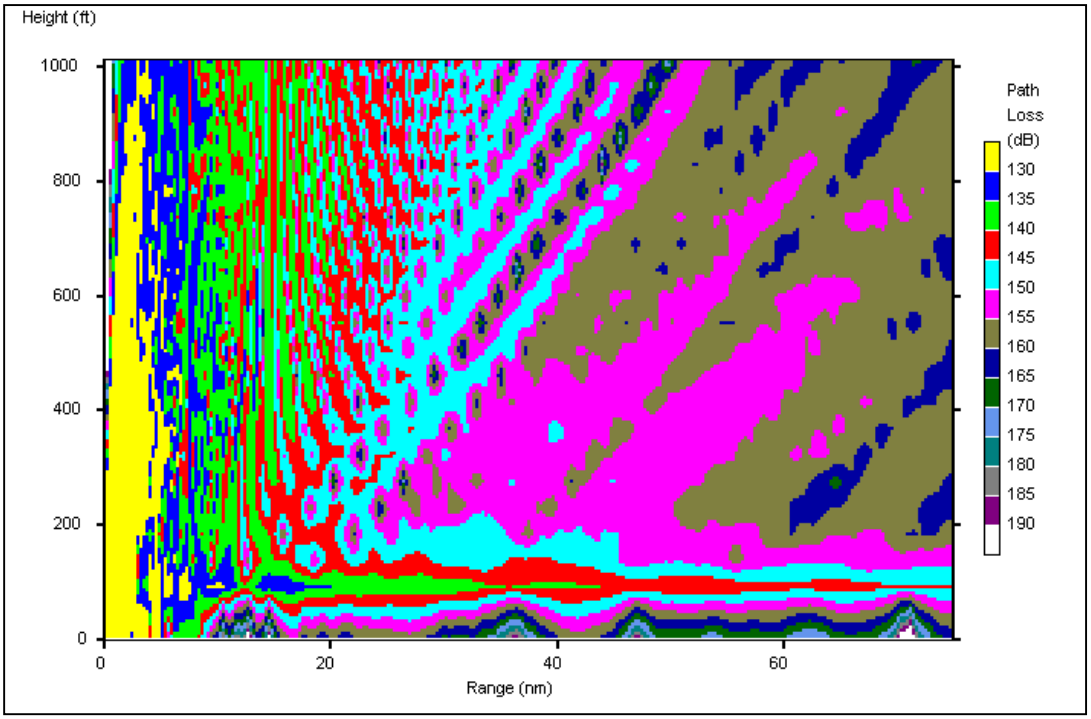

Figure 91. 03May X Band. Coverage diagram – EEMS.

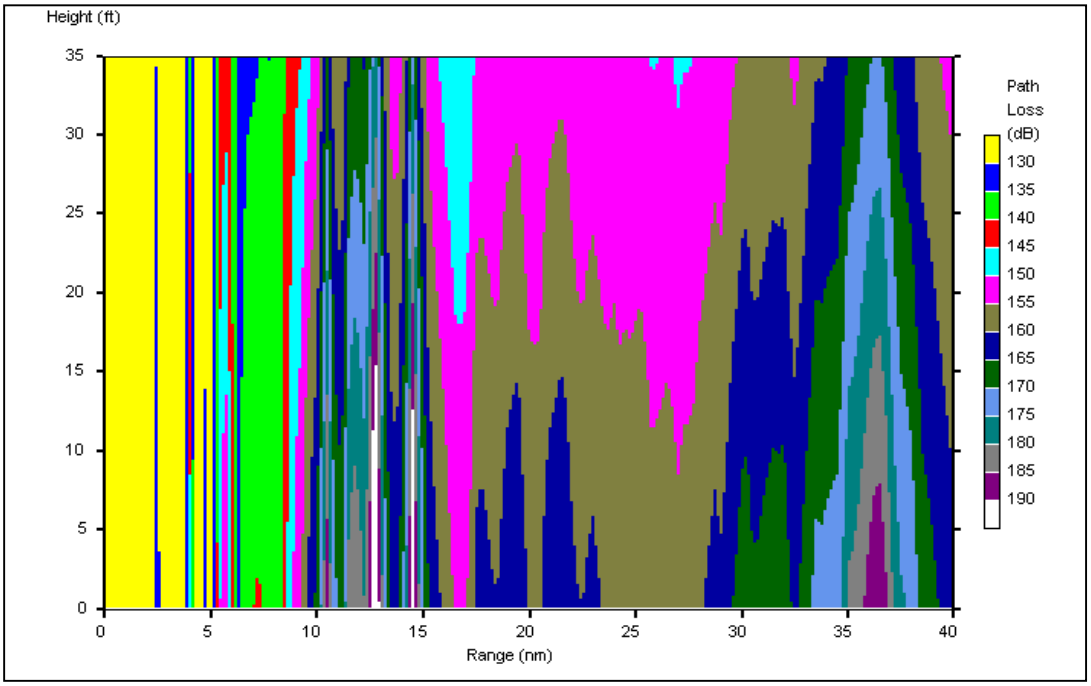

Figure 92. 03 May X Band. Low-level coverage - EEMS

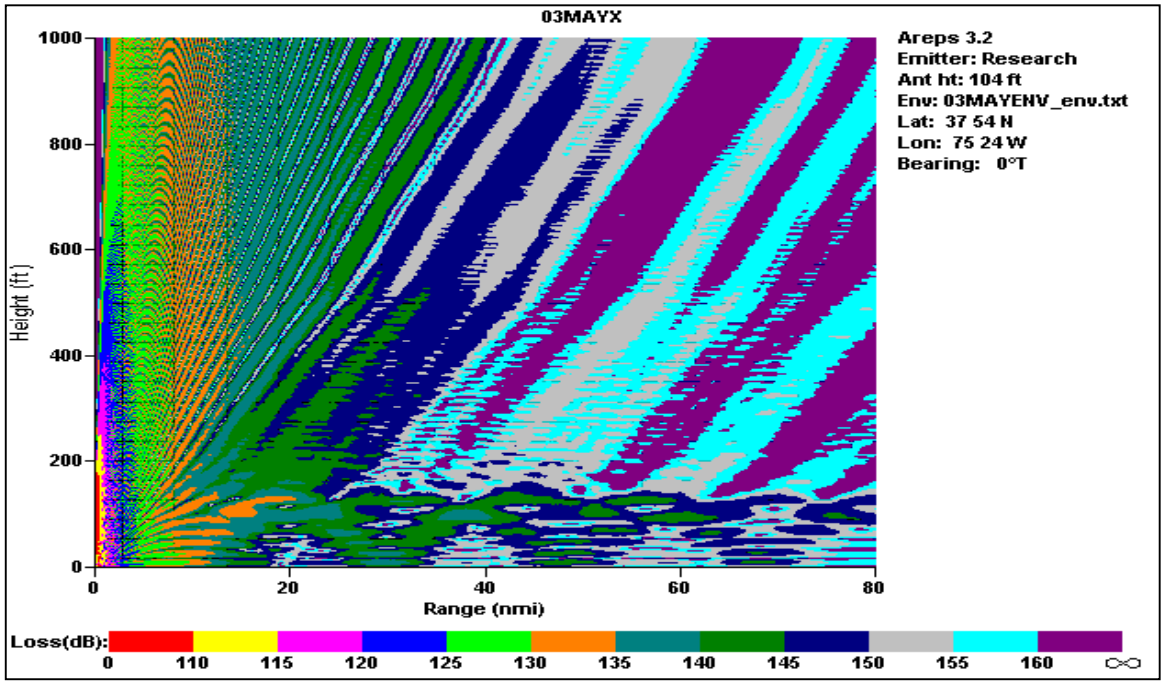

Figure 93. 03 May X Band. AREPS – Paulus-Jenske.

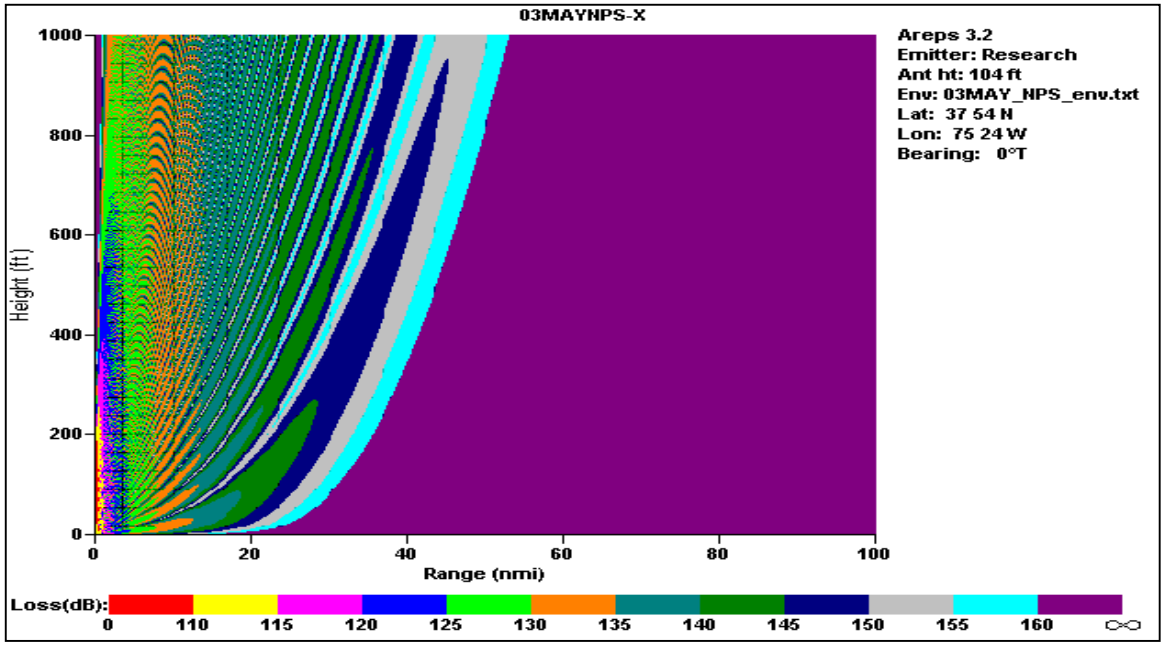

Figure 94. 03 May X Band. AREPS – NPS.

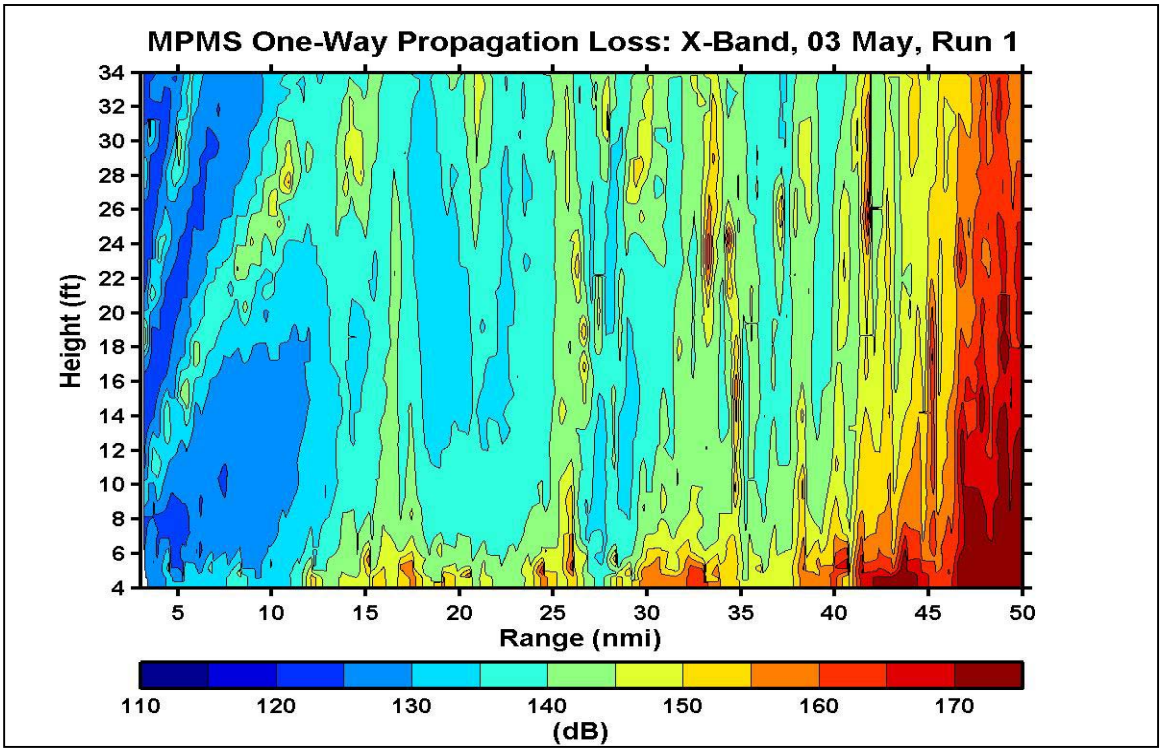

Figure 95. 03 May X Band. Low-level coverage diagram – MPMS II.

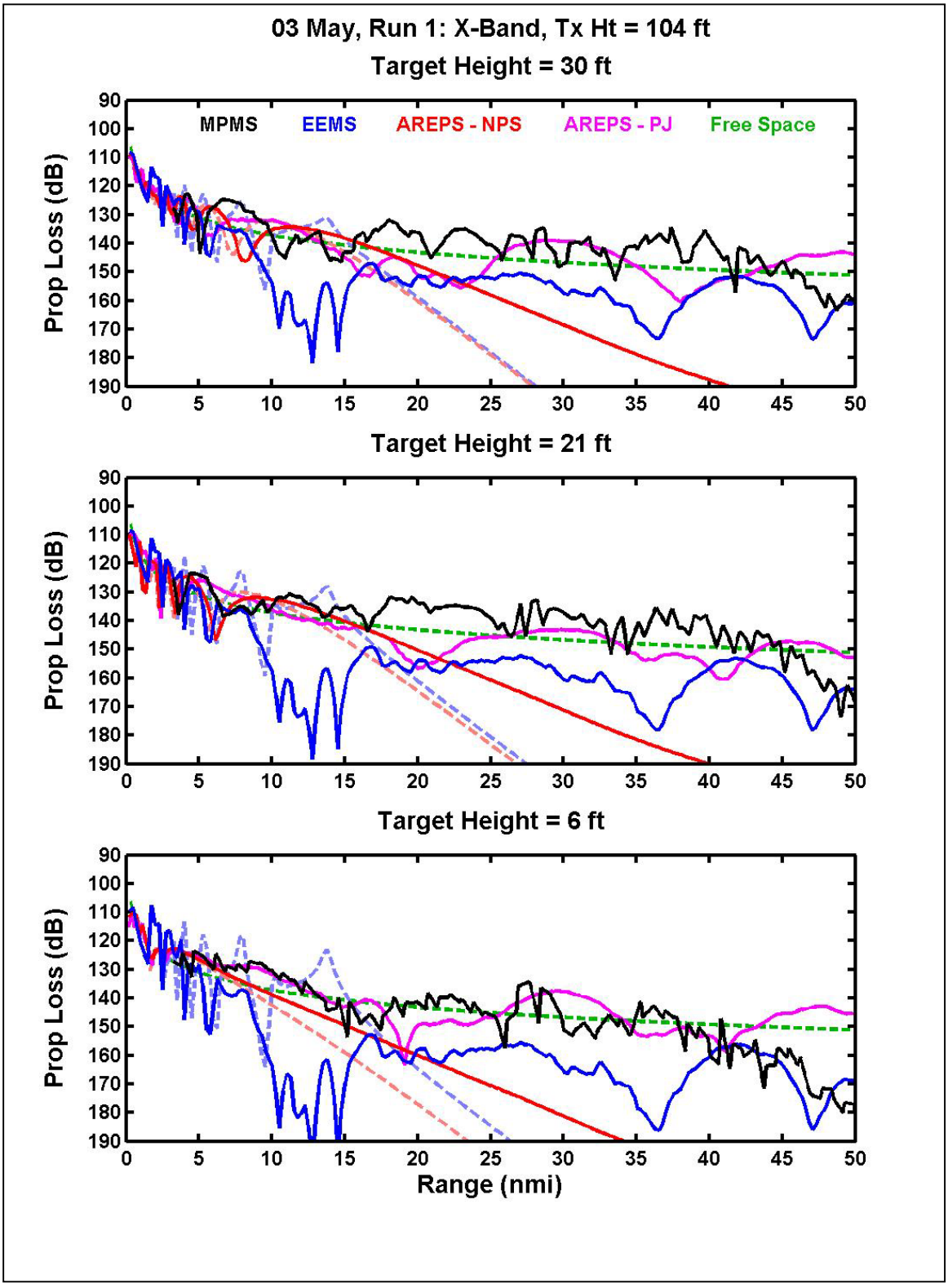

Figure 96. 03 May X Band. Propagation loss curves for EEMS, AREPS, MPMS II.

THIS PAGE INTENTIONALLY LEFT BLANK

XII. SUMMARY AND CONCLUSIONS

A. PROPAGATION MODEL PERFORMANCE

The results derived from interpretations of predicted and field-test observed data demonstrate two main outcomes relative to operational applications:

- That each one of the model configurations converged during one or more runs to an acceptable result in comparison with the MPMS II measured data (i.e. within 2-4dB).
- Notwithstanding the above result, the models diverged away from the MPMS II measured data, far more than they converged.

The first result demonstrates that each of the models, with test data, is capable of producing accurate representations of the propagation conditions when the environmental conditions are relatively homogeneous and when accurate and high quality data is available for input.

The second result makes it abundantly evident that even realistic METOC data, in a complex coastal environment, will yield modelled propagation that is very significantly at odds with reality. Under normal operational conditions, data will be scarce and the METOC officer will often be faced with using only the limited data available. While this may be acceptable in areas farther out to sea, within the littoral zone, the normal operational practice is likely to produce results which are at best, inaccurate and at worst, potentially dangerous. This could only be demonstrated with a study such as this.

Each of the profile combinations was selected for its level of complexity and variation in both synoptic and meso-scale meteorological forcings. The resulting vertical ascents and refractive profiles were intrinsically dependant on the pattern of previous synoptic events. Atmosphere profiles adjust to various environmental forcings with a certain time lag. Such considerations can result in very complex vertical profiles, with multiple areas of hydrolapses and inversions, wide variations in static stability, each of which will affect the refractive profile. The model results clearly show that the sampled environment was generally extremely complex and varied significantly in a relatively short spatial scale.

That the models not only diverged significantly from the measured losses, but also from each other, is an important result and of great interest. Previous studies have indicated that the propagation models (TERPEM and APM) generally produce similar results, for example Thomson (2002). In this study considerable differences occurred between the propagation models (TERPEM and APM) predicted 2-way losses, using identical METOC input data. Where the models must be differing is in their application within AREPS and EEMS. EEMS and AREPS use a variety of evaporation duct models, and the varying results of the ED calculations were discussed in Chapter XI, where significant differences in the results were found. The process of merging the resultant ED and the rocketsonde profile also varies within each TDA, and again this must play a part in causing the differing results. The role of the evaporation duct is vital in determining the surface propagation conditions for examined frequencies, especially X-band. Because of the impact of a surface-based duct, the effect of refractivity was seen to be extremely sensitive to small variations in the vertical profile. Both the near-surface evaporation duct and the both factors were seen to be likely dominant causes of error in the resultant model output.

The performance of AREPS, using the NPS ED model only, was on occasions remarkable, most often being capable of exceeding the accuracy other two model runs on a number of occasions within 15nm. This implies that it would be extremely useful and productive to be able to examine the results of this model appended to the upper air profile, which must certainly improve the final accuracy of the modelled propagation.

Of the four sampled days, only two (10th April and 1st May) produced conditions under which any of the model predictions might be deemed to be of an acceptable accuracy, i.e. spatially smoothed loss profiles within 3-5 dB of the observed profiles. Further, even during these days, the S band results were acceptable, but the X band results diverged significantly. Of importance, on the 1st May, the wind was considerably stronger than on other days; 9.83 m/s (each of the other runs did not exceed 4m/s), and on this occasion the EEMS run was particularly accurate (within 2-3dB). This demonstrates that the sea clutter (roughness) effects algorithm incorporated within this model worked extremely well on this particular occasion.

On the other two days, 29th April and 03rd May (which were both characterised by strong surface based ducting), the varied nature of the differences between measured and modelled results, was very significant, often varying by 20-30dB. Much of this variability is undoubtedly due to the complexity and presumed temporal and spatial variance of the atmosphere along the MPMS II measurement path. During these two days containing strong surface- based ducting, the MPMS II obtained loss profiles exhibited multipath interference, signal fade and skip zones. These areas were not distributed evenly, but rather, increased in their strength, or actually began down-profile in an offshore direction. The conclusion is that this was caused by, an almost classical development, of an offshore duct.

The coastal or littoral environment, in which naval and joint military operations are being increasingly conducted and concentrated, often exhibit a great deal of inhomogeneity, a principle which can often be neglected when operating in an air mass far offshore in open water. In such a case a single profile may produce a representative sample of the environment, which can be extrapolated for many miles in each direction. This thesis has clearly shown, however, that even in a relatively straightforward synoptic situation, the resultant atmospheric profile, within coastal regions, is potentially extremely variable in both the horizontal and vertical spatial scale. The consequences of this fact mean that the characterization of the battlespace environment for the warfighter is liable to be fraught with error.

Command requires accurate, timely and dependable tactical advice regarding the effect of the environment on weapons systems and sensors. The fact that the coastal environment demonstrates such a large amount of vertical and horizontal, variability, inevitably leaves the consequence that this may not always be the case. This study has shown that the coastal environment, can occasionally be well described by a single profile, but this is by no means the normal situation. More often, the modelled environment is significantly in error in respect to the actual conditions. The operational and tactical effects of the environment were discussed in Chapter V, which outlined how features such as the evaporation duct or surface based duct can be used for significant tactical advantage. If, however, the presence of such features is not accurately forecast, then any tactical advantage the environment may provide is lost to the warfighter.

B. RANGE DEPENDANT CONSIDERATIONS

This thesis has concentrated on a range-independent method of calculating the propagation conditions. This limitation was brought into several discussions on range dependent differences between observed versus model predicted interference patterns. The rationale behind this decision was, simply, that this is how the majority of naval operations are supported. Under operational conditions, the luxury of multiple vertical ascents, whether measured by rocketsonde, radiosonde or dropsonde is unrealistic. The collection of such data under fire would be time consuming and potentially hazardous. On occasions under periods of heavy operational activity, the use of a single rocketsonde or radiosonde may be prohibitive, due to EMCON policy or indeed, flying movements. In such a case, only the surface meteorological measurements may be available for use in a propagation model. This makes the fact that AREPS, using just the NPS evaporation duct model, often exceeded the accuracy of the other two runs (in the 5-15nm range) in a number of runs of greater significance.

In the absence of high quality data, the production of tactical forecasts must often rely on one of two options:

- A highly experienced and skilled METOC forecaster, who is able to interpret the results and adjust advice accordingly to their judgement.
- The input of various parameters, output from atmospheric models.

There are disadvantages to both approaches:

- Forecasters vary significantly in experience, and for that matter, also ability, and thus there is likely to be little consistency in the advice given to Command.
- Current models, such as, the US Navy's COAMPS or the UK Met Office's Meso-scale model have yet to prove their ability to accurately and consistently handle the complexities of the land/sea boundary, or to produce sufficient vertical resolution for accurate inputs in to EM propagation TDAs.

C. ATMOSPHERIC MODELLING

The RN and USN currently use a suite of atmospheric models to forecast various environmental parameters, not least the state of the atmosphere, or more normally, a weather forecast. Both EEMS and AREPS are designed to directly ingest data from

COAMPS or the Meso-scale model. Both models are proven to produce good approximations to the state of the atmosphere. The characterization of the refractive profile and subsequent propagation conditions is particularly sensitive to small errors. The spatial scales over which horizontal and vertical changes occur, are very small in relation to current model parameters, with important features often smoothed or missed by the resultant forecasts. In particular, within the coastal boundary, the description of the marine atmospheric boundary layer (MABL) is frequently poorly modelled. As discussed in Chapter V, this zone is characterised by strong temperature and humidity gradients, which undergo significant variation in relatively small horizontal scales. The coast of California is dominated by variations in this MABL, for much of the year, and both the weather and refractive conditions are intrinsically dependant upon its character. Current models rarely produce satisfactory and reliable forecasts of the variation of this feature, which is potentially significant for the concept of port protection.

D. OPERATIONAL AND TACTICAL CONSIDERATIONS

This study has illustrated, using high quality in situ measured data, that in a simulated operational scenario, there are still significant problems in forecasting propagation conditions in the littoral zone. This is a region in which both the Royal Navy and United States Navy are increasingly engaged, often in coalition. The threat from potential adversaries is becoming increasingly diverse, and technology increasingly lethal. Surface vessels are vulnerable to attack from submarines, surface, air, and land launched sea-skimming missiles, the traditionally posed threat. However, recent events have shown that adversaries in small craft armed with shoulder-launched weapons, limpet-type bombs and/or simply packed with explosives are increasingly a threat. Such threats can also be directed at ports and other major coastal installations, such as oil refineries.

Radar can and is used to detect and protect our assets by the detection of aircraft, missiles, un-manned airborne vehicles, periscopes, small-craft and potentially swimmers. The concept of Sea Shield, Sea Strike and also Homeland Defence, whether in protection of UK or US interests, can be intrinsically dependant on the effectiveness of radar and the description of the battlespace environment. The effectiveness of radar is undoubtedly

dependant on the accurate portrayal of the refractive medium in which it is being utilised and the temporal and spatial variations that subsequently occur.

Propagation models have been shown to be capable of producing excellent results, in both this study and others, but the variability of the atmosphere, especially in the littoral region produces significant challenges to accurate predictions. To achieve the goal of an accurate characterisation of the littoral zone, requires further research, such as that conducted at Wallops Island, with emphasis on the production on atmospheric models which concentrate on the very fine detail required for propagation forecasts and also propagation models that fully utilise the near surface data field to accurately predict the evaporation duct.

Until higher quality data and models are available, the Royal Navy and United States Navy must continue to rely on the decisions made by highly trained, experienced and specialised forecasters to provide the tactical edge to the warfighter.

LIST OF REFERENCES

Babin, S. M., G. S. Young and J. A. Carton, 1997: A New Model Of The Oceanic Evaporation Duct. *J. Appl. Meteo.,* **36**, No. 3, 193-204.

Battaglia, M.R., 1985: Modelling the radar evaporative duct, *RANRL Technical Note* **3/85**, Department of Defence, Defence Science and Technology Organisation, Weapons Systems Research Laboratory, RAN Research Laboratory, Australia.

Baldauf, Brian K., 1996: Evaluation of Low Altitude Rocket Dropsondes for Shipboard Atmospheric Profiling and Electromagnetic Propagation Assessment, MS Thesis, Naval Postgraduate School, Monterey, CA, December 1996, 149 pp.

Ballantine, S., 1928: The Lorentz reciprocity theorem for electric waves. *Proc. I.R.E.*, **16**, 513-518.

Bean, B. R., and E. J. Dutton, 1968: *Radio Meteorology*. Dover Publications, New York, pp. 435.

Call, D. B., 1994: LARDS A Low Altitude Rocket Dropsonde With PS Wind-Finding, Atmospheric Instrumentation Research Inc., Boulder, CO, 12 pp.

Chief of Naval Operations, 2000: *Navy Strategic Planning Guidance With Long Range Planning Objectives,* 90 pp.

Department of the Navy, 2003: *Naval Transformation Roadmap: Power and Access...From the Sea*. 68 pp.

Director of Naval Oceanography and Meteorology, 1994: The Effects of the Environment on Radio and Radar Wave Propagation. *Naval Oceanography and Meteorology Memorandum* No. 1/94.

Directorate of Naval Staff Duties, 1995: *The Fundamentals of British Maritime Doctrine.* BR 1806. HMSO, London. 256pp.

Dockery, G. D., 1988: Modelling Electromagnetic Wave Propagation in the Troposphere Using the Parabolic Equation. *IEEE Trans. Antenn. Prop*, **36**, 1464-1470.

Dockery, G.D. and Goldhirsh, J., 1995: Atmospheric Data Resolution Requirements for Propagation Assessment: Case Studies of Range-Dependant Coastal Environments. In: Propagation Assessment in Coastal Environment. *AGARD Conference Proceedings*, vol. **567.** Paper 7.

Dockery, G. D., 1997: Meteorological Data Requirements For Assessment of Aegis Air Defense Capability. *Proceedings Electromagnetic/Electro-Optics Prediction Requirements & Products Symposium*, Naval Postgraduate School, Monterey, CA., 121-130.

Fairall, C. W., E. F. Bradley, D. P. Rogers, J. B. Edson and G. S. Young, 1996: Bulk Parameterization Of Air-Sea Fluxes For Tropical Ocean-Global Atmosphere Coupled-Ocean Atmosphere Response Experiment. *J. Geophys. Res*., 101, 3747-3764.

Frederickson, P., K. L. Davidson, F. K. Jones, T. Neta, 2000: Flux Buoy Data Report. Draft Memo, Naval Postgraduate School, Monterey, CA., 8 pp., 21 July 2000.

Frederickson, P. A., K. L. Davidson, and A. K. Goroch, 2000: Operational Bulk Evaporation Duct Model For MORIAH. Draft Memo, Naval Postgraduate School, Monterey, CA, 03 January 2000. 70 pp.

Frieden, D. R., 1985: *Principles Of Naval Weapons Systems*, Naval Institute Press, Annapolis, MD, 27-88.

Goldhirsh, J. and G. D. Dockery, 1997: Statistically Derived Propagation Factor Errors for the Mid-Atlantic Coast Region Due to Assumption of Lateral Homogeneity of Atmospheric Refractivity. *Proceedings Electromagnetic/Electro-Optics Prediction Requirements & Products Symposium*, Naval Postgraduate School, Monterey, CA., 121-130.

Levy, M.F., 1989: Combined Effects of Atmosphere and Terrain on UHF/Microwave Paths. In: Multiple Mechanism Propagation Paths(MMPPs): Their Characterisation and Influence on System Design. *AGARD Conference Proceedings*, vol. **543.**Paper 10

Levy, M.F., 1995: Fast PE Models for Mixed Environments. In: Propagation Assessment in Coastal Environment. *AGARD Conference Proceedings*, vol. **567**.Paper 8.

Miller, A.R., Brown, R.M. and Vegh, E., 1984: New Derivation for the Rough-Surface Reflection Coefficient and for the Distribution of Sea-Wave Elevations. *IEE Proc*. Part H, **131,** 2, 114-116.

Naval Surface Warfare Center, 2000: Site Test Plan And Procedures For The Microwave Propagation Measurement Experiment At The Surface Combat Systems Center (SCSC) Wallops Island Test Facility, Naval Surface Warfare Center (NSWC), Dahlgren, VA., 36 pp.

Pappert, Paulus, & Tappert, (1992): Sea echo in tropospheric ducting environments. *Radio Science*, vol. **27**, 2, 189-209.

Philips, O.M., 1966: *Dynamics of the Upper Ocean*. Cambridge University Press. 367pp.

Space and Naval Warfare Systems Command 2000: *User's Manual (UM) for Advanced Refractive Effects Prediction System Version 2.0*, Draft, Space and Naval Warfare Systems Command, METOC Systems Program Office (SPAWAR PMW-185), San Diego, CA.

TERPEM User Guide. 1998 (June). TERPEM User Guide. Signal Science Limited, 20, Alexander Close, Abingdon, Oxon. OX14 1XA. UK. Code version 5.1.

Thomson, A.D., 2002: TERPEM evaluation. Presentation to *TTCP SEN TP-6* annual meeting at Defence R & D Canada – Ottawa.

Web-sites

NOAA Air Resources Laboratory [http://www.arl.noaa.gov]. Accessed June 2003.

THIS PAGE INTENTIONALLY LEFT BLANK

INITIAL DISTRIBUTION LIST

1. Defense Technical Information Center
   Ft. Belvoir, VA

2. Dudley Knox Library
   Naval Postgraduate School
   Monterey, CA

3. Director of Naval Surveying, Oceanography and Meteorology
   MINISTRY OF DEFENCE
   London. United Kingdom

4. Ms Wendy Townshend
   Maritime Warfare Centre
   PORTSMOUTH, Hants. United Kingdom

5. Professor Kenneth L. Davidson
   Meteorology Department, Code MR
   Naval Postgraduate School, Monterey, CA

6. Professor Wendell A. Nuss
   Meteorology Department, Code MR
   Naval Postgraduate School, Monterey, CA

7. Professor C. H. Wash
   Meteorology Department, Code MR
   Naval Postgraduate School, Monterey, CA

8. The Oceanographer of the Navy
   United States Naval Observatory
   Washington, DC

9. Commanding Officer
   Fleet Numerical Meteorology and Oceanography Center
   Monterey, CA

10. G. Daniel Dockery
    The John Hopkins University
    Laurel, MD

11. Richard Paulus
    SWAWARSYSCEN-SD, 2858
    San Diego, CA

12. Wayne Patterson
SPAWARSYSCEN-SD, 2858
San Diego, CA

13. Janet Stapleton, Code T44
Naval Surface Warfare Center, Dahlgren Division (NSWCDD)
Dahlgren, VA

14. Commander
Space and Naval Warfare Systems Command (PMW-155)
San Diego, CA

15. Kenneth Andreson
SWAWARSYSCEN-SD, 2858
San Diego, CA

16. Dr Spephen Burk
Naval Research Laboratory
Monterey, CA

17. Robert E Marshall, PhD
Naval Surface Warfare Center
Dahlgren, VA

18. Lt Cdr Andrew J Moys RN
Monterey, CA